THÈSE

Pour obtenir le grade

DOCTEUR DE LA COMMUNAUTÉ UNIVERSITÉ GRENOBLE ALPES

Spécialité : **MBS - Modèles, méthodes et algorithmes en biologie, santé et environnement**

Arrêté ministériel : 25 mai 2016

Présentée par

Alessio TREBBI

Thèse dirigée par **Yohan PAYAN**, CNRS
et co-encadrée par **Antoine PERRIER** et **Mathieu BAILET**

préparée au sein du **Recherche Translationnelle et Innovation en Médecine et Complexité** dans **l'École Doctorale Ingénierie pour la Santé la Cognition et l'Environnement**

Définition d'une méthodologie pour évaluer les modèles éléments finis du talon humain pour la prévention des escarres

Thèse soutenue publiquement le **7 décembre 2022**,
devant le jury composé de :

Monsieur Amit GEFEN
PROFESSEUR, Tel Aviv University, Rapporteur
Monsieur Estavam Barbosa LAS CASAS
PROFESSEUR, Universidade Federal de Minas Gerais, Rapporteur
Madame Chiara Giulia FONTANELLA
PROFESSEUR ASSISTANT, Università degli Studi di Padova, Examinatrice
Monsieur Pascal PERRIER
PROFESSEUR, Grenoble INP, Examinateur
Monsieur Claudie VERDIER
DIRECTEUR DE RECHERCHE, CNRS, Examinateur
Monsieur Yohan PAYAN
DIRECTEUR DE RECHERCHE, CNRS, Directeur de thèse

Dédié à mes parents

Viviana Zinetti et Gianfranco Trebbi

« Avevamo tutti più o meno quell'età

in cui non hai ancora deciso se mettere su famiglia

o perderti per il mondo. »

- Mediterraneo, 1991

Summary

In a context of an aging population and an increasing prevalence of diabetes, the problem of pressure ulcers continues to grow. Despite the attention received in the past decade in order to reduce the humanitarian, social and economic costs, there is still a lack of understanding in the pathophysiology of pressure ulcers. These injuries not only represent major challenges for the quality of life of patients, but also a great burden for healthcare system. The costs associated with the management of pressure ulcers are considered to be very significant in many countries being on a scale of billions of euros. The prevalence of ulcers in hospitalized patients is around 10% with the heel and sacrum being the most common sites. These two body locations are substantially different in matters of anatomy, histology and loading configurations. This thesis will specifically focus on the prevention of diabetic foot ulcers. Precisely, the heel can experience two different processes of ulcer formation. In one case, with a subject laying on his back, the mechanical forces due to the leg and foot weights are transferred to the heel bone, the calcaneus, through a relatively thin layer of soft tissues which includes fat, skin, muscle and tendons. In the other case, specific to diabetic patients, neuropathy prevents the subject to detect an improper shoe fitting or an incorrect gait that would generate high and repetitive loads on a specific part of the foot. Over time, these internal strains in tissues and cells can cause tissue breakdown and start a pressure ulcer. In this thesis we will specifically address these ulcers with a focus on the fat pat plantar region of the heel.

It is believed that a solution that would track internal tissue strains and alert when their values are too high could contribute in the prevention of heel pressure ulcers. This is a complex task as it is not possible to measure directly the strains that occur in the deep layers of the tissues. Medical imaging, external measurements, and cadaveric dissections can each offer only a partial information required to fully understand the role of the internal structures. Hence common solution to measure real time strains that occur in deep layers resulting from loading applied on the skin surface are computational simulations. In this regard, finite element (FE) modeling is a technique that permits the prediction of the deformations of structural and mechanical systems. These simulations provide useful clinical information, like internal strains, which is difficult to measure with experimental procedures. In the last decade the first FE heel models started to be developed in order to simulate the stress propagation in the heel while the subject is walking or is laying on a bed. However, the subjects intervariability in terms of tissue morphologies and mechanical tissue properties makes this a complex task requiring personalized models. Additionally, the heel is by itself a complex organ involving a very specific structure, the heel pad, composed by various tissues with different mechanical properties in close contact between each other. FE models are complex

simulations that require a consistent and robust methodology for validation through rigorous experimental measurements. In the literature, there are two main gaps regarding this aspect. First, the scarcity of experimental tests to define *in vivo* material properties of the human fat pad. In general, researchers keep implementing parameters that reference to outdated studies made on ex vivo specimens. Second, little has been done to establish the validity of FE models via experimental measurements. Usually, data from previous studies literature is used to compare the results of contact pressures and strain propagation in internal tissues. However, as all published studies suffer from the same limitations, most of them do not provide any meaningful validation of their results.

This therefore leads us to the main research purpose of this thesis: «Definition of a methodology to evaluate finite element models of the human heel for diabetic foot ulcer prevention».

To cover this objective, the manuscript is divided in six main parts.

The first part is an introduction to the topic from biomechanical and medical perspectives. This section will briefly describe the problem and the structure of this thesis.

In the second part, a systematic review of the literature is conducted on FE models of the heel to find the areas where it is possible to contribute to the medical and biomechanical studies on the topic.

In the third part, a Magnetic Resonance experiment is defined to provide a dataset of 3D images and boundary conditions that will be used to build and to evaluate FE models of the human heel.

In the fourth part, the measurements of internal strains in the biological tissues of the heel through Digital Volume Correlation based on image registrations are described.

In the fifth part an FE model of the heel is build and evaluated with the dataset defined in the previous two chapters.

The sixth part will draw the conclusions of the studies described in this thesis resuming the implications and the future steps.

Acknowledgments

I would like to express my gratitude to my supervisor Professor Yohan Payan for having believed in me since the very beginning. He has been a great and competent advisor always giving me valuable support and suggestions through the development of the thesis. I appreciate in particular his friendly mood that always accompanies his personality.

I also want to thank my co-supervisors Mathieu Bailet and Antoine Perrier for their complementary knowledge and suggestions that helped me especially in the beginning of my project.

I would like to express my appreciation to my friend and colleague Ekaterina Mukhina for all the funny moments that accompanied our moments in the lab.

I would finally thank my mother Viviana Zinetti and my father Gianfranco Trebbi that always supported me in my life decisions allowing me to study and travel making me become the man that I am today.

Table of contents

List of publications

Journal articles

1. **Alessio Trebbi**, Antoine Perrier, Mathieu Bailet, Yohan Payan. **MR-compatible loading device for assessment of heel pad internal tissue.**
   Medical Engineering and Physics, Volume 98, December 2021, Pages 125-132.
   Impact factor: 2.356
2. **Alessio Trebbi**, Ekaterina Mukhina, Pierre-Yves Rohan, Nathanaël Connesson, Mathieu Bailet, Antoine Perrier, Yohan Payan. **MR-based quantitative measurement of human soft tissue internal strains for pressure ulcer prevention**
   Medical Engineering and Physics, Volume 108, October 2022, 103888.
   Impact factor: 2.356
3. **Alessio Trebbi,** Nolwenn Fougeron, Yohan Payan. **Definition and evaluation of a finite element model of the human heel for diabetic foot ulcer prevention under shearing loads**
   Journal of Biomechanics 2022 (submitted).
   Impact factor: 2.789
4. Ekaterina Mukhina, **Alessio Trebbi**, Pierre-Yves Rohan, Nathanaël Connesson, Yohan Payan. **Definition and evaluation of a finite element model of the human heel for diabetic foot ulcer prevention under shearing loads**
   Journal of Tissue Viability 2022 (in press).
   Impact factor: 3.374

International conferences

1. **Alessio Trebbi**, Antoine Perrier, Mathieu Bailet, Yohan Payan. **Tissue internal strains computed by a finite element model of the human heel and measured from MR images.**
   European Society Biomechanics. Porto 2022
2. **Alessio Trebbi**, Antoine Perrier, Mathieu Bailet, Yohan Payan. **Development of a finite element model for the heterogeneous structure of the calcaneal foot pad to study its loading distribution. Insights for stress-related injuries.**
   European Pressure Ulcer Advisory Panel. 2021. Virtual meeting 2021
3. **Alessio Trebbi**, Antoine Perrier, Mathieu Bailet, Yohan Payan. **Strain Calculation from MR Image Registration An Application for Foot Pressure Ulcer Prevention**
   European Pressure Ulcer Advisory Panel. Virtual meeting 2021

4. **Alessio Trebbi**, Bethany Keenan, Mathieu Bailet, Antoine Perrier, Yohan Payan. **Human heel internal tissue displacements and strains calculated from Magnetic Resonance Images**
   European Pressure Ulcer Advisory Panel. Prague 2022
5. **Alessio Trebbi**, Bethany Keenan, Yohan Payan. **Heel Internal Tissue Displacements and Strains Calculated from Magnetic Resonance Images**
   BioMedEng. London 2022

List of figures

List of tables

List of abbreviations

FE – Finite element modeling

PU – Pressure ulcer

MR – Magnetic resonance

IR – Image registration

DVC – Digital volume correlation

1. Chapter 1

General Introduction

The following chapter will give a brief overview on the themes that will be discussed in this thesis. Initially the problem of pressure ulcers on the diabetic foot is described. This involves the aetiology and the currently implemented solutions to prevent this type of injuries. A specific attention will be given to FE modeling and its current methodologies of evaluation as this will be the main goal of this thesis. Finally, the outline of the thesis will be given with a description of the content of each of the following chapters.

The thesis is composed by an initial literature review about the analyzed topic. Subsequently three sequential studies strongly connected within each other are proposed. Each chapter will present one of these studies. The chapters are presented in the format of a scientific journal article to facilitate the reader in the comprehension of the text (introduction, methods, results, discussion, conclusion).

1.1. The etiology of PU and the dramatic consequences of high mechanical strains.

Constant mechanical loading on the skin surface can lead to soft tissue damage or ulceration. In fact, normal pressure and frictional shear forces can cause deformation and injury to the internal soft tissues, in particular over bony prominences. Pressure ulcers are a relevant problem that has still not been fully solved at a significant level, therefore the development of new strategies for prevention is required. The aetiology of pressure ulcers is complex, considered to involve many different biomechanical, physiological, and biochemical processes [1]. It is assumed that ischemia, impaired lymphatic drainage, reperfusion and sustained deformation of cells may play a crucial role [2][3]. However, sustained mechanical loading is believed to be the main crucial cause of pressure ulcers. For this reason, we will focus in this thesis on the biomechanical factors that lead to tissue damage without considering multi-physic or multi-scale approach [4].

In order to prevent pressure ulcers, healthcare professionals should be able to predict whether a certain state of mechanical loading would produce high strains in the tissues generating irreversible damage [5][6]. Currently, there is no *in vivo* biomarker that allows to observe (in an ergonomic embedded way) the levels of these high strains. Researchers have therefore proposed to build subject-specific FE models to use "numerical mechanical biomarkers" with the computation of max shear strains and compressive strains [ref [114] Ceelen et al. 2008]. To be accepted by clinicians, such models should be evaluated (and ideally validated) with comparisons with real data collected on subjects. Many physical entities could be used for such comparisons such as interface pressures or foot global deformations. However, a full validation of the models should be based on *in vivo* internal strains since these entities are considered the goal measurement of interest in terms of pressure ulcer prevention.

1.2. Finite element modeling

FE modeling is a widely used computational technique for estimating internal stress, strain and deformation under specific boundary conditions. This tool can therefore be used to predict damage where the computed strains exceed related thresholds [7].

Medical imaging can provide accurate, patient-specific details of the anatomical geometry of the considered body part. The obtained surfaces are meshed and assigned material properties, boundary conditions and external loads. Simulations are finally performed in a non-linear FE solver to assess the behavior of the tissues under the considered boundary conditions [8].

Measuring the mechanical properties of soft tissues is a complex task. There are indeed many variables involved generating many potential errors and uncertainties in proposing the constitutive models.
Published data is therefore often subject to large and unknown uncertainties. Due to the complex structure and unusual properties of soft tissues of the heel, it is difficult to generate an FE model that accurately simulate the mechanical behavior.

1.3. Validations

It is considered that further work is needed to develop models that are sufficiently robust and properly validated to draw reliable clinical conclusions. Although the studies that have been published to date demonstrate the potential of FE modeling and show some interesting preliminary conclusions, in general they all have limitations in their validations against independent experimental measurements. Indirect validation (data from existing literature) is commonly used to compare the contact pressure and stress/strain behavior [9]. However, since the published studies share the same limitations, this does not provide any actual validation of the results.
Additionally, many have significant limitations in relation to the implementation of generic "soft tissue" properties, instead of correctly modeling the subject-specific tissues. As computational models involve complex procedures for their definition, a consistent and robust methodology for model validation through rigorous experimental measurements is required [10].
Medical Resonance (MR) imaging now offers the possibility to analyze the tissue internally; it permits therefore to observe tissue deformations due to any external load. In particular, Digital Volume Correlation (DVC) based on the non-rigid registration between two MR images (one with the tissue at rest and the other one with tissue deformed) can be used to measure *in vivo* tissue strains. This provides therefore a way to validate computational models.

1.4. Aim of this thesis

The main goal of this thesis is to develop a methodology to evaluate finite element models of the human heel for diabetic foot ulcer prevention. To this respect, a sequence of sub-goals are defined.
The first sub-goal goal is to design an MR experiment that will provide a complete dataset for the generation and the evaluation of an FE model of the heel. This experiment will provide the *in vivo* response in terms of deformations of the soft tissues under a known load. All the important anatomical structures

involved (skin, fat, muscle, tendon) will be included in order to generate the geometry of a subject specific model of the heel.

The second sub-goal will focus on the definition of a methodology to measure internal strains from non-rigid image registration. To this respect, the MR image acquired with the foot in a rest position will be registered with MR images of the deformed foot. Different operations using image transformations and artificial images will be used to validate this methodology.

The third sub-goal aims to build and evaluate a novel FE model of the heel. The geometry and boundary conditions will be obtained from the MR experiment performed for the first sub-goal. The constitutive behaviors will be defined by curve fitting hyper-elastic laws from published experimental tensile and compression tests. The simulations provided by the FE model will finally be evaluated by comparisons with the results obtained in the second sub-goal. To this respect, the strains magnitude and locations predicted by the FE model will be compared with the strains measured from the MR experiment.

1.5. Outline of this thesis

This paragraph will describe the content of each chapter (Figure 1).

The second chapter of this thesis will focus on a literature review on the etiology of pressure ulcers and how computational modeling can provide insights in their prevention. The second part of this chapter will provide a literature review of the current adopted techniques for biomechanical modeling of the human heel and their limitations.

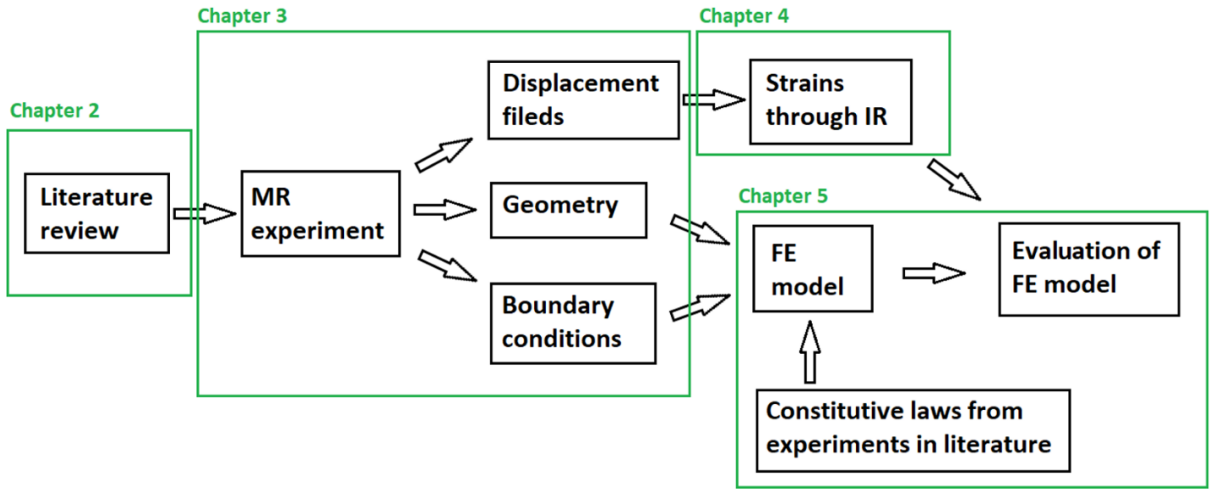

Figure 1: General overview of this thesis. The current chapter 1, introduction, and chapter 6, conclusion, are not represented.

The third chapter will describe the design of an MR-compatible device for the application of shearing and normal loads on the human heel. Magnetic resonance imaging is a key feature that allows to monitor deformations of soft tissues after loading in a non-invasive way. Measuring applied forces in an MR-environment is challenging due to the impossibility to use magnetic materials. In the device we will develop, forces are applied through the compression of springs made of polylactide. Shearing and normal loads were applied on the plantar skin of the human heel through a flat plate while acquiring MR images. The device materials did not introduce any imaging artifact and allowed for high quality MR deformation measurements of the internal components of the heel. The obtained subject-specific results are an original data set that can be used in validations for Finite Element analysis and therefore contribute to a better understanding of the factors involved in pressure ulcer development.

The fourth chapter will propose an *in vivo* solution to measure internal strains based on the 3D non-rigid registration between two Magnetic Resonance (MR) images, one in an unloaded configuration and the other deformed by means of the plate. From the results of the image registration, the displacements field and subsequent strains maps for heel soft tissues will be computed. An extensive study, considering different cases (on heel pad but also on sacrum regions, in collaboration with my colleague Ekaterina Mukhina), will be performed to evaluate the reproducibility and trueness of the results obtained with this methodology. The implemented technique gives insight for several applications. It adds a useful tool for better understanding the propagation of deformations in the heel soft tissues that could generate pressure ulcers. This methodology can be used to obtain data on the material properties of the soft tissues to define constitutive laws for FE simulations and finally it offers a promising technique for evaluating FE models.

The fifth chapter will propose and validate an FE model of the heel for diabetic foot ulcer prevention. Constitutive laws and parameters are defined through curve fitting experiments found in the literature of the respective tissues. The model will then be validated by using a digital volume correlation methodology implementing image registration from MR images. For an additional evaluation, different sets of constitutive models found in the literature will be into the proposed FE mesh and simulated with equal boundary conditions, in order to compare their influence on the numerical results.

Finally, a conclusion will resume the implications relative to the findings of this thesis and reflect on the current state of finite element modeling of the human body.

2. Chapter 2

Biomechanical modeling of the heel for the diabetic foot pressure ulcer prevention: a review

In this chapter a review of the biomechanical modeling of the human heel for prevention of diabetic foot pressure ulcers is presented. Initially, the aetiology of pressure ulcer is described and the cascade of events that originate these injuries are described. The impact that this issue has on society and the importance of new solutions for prevention is expressed. The focus is then given to the biomarkers that are considered crucial to detect dangerous regions where pressure ulcers could occur. FE models that aim to quantify these biomarkers proposed in literature are then presented. A particular emphasis will be given in the techniques used to evaluate these kinds of models. Finally, the new possible lines of further investigations resulting from our analysis are listed.

2.1. Costs of pressure ulcers

Pressure ulcers are delimited regions of tissue breakdown in skin and/or underlying tissues [11]. Typically, they can occur in general situations in which people are exposed to sustained mechanical loads, however they are especially common in patients who are bedridden, using a prosthesis or orthosis, or wheelchair bond. Ulcers are hard to treat, painful and represent a serious issue in terms of health care and money. As a result, they can affect the quality of life of both elderly and young individuals [12].

Nowadays two-fifth of the patients being taken in charge by a reanimation or a geriatric unit will eventually develop a pressure ulcer. Within these, 40% will be located on the posterior side of the heel, mostly because patients stay for hours lying in a supine positon without moving [13]. This condition, in the worst case, can require an amputation of the foot. In 2007, in the US, the cost of pressure ulcers was estimated to be 48 billion USD and the survival rate after 5 years was only 50% following a foot amputation [14][15]. In the United Kingdom, the cost of healing a pressure ulcers varies from 1,214 to 14,108 pounds with the overall daily costs in the region of £1.4 million [16]. Global pressure ulcers prevalence rates can vary considerably across regions and clinical settings, with the UK considered to have the highest point prevalence of 26.70% in a recent systematic review [17]. Pressure ulcers management is therefore a considerable problem that still has to be fully addressed. The development of new intervention strategies to prevent pressure ulcers prevention seems thus required.

2.2. Aetiology of pressure ulcers

The etiology of pressure ulcers can follow mainly two different processes: they can develop either superficially or from within the deep tissue, depending on the biomechanics of the loading. The first category develops on the skin layer and is mainly caused by shear stresses applied on the skin surface. If not promptly treated, this initial irritation may form an ulcer, which can be easily detected by scanning visually the skin [18][19] (Figure 2).

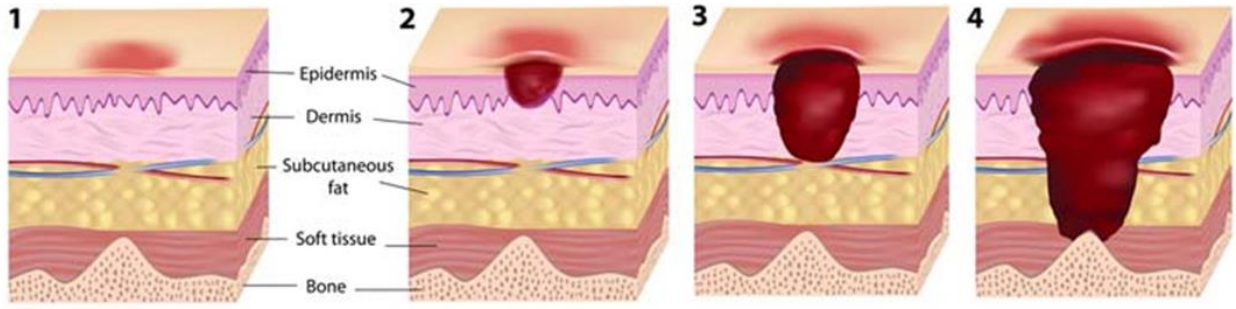

Figure 2: *Stages of superficial pressure ulcers. Initially the skin starts irritating as a result of an applied load. If not promptly treated, the skin tissues start being subject to permanent damage that keeps growing towards the deeper tissues.*

Alternatively, deep ulcers originate on deep muscle and fat layers that surround bony prominences and are mainly caused by sustained compression of the tissue [20][21][22]. This type of pressure injury is very serious, as it develops faster than the superficial ulcers and easily affects a larger portion of biological tissue [23]. Subsequently, the damage starts to increase in volume and affect portions of muscle, adipose, and subcutaneous tissues while only minor signs of tissue breakdown are shown on the skin surface. Therefore, the signs that could lead to an early diagnosis of the most severe ulcers are buried in the deep tissues making them hard to identify with a simple visual scan. This strongly delays clinical interventions and easily aggravates the outcomes [2] (Figure 3).

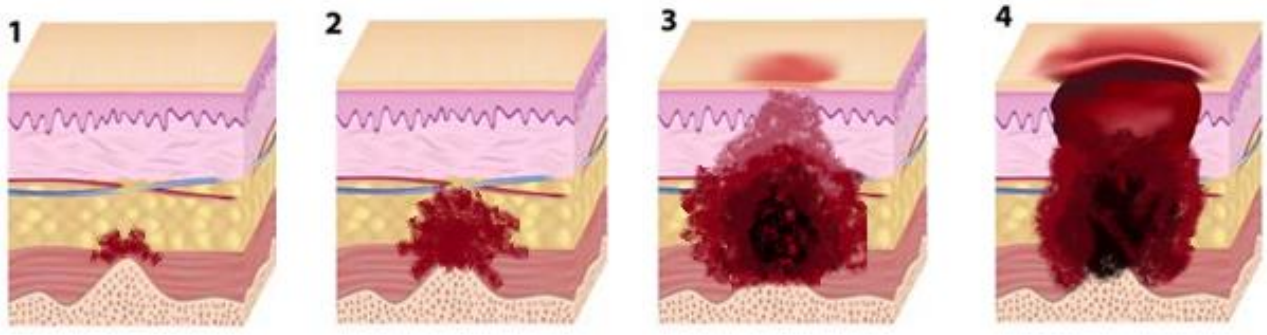

Figure 3: *Stages of deep pressure ulcers. An external load is applied on the skin surface that creates a high stress on the soft tissues that bound a bony prominence. A portion of deep internal tissue is therefore subject to damage. The necrosis keeps growing and the injury is only visible when a significant part of tissue is already damaged.*

Initially, pressure ulcers were assumed to mainly result from prolonged ischemia [20][24]. In accordance, when external loads are high enough to occlude blood vessels, cells start to experience shortage of oxygen and harmful waste products accumulate in the surrounding area. This will indeed cause cell death. Additionally impaired interstitial fluid and lymphatic drainage can contribute in the generation of an hostile environment for cells [25]. Finally, reperfusion might aggravate the circumstances when the blood flow is restored [26]. However all these effects do not fully explain why in some cases severe wounds can develop much faster than the usual time for cell death related to the deficiency of oxygen [27]. This can be addressed considering the impact of "direct deformation damage" that occurs when the threshold for deformation damage exceeds the normal physiological values and originates cell death by mechanical strains. These unusual high values have been reported in studies related to sitting [28], lying on a stiff surface [29] or because of irregularities as seams and folding in clothes or bed sheets, or even due to interventional medical devices.

2.3. Strain as a danger index

It is nowadays well known that pressure ulcers are mainly caused by sustained mechanical loading applied on the body soft tissues. However, the prevention of these kind of injuries remains difficult. This occurs partly because the underlying pathways whereby mechanical loading leads to tissue damage are still to be properly investigated. Specifically, it is not clear how external loading conditions transfer to localized stresses in the deep soft tissues and how these localized stresses in turn cause tissue break down. Researchers have been working on the most effective way of measuring pressures at the skin level with the objective to reduce them [30][12]. However, it is important to keep in mind that surface pressures are not representative of the internal mechanical loadings that develop in the deep soft tissues, which are actually the most crucial for pressure ulcer prevention. This has a particular impact when geometries are complex and different tissues with different mechanical properties are close to each other. In fact, these conditions may result in high inhomogeneous distributions of the superficial loadings. In order to address the response of internal tissues to mechanical loading, the specific mechanical environment within these layers has to be known. Additionally time and strain give an inversely proportional contribution to ulceration. In fact, higher strains around 40% will require a shorter time to cause tissue breakdown, in the order of a few minutes. On the other hand, lower strains around 20% will induce ulceration only after a constant application, from two to four hours [31]. Therefore, in addition to strain levels, it is crucial to consider the amount of time for which the load is applied. A possibility offered by computational

simulations consists in calculating the transition from superficial external loads to local internal stresses [32][33]. These models may in fact provide a better understanding of the tissue layers mechanical conditions from the superficial skin down to ones proximal to bone prominences. Additionally, experimental research will have to be conducted in parallel in order to provide insight on how internal stresses lead to tissue breakdown.

2.4. Ulcer location

Hospital patients who have limited moving abilities have in general a higher risk of developing a pressure ulcer. In fact, lying on a bed or sitting on a wheelchair, without changing position for a long time, will generate constant pressures on specific body parts that become the starting point of a pressure ulcer. According to the position of the body, the areas subject to loads may vary, however there are specific regions that have a relatively higher risk: sacrum and heels (Figure 4).

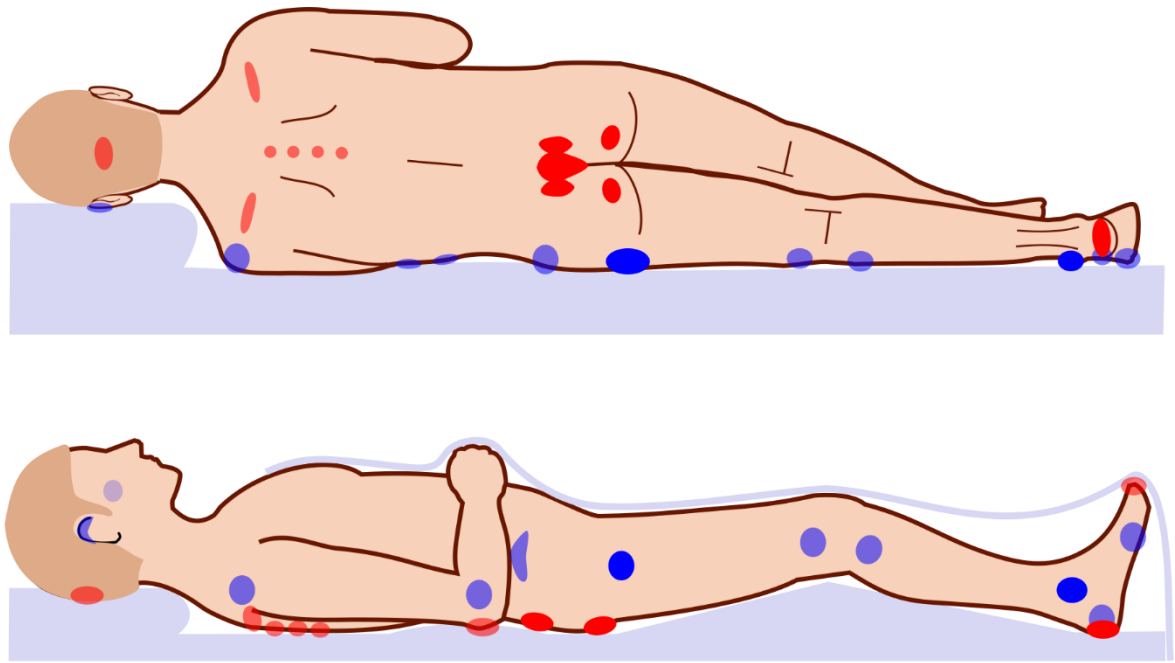

Figure 4: *Body locations where pressure ulcers are more likely to develop and the respective body positions that can cause them. Red: In supine position. Blue: in side-lying position (Image from Wikimedia).*

In the case a hospital patient had developed a pressure ulcer, this ulcer will be located on the sacrum for 28.6% of all cases, and on the heel for 26.0% of the cases. Also ischium, ankle, elbow and hip have relative higher prevalences being each around 10% [34]. Many researchers have implemented finite element analysis to understand how the loads generated by lying in different configurations lead to deep internal stresses [35][36][37][33]. Despite being the second most common type of pressure ulcers, heel ulcers are considerably understudied compared to the rest of the ulcer literature, having a relative low number of groups actively investigating in this area [8][32][33]. As a consequence, additional research towards heel ulcer prevention should be performed.

2.5. Heel Ulcers

Ulcers are among the most severe pathologies that can develop on the human heel. Bone removal is a required procedure from 15% to 27% of all ulceration cases [38]. Heel ulcers can be divided into two categories: plantar or posterior. The main difference relies on the source of high sustained load and indeed in the location of the application. The first category corresponds to high loads resulting from standing and locomotion applied on the lower part of the heel. Accounting for ulcer development in the complete plantar region of the foot, the plantar heel and the hallux, respectively 21% and 40%, are the regions with the highest incidences [39].

Posterior heel ulcers develop mainly in patients that are required to lay on their back for hours without having the possibility to change position [13]. This condition will generate a permanent load on the posterior part of the heel that can be the starting point of an ulcer. The main causes of posterior foot ulcers are considered to be elevated plantar pressures, foot skeletal deformities, peripheral neuropathy, and peripheral vascular disease [40][41]. Load tolerance has been shown to vary significantly with anatomical location. Some areas, such as the posterior part of the heel, are highly vulnerable to injuries [34]. On the contrary, the plantar region has evolved to tolerate routine surface pressures of more than 1000 kPa [42]. Plantar skin has a specific composition and morphology, and it is hypothesized that these features enhance its load tolerances [43]. According to the morphology, the stratum corneum is much thicker in plantar skin; moreover plantar epidermis has a unique cytoskeletal profile that is believed to enhance the load tolerance [44]. Fitting high-risk patients with specific dressings or shoes to reduce loads can help in ulcer prevention [45]. However, no definitive injury strain threshold can be accounted for a systematic prediction of heel ulcer formation [46]. Collagen changes induced by hyperglycemia can result in stiffening the plantar fat pad and leading to an increase of internal stresses close to the bony prominences [47].

Therefore, severe pressure ulcers can begin in deep, subdermal, tissue layers [48]. This, combined with neuropathy, makes this pathology hard to detect, and when the first actual symptoms appear, serious complications are already present. In order to understand the modeling challenges that have to be overcome to consistently simulate the biomechanics of the heel, it is crucial to have a clear overview of the heel anatomy and histology.

2.6. Diabetic foot ulcers

Ulceration of the diabetic foot is another common disease. The main difference with posterior heel ulcers are the causes that generate them. In this case, the peripheral neuropathy of diabetes results in abnormal forces being applied to the foot [49]. This can be caused by improper shoe wearing, constant applied excessive loads, unnatural repetitive strains generated by an improper gait. Additionally, diabetic ischemia renders the skin less able to withstand these high loads. Other complications contributing to ulceration development include limited possibility to visually scan the related region, limited joint mobility, and the consequences of cardiovascular and cerebrovascular disease [50]. However, the most common precipitant is ill-fitting footwear. The regions of the foot that are more frequently subject to such ulcerations are the heel, forefoot and toes.

Diabetic foot ulcers are disabling and frequently lead to amputation of the leg as healed ulcers often recur [51]. The pathological processes are difficult to be understood and therefore poorly taught. The communication between most specialties involved can then be disjointed and insensitive to the needs of patients.

In this thesis we will specifically focus on these type of ulcers that occur in the heel plantar region.

2.7. Heel anatomy and histology

The central structure that constitutes the heel around which all the biomechanical forces are exchanged is the calcaneus. This bone is inserted between the talus and the cuboid bones and is attached to the ligament of the plantar fascia and the Achilles tendon, two crucial structures in foot biomechanics (Figure 5).

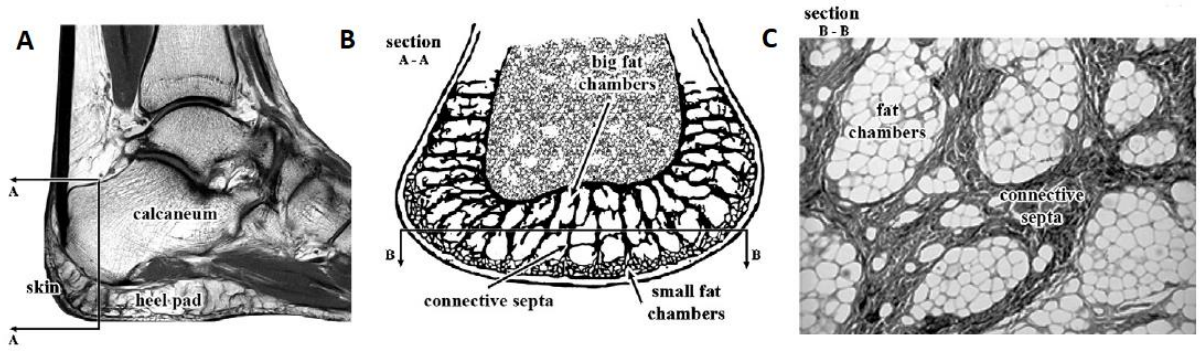

Figure 5: A) Sagittal view of an *MRI of the heel where it is possible to see the heterogeneous structure on the heel pad that surrounds the calcaneus. B) Section on the coronal plane to illustrate the distribution of the fat chambers in the heel pad. C) The composition of the fat chamber made by fully grown adipocytes. The fat chambers are included in the fibrous septa structure. Image taken from Natali et al.* [52].

The redistribution of plantar pressures is to some extent performed by the heel fat pad, a complex structure of connective and adipose tissues situated in the lateral and lower side of the calcaneus bone. These two biological tissues are arranged in a honeycomb configuration where fibrous septa envelop the adipose chambers [53]. The fibrous septa provide structural integrity by constraining the deformations of adipose chambers and are mainly composed of collagen and elastin. This three-dimensional structural net is anchored from the plantar aponeurosis and the calcaneus and extends until the dermis. The walls and columns of fibrous septa are also reinforced internally with a composition of diagonal and transverse elastic fibers that connect the internal structure of the fat chambers [54]. The adipose tissue determines the bearing properties acting precisely as a pad between the calcaneus and the ground. The integrity and the correct ratio of both the fibrous septa and fat chambers are mandatory requirements for the proper functionality of the plantar fat pad [55]. Wang et al. measured that connective septate has a thickness of 151 ± 56 µm in healthy subjects and 270 ± 61 µm in diabetic patients [56]. Natali et al. reported a thickness of 1800 µm in big fat chambers and 400 µm for the smaller ones [57]. The fat chambers connecting directly with the internal part of the dermis are relatively smaller than the ones loaded deeply close to the calcaneus. Therefore, the heel pad is anatomically divided into a superficial layer of micro-chambers and an internal one of macro-chambers [55] (Figure 5B).

Natali et al. reported fat chambers to range from 1000 to 5000 µm in diameter in heathy subjects [57]. Fat chambers are filled with adipocytes with a diameter from 100 to 200 µm [58]. Wang et al. measured a minimum adipocyte diameter of 40.7 ± 5.6 µm in healthy condition and 45.0 ± 4.9 µm in diabetic subjects [56] (see Figure 5C for a picture of adipocytes inside fat chambers).

Finally, the skin binds up the calcaneal pad and constitutes an important element on the deformations derived by the application of external loads [59]. Plantar skin thickness is assumed to range from 1815 ± 668 μm in healthy subjects and 2056 ± 662 μm in diabetic conditions [56]. The ratio between the connective septa and the adipose chambers can be altered by degenerative phenomena as pathologies, trauma, or aging. These situations can cause an increase in the thickness of the connective septa, rupture of the elastin fibers, and fragmentation of collagen bundles [60].

In order to develop computational models able to simulate the described tissues, it is fundamental to measure their mechanical properties in order to propose realistic constitutive materials. To this purpose, various experiments on the heel tissues have been performed ; they are discussed in the next section.

2.8. Heel Experiments

The experiments that have been performed to gain insight on the mechanical properties of the heel soft tissues can be divided into two main categories *ex vivo* and *in vivo*. *Ex vivo* mechanical properties identification are performed on cadavers experiments where a specific tissue type can be investigated independently of each other. However, it is clear that for a clinical implementation, patient-specific *in vivo* noninvasive experiments are required. Therefore, it is important to develop a testing protocol that is able to give enough information to identify the required mechanical properties of the analyzed tissues.

2.8.1. *In Vivo* Compression Tests

The most common *in vivo* experiment performed on the calcaneal pad consists in generating mechanical loading by means of an indenter applied on the plantar region of the heel. This application requires the design of a loading device that is capable of holding the foot in a fixed position and applying a controlled deformation while measuring the resulting load, or vice versa. This measurement combination is done in order to plot the characteristic load/displacement curve that is the base for constitutive analysis of the soft tissues. For these purposes, several devices have already been designed for the plantar region of the foot. Fontanella et al. developed a device that uses a stepper motor for actuation and position measurements while the forces are measured by a load cell and the foot is fixed by Velcro straps [61]. Hsu et al. additionally implemented an ultrasound transducer to monitor the thickness of the layers of adipose micro-chambers and macro-chambers [55] (Figure 6).

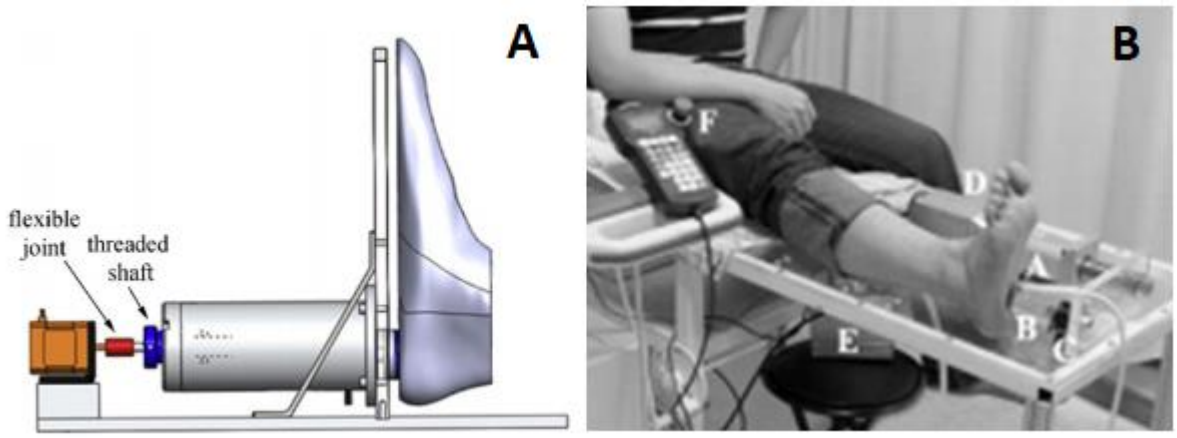

Figure 6: *Loading devices respectively designed by Fontanella et al. (A)* [61] *and Hsu et al. (B)* [55].

In order to obtain a complete vision of the displacement of the internal tissues, MRI compatible devices have also been developed. This solution, however, introduces the additional challenge of limiting the selection of materials for the device to only the ones that do not interfere with the magnetic fields of the MR machine [62][63]. Williams et al. solved this challenge by using a hydraulic piston to apply the loading and keeping the pump far from the magnetic fields [64]. Gefen et al. implemented an additional solution to measure loading in a MRI environment by using an optical sandwich [65] (Figure 7).

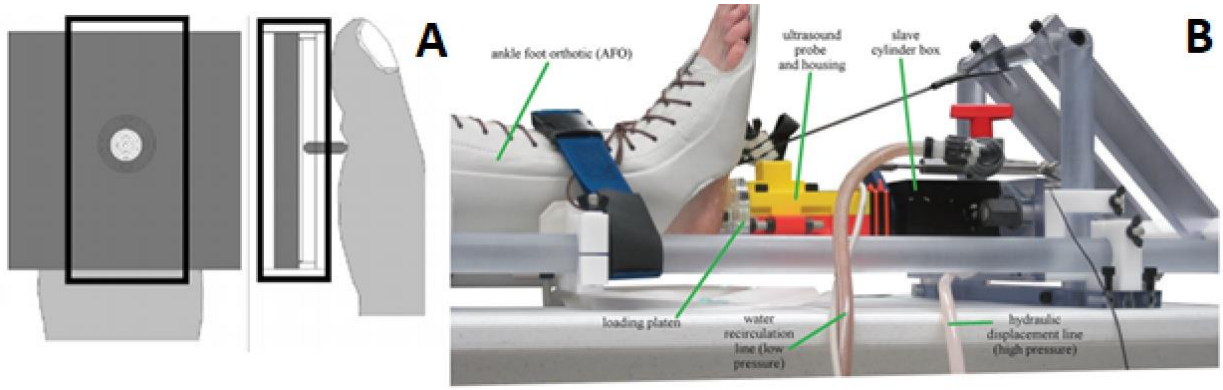

Figure 7: *Loading devices respectively designed by Gefen et al. (A)* [65] *Williams et al. (B)* [64].

Experiments vary in terms of the geometry of the indenter. Some researchers have used cylindrical indenters with their vertical axis aligned with the longitudinal axis of the foot and centred on the lower part of the calcaneus [66][67].

In general, these types of compression tests displayed a nonlinear load-deformation behavior with an initial compliant region and subsequently, with an increase of force, a stiffer one. Williams et al. shown

that a subject with diabetes, had stiffer tissues than a healthy subject. In particular, for similar strains, the heel pad stiffness was between 1.73 and 3.46 times stiffer [68]. This demonstrates how mechanical properties of soft tissues can strongly vary between subjects and also how pathologies can affect them.

2.8.2. *Ex vivo* Experiments

Cadaveric experiments allow for more specific tests that would not be feasible on living subjects. In fact, studies performed on living subjects can only give the structural properties of the calcaneal pad, and getting information for the different soft tissues is challenging. A common technique, in order to analyze specifically the adipose and connective tissue of the fat pad, is to extract some cylindrical samples of heel pad tissue to perform static and dynamic experiments. Miller-Young et al. performed three different types of tests in order to analyze various material properties [69]. Cylindrical samples with a diameter of 8mm were extracted from different areas of the plantar heel and compressed between stainless steel platers to minimize friction. These results were then used by the authors to estimate the parameters of assumed constitutive models of the tissue. The parameters and the type of constitutive equations will be described in the paragraph *tissue models*.

2.8.3. Gait Experiments

In order to characterize the heel pad during its normal functions, walking experiments were performed in the literature. In relation to these kinds of tests, the energy absorbing properties of the calcaneal pad are of particular interest. This function of the heel pad is in fact fundamental for the impact attenuation during the stance phase of gait and the preservation of the skeletal structure of the foot. For this application, a device to measure ground reaction forces is combined with an imaging system. Such a system is often based on digital radiographic fluoroscopy. This technique uses X-rays to obtain real-time moving 2D images of the interior of the human body. For measuring the ground reaction forces a mat with pressure sensors is often used. Gefen et al. were one of the firsts to implement this experimental configuration and found an energy dissipation during heel strike of 17.8±0.8% [70]. Subsequently Wearing at al. performed an experiment in similar configuration where the properties of a healthy heel pad were compared with the ones of a heel affected by pain. It was found that the fat pad of symptomatic feet had a lower energy dissipation ratio of 55±17% versus the 69±8% of the asymptomatic one [71].

2.8.4. Elastography

A completely different technique to gain insight in stiffness parameters of the internal biological tissues is MR elastography. This solution combines MR image acquisition with a source of vibration that generates internal tissue displacements. Synchronizing the sampling rate of the MR with the frequency of the vibration, it is possible to obtain the image of the displaced tissues from the loads generated by the source of vibration. Weaver et al. used harmonic waves to find the difference of shear modulus between an unloaded fat pad and a loaded one. The shear modulus increased from 8 kPa to 12 kPa in the transition from the unloaded to the loaded configuration [72]. Another similar experiment was carried out by Cheung et al. this time comparing the elastic modulus between a healthy and a diabetic group. MR elastography was able to capture a small difference between the two groups measuring 4.85 kPa and 5.26 kPa for the healthy and diabetic group respectively [73].

2.9. Tissue models

Experiments applied on biological soft tissues show that they have a strong nonlinear behavior and are capable of large deformations. They are therefore often considered to have hyperelastic properties. Such tissues can also demonstrate a time dependent-nature as a viscoelastic property and additionally have a large variance in properties as a matter of inter-subject variability, sexual differentiation and age dependency. Luboz et al. showed how relatively small changes in the soft tissues stiffness can generate strain variations up to 50% within the same loading conditions [74]. In particular it was demonstrated that fat and muscle stiffness have an important influence on the strain variations, while skin stiffness is less influential. The authors showed also that tissue thickness can influence the results in a significant way. This demonstrates the dependence of the obtained numerical simulations from chosen material properties and subject-specific geometric model. Therefore, it is crucial to use subject-specific material properties and geometries when available.

The following paragraphs will describe the common constitutive laws implemented in the literature for simulating the mechanical properties of the heel biological tissues.

2.9.1. Hard Tissues

Biological tissues are divided in two categories: soft and hard. The difference is given by the existence of an inorganic phase. This mineral component makes bones stiffer of at least three orders of magnitudes than the other soft tissues. Bones are therefore often modeled as linear elastic, isotropic materials (with, for example, an elastic moduli of 7 GPa and a Poisson's ratio of 0.3 [67][33]). However, in applications where bone deformation is minimal, as a matter of the low loadings, or irrelevant as the focus is on soft tissues stress and strains, the geometry of skeletal structures becomes far more important than their actual mechanical properties. Therefore, some researchers model bones as rigid bodies in order to reduce the computational cost in simulations [75][76]. Two tendons are attached on the calcaneus bone: the Achilles tendon, and the aponeurosis (Figure 8).

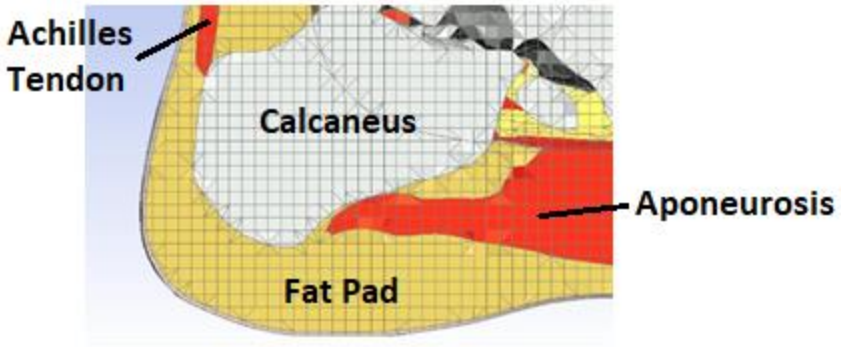

Figure 8: *Computational model of the heel where is shown the internal division of the different materials composing the heel.*

In general these types of tissues have a special importance in studies that focus on the complete foot biomechanics, as such tendons play a fundamental role in gait and the structural integrity of the foot bones. This is the case of the musculoskeletal foot model developed by Perrier *et al.* where accurate simulation of tendons and muscular activation is fundamental for dynamic biomechanical evaluations [77]. In this case, ligaments are modeled as linear elastic materials with a stiffness of 395 MPa. On the other hand, considering the additional computational costs that such structures require, with specific materials and boundary conditions, many researchers prefer to merge these tissues with the surrounding materials [33].

2.9.2. Soft Tissues

Soft tissues of the heel mostly include skin, fat, and muscles. According to the objective of the research intended to develop, there is the possibility to define a homogenous structure to simulate the combined mechanical behavior of different soft tissues together. Chokhandre *et al.* developed an FE model of the human heel merging all soft tissue in a single structure [77]. Gu *et al.* focused on the skin of the heel to address the early detection of superficial heel pressure ulcers [78]. To do so, the skin was modeled as a separate material from the rest of the soft tissues, while the fat and the muscle were considered to be a unique structure. The solution of combining different soft tissues together simplifies the model and reduces computational times for simulations. The tradeoff concerns the loss of information regarding the exchange of stresses in the interfaces between the merged materials. Studies that are interested in the internal layers of the human heel must define different constitutive materials representing skin, muscle and fat. Many numerical approaches have been provided based on *in vivo* and *ex vivo* test data. For the mechanical properties of biological soft tissues, the constitutive equations that were proposed to model rubber materials are often used. These materials have indeed similar properties to the biological tissue as they are hyperelastic and quasi-incompressible. Among the most commonly used constitutive laws is the Ogden material model, which is quite complex in its original form since based on a power law development, but can be simplified with specific values of its parameters. Other constitutive models such as Neo-Hookean, Mooney-Rivlin or Yeoh materials assume a polynomial form of the Energy fuction [79]. The differences between these laws are based on the number of parameters and the achievable curves of stress-strain relationships. In general, the lower is the amount of parameters to tune and the easier will be the process of optimization and identification of their values. The Neo-Hookean model is one of the most commonly used to model plantar soft tissues [76][33] since it involves only two parameters (the shear modulus and the Poisson ratio)that can be easily estimated from commonly known material properties. Moreover, Neo-Hookean models give a faithful representation of biological soft tissues especially in compression which is usually the case regarding plantar soft tissues.

Hsu et al specifically studied the different functions of adipose and septa concluding that the macro-chamber layer responds to loading with large deformations while the micro-chamber layer has a higher degree of tissue stiffness [80].

One of the most detailed model of the heel pad was proposed by Fontanella *et al.* where the fat is defined by two different material structures representing the adipose chambers and the fibrous septa. Adipose

chambers were modeled as ellipsoids and are distributed in a hexagonal scheme inside a matrix that represents the connective septa [57] (Figure 9).

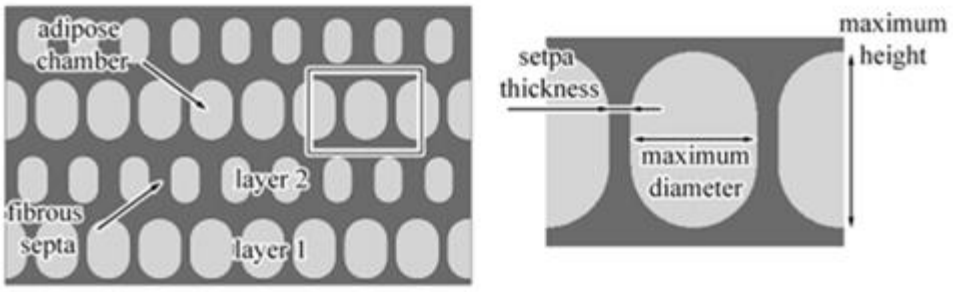

Figure 9: *The model structure presented by Fontanella et al. to simulate the fat pad structure. Fat chambers are represented as cylinders inserted in a matrix that models the fibrous septa. Image taken from Fontanella et al.* [57].

To simulate the pathological condition of diabetes, the model is used by thickening the connective layers, which causes the stiffening of the pad structure. In this case, an almost incompressible isotropic hyperelastic strain energy function is assumed for the adipose tissue. While for the fibrous septa a hyperelastic formulation is implemented which accounts for its fiber reinforced composite configuration.

2.10. Finite Element Heel Models

This paragraph starts with the description of the techniques currently used to define FE models of the heel and then focuses on the most relevant computational models developed in the last decade. In a second step, the evaluation methods and the implementation are described.

2.10.1. Heel Model Development

In the past decade, many models have been developed to understand the biomechanics of the human foot. However, few teams focused on modeling specifically all constituents of the human heel. We are going to refer extensively below to three research groups that developed 3D FE models of the heel region that differentiate from other models for specific peculiarities: the team of A.N. Natali from Padova, A. Gefen from Tel Aviv, and Y. Payan from Grenoble (Table 1).

Central article on Heel FEM	Fontanella 2016 [8]	Levy 2015 [33]	Luboz 2015 [32]
Imaging	CT	T1 weighted axial MRI	CT and MRI
Segmentation	Simlpleware [66]	Simpleware	AMIRA
Element type	Hexa	Tetra	Hexa
N elements		170 000	122 000
FE analysis	ABAQUS[81]	ABAQUS[82]	Artisynth
Area	plantar	posterior	posterior
Fat pad subcomponents	yes	no	no

Table 1: Comparison on the methods to generated the FE models of the heel by Fontanella et al. [8] Levy et al. [33] and Luboz et al. [32].

The generation of FE models of body parts starts with the definition of the geometry of the bones and soft tissues. This process is performed by the 3D segmentation of computer tomography (CT) or magnetic resonance (MR) imaging, which can be taken from pre-existing online libraries or obtained by scanned patients. Both techniques are currently used though CT scans are invasive exposing the patient to a small amount of radiation which suggests not acquiring several consecutive scans from the same subject. MR images provide a higher level of detail for soft tissues while CT scans faithfully outline the bone inside the body. The 3D surfaces are then generated by a segmentation process which implies the semi-automatic boundary definition from 2D slices of the acquisitions. Various commercial software can be used for this, the most common are AMIRA (Mercury Computer Systems Germany) or Simpleware (Simpleware Ltd., UK). The meshing procedure can be developed with specific software such as Hypermesh but generally, FE platforms also have their own meshing tools. Most of the biomechanical FE models implement a tetrahedral mesh since it's easier to generate as it adapts to the complex geometries of the biological tissues. On the other hand, hexahedral meshes are more complex to generate as it's hard to define good quality elements in highly irregular shapes. However models in hexahedral meshes are often preferred as they are considered more precise and less time consuming [83]. In addition, these hexahedral meshes don’t suffer from numerical locking that can occur in tetrahedral meshes when a quasi-incompressible behavior is assumed for the material.

In the case additional external geometries have to be included in the model, as dressing, footwears or indenters, solid modeling computer-aided design are used such as SOLIDWORKS (Dassault Systemes, SolidWorks Corp., USA). Finally, in relation to the meshing process and FE simulations, ABAQUS (ABAQUS Inc., Pawtucket, RI, USA) and ANSYS (ANSYS Inc., Canonsburg, PA, USA) are the most commonly used softwares. According to the type of application, platforms that combine multibody simulation with FE models, such as implemented by Artisynth [84], can be used. This solution is generally preferred when the model should involve muscle actuators and collisions, which often happens in modeling the whole human foot or joints like the ankle.

Generating geometries from medical imaging of a specific subject will, in fact, define a model of that specific person. This is useful for preliminary studies that are typically done on healthy subjects, however, for future clinical implementation of the model, the geometries have to be adapted to match the shapes of every single patient. Luboz *et al.* showed how the variation of the calcaneus shape between subjects can strongly impact the stress and strain distributions when the heel lies on a mattress [32]. To this aim, a patient-specific process to generate a numerical clone (or "digital twin") of the patient foot was proposed by Bucki et al [31]. This technique is based on a generic atlas model whose geometries can be adapted (through the tuning of some parameters) to the shapes of every single subject. This process of transformation from a general atlas model to one of a single patient is called non-rigid registration (or "Mesh Matching method", [85]. The registration is divided into three steps: rigid, affine, and local elastic registration. This solution avoids the tedious and time-consuming generation of a new patient mesh and can rapidly create a numerical clone for each patient.

A useful technique that is becoming popular in biomechanics is multiscale modeling. This solution involves the generation of several hierarchies in the structures of organs and tissues, from the macroscale of the human limbs down to the microscale of cells. The different scales are then linked to each other for the exchange of information such as forces and displacements [4]. This technique, therefore, could permit to extensively analyze the biomechanical behavior of single tissues of very specific areas of the fat pad (as the septa and adipose chambers) starting from a macro model of the whole heel. On the other hand, multiscale modeling can also be implemented starting from the stiffness evaluation of smaller scales and progressing to the overall stiffness of bigger bulk structures where all tissues are modeled together [81].

2.10.2. Model Validations and Applications

Regarding biomechanical models, there are currently two types of possible validations: direct and indirect validation. Regarding direct validation, an experiment is performed a posteriori specifically to evaluate the developed model. In this case, results from the model and the experiments are compared to verify if they match. On the other hand, in indirect validation, a comparison is performed between the model prediction and previous studies or experiments performed a priori, in which the settings of the experiments cannot be anymore controlled by the model developer [10].

The plantar heel model of the team of Natali was evaluated by an inverse analysis that compared the numerical model results with experimental data [81]. This procedure was divided into two stages: a first in vitro stage for preliminary constitutive parameter values, and a second in situ part, where the value of the parameters were updated. The *in vitro* section was based on a previous experiment performed by Miller-Young et al. where cylindrical samples of soft tissues of the heel were harvested from cadavers and mechanically tested [69]. The cylinder had a diameter of 8mm and contained only the tissues of the fat pad: adipose chambers and fibrous septa. By compressing the samples, the stress/strain relationship was measured. Natali then used a cost function to reduce the discrepancy between experimental data and results obtained from the analytical models. In order to consider interactions with surrounding tissues, structures, and geometries a second in situ inverse validation was performed. The procedure was similar to the initial one, by the implementation of a cost function, with the difference that a complete cadaveric heel was considered. The authors fixed the calcaneus and used an indenter to generate stress/strain relationships. The purpose of this work was to investigate the relationship between mechanical functionality and the structural configuration of the heel fat pad in healthy and degenerative phenomena. It was found that the loss of continuity of the fibrous component, and specific properties of degenerative septa, induce the increase in stress values, suggesting the distortion of heel functionality.

The posterior heel model of Gefen and colleagues was calibrated by directly reproducing a physical experiment with his computational model. In this application, the focus was on the posterior part of the heel [33]. The experiment consisted of lying the heel down with the patient in a supine position, measuring the contact pressure between the heel and rigid support, and acquiring MRI scans. The model was then evaluated by reproducing the same configuration and considering the difference in total soft tissue thickness (skin, fat, and tendon). The main objective of this work was to evaluate the biomechanical efficacy of heel dressing for prevention of pressure ulcers. The main result was that the peak strains

occurred in the subdermal fat adjacent to the bone-fat interface and that the use of a multilayer heel dressing consistently reduced the elevated strains in the soft tissues.

The model developed by Perrier from the team of Payan also adopted a direct validation that was performed with the complete foot model [77] and carried on for a static weight-bearing position. The experiment consisted in a subject standing on a mat with pressure sensors. The measured contact pressures were then compared with the simulated ones computed by applying on the tibia half of the subject weight. The main findings were that the geometry of the calcaneus has an influence in the formation of pressure ulcers with a mean variation of over 6.0 percentage points over 18 different subjects [32]. Another outcome was that the stiffness of the mattress on which the heel is lying has an influence on the development of pressure injuries. A softer support will generate lower internal strains and therefore will have less probability to develop pressure ulcers in the patient.

2.11. Heel model limitations and possible lines of investigation

This section analyzes the various challenges that are involved in the process of defining computation models of the human heel for clinical applications. As it was presented in the previous paragraphs, the results obtained by different research groups have a significant variance. This is detected from the very early stages of the anatomical and histological analysis up to the final results of the FE simulations. This suggests that a considerable progress has to be made before the computational simulations of the human heel can become a clinical tool for prevention of pressure ulcers and other foot pathologies. This section will focus on describing the discrepancies between the achieved results according to the related area of investigation of different research groups and proposes possible solutions and future steps.

2.11.1. Anatomy

Regarding the anatomy of the heel pad at a macro level, authors tend to agree on the morphology and the internal dimensions of bones and soft tissues (as fat muscles and skin) as MRI and CT scans offer optimal images of the internal heel parts. On the other hand, in a meso level, related to the dimension of fat chambers and septa thickness, literature is scarce and discordant. Wang *et al.* reported a septate thickness that is 10 times smaller than the one used by Natali et al. in their models [10]. This difference might be caused by the different locations from which the septa were measured as the macro-chambers area or the micro-chambers. Additionally, the dimension of the fat chambers is not clear and exhaustively addressed,

specifically the difference in their dimension between macrochambers and microchambers. Therefore, not enough information have been found to get a clear overview of the morphology of the fat pad sub-components.

2.11.2. Loading

According to the loading protocols, a variety of indenters has been used to generate soft tissue displacements in the calcaneal pad, such as cylindrical pistons, plates and ultrasound probes. The various geometries implemented generate different force/displacement responses, making hard to compare results of different experiments. Additionally, the foot positioning and the angulation of the applied pressure is often not clear and often varies between different studies. The definition of a standard foot position and a loading protocol to define geometry and pressure angulation could help for comparison of results obtained by different research groups.

The results from compression *in vivo* tests on the heel pad are often presented in terms of force/displacement, or stress/displacement assuming the contact area to be constant [86][87]. This is because the information about internal soft tissue displacements was scarce or absent. Additionally the biomechanical properties of the soft tissues would have been influenced by boundary conditions as confinement by the surrounding skin, the bony geometry, and friction with the ground. Therefore, the majority of studies that have been carried to examine the heel pad mechanical properties *in vivo* have measured only its structural properties, and not the parameters of the single tissues. MRI and CT scan can display 3D images of internal tissues; therefore a combination of these techniques with a loading device could allow obtaining stress/strain relations. This would permit for more specific analysis of the different roles played by the heel internal components.

An aspect that has not been investigated sufficiently is the application of shear loadings on the heel surface. Experiments have shown that the plantar surface of the foot experience a significant amount of shear loading during gait [88]. Also, lying on hospital beds can generate high amounts of shear due to friction between the skin and blankets [33]. It is also theorized that friction play a significant role in the development of pressure ulcers [89]. One study analyzed the deformations resulting from shear loading applied on the metatarsal part of the foot but applications on the heel are quite scarce [90].

2.11.3. Material properties

Biological tissues exhibit a complex non-linear and time dependent mechanical behavior; therefore, their modeling is inherently difficult. Moreover, biomechanical properties of soft tissues vary significantly between subjects, but also within the same person according to age and region of interest. Many reviewed studies used constitutive material found in the literature, even though the real challenge is being able to identify material properties on a patient specific base. Williams *et al.* showed that heel pad stiffness of a diabetic subject was between 1.73 and 3.46 times stiffer for similar strains than a healthy subject. Therefore, differences in biomechanical properties must be identified and taken into account when developing a computational model of the heel [68]. To be applicable on a clinical basis, *in vivo* testing techniques will have to be non-invasive and easy to perform, providing results that are robust and fast to get.

2.11.4. Modeling

Heel models have been implemented to simulate very different configurations. The most accurate and recent ones have focused on simulation of the heel of a patient lying on a hospital bed. This is the case of Levy *et al.* that modeled heel dressings to monitor shear loadings generated by frictions [33]. Luboz *et al.* simulated the strain configurations developed in the heel lying on mattresses with various stiffness [32]. However, up to this date, Fontanella *et al.* were one of the only ones that have ventured in the attempt of modeling the fat pad sub components using multiscale modeling [8]. This model however accounts for simplified and homogeneous geometrical conformation and properties of the pad. A more complex and irregular conformation of the sub-components could actually be a closer model of the reality. Additionally, the septa and adipose chambers were modeled in a meso scale, separated from the macro model of the heel. This assumption removes the possibility to simulate the interface between the septa and the surroundings of the fat pad as the calcaneus, skin and tendons. Interfaces between materials with different Young's moduli are known to create stress concentrations. In fact local regions experience stresses far higher than the global mean stress [91]. This demonstrates the importance of modeling separately the fat pad sub components as they have very different mechanical properties. This could in fact show much higher stress concentration that would not be detected with simpler models. In turn, being able to calculate these hidden stresses could give an important advantage in terms of pressure ulcer prevention. However, the tradeoff relies in the computational cost that this implementation would add in the

simulation. A possibility to overcome such additional computational cost relies into the use of peculiar modeling components such as shell elements or dimensionless springs.

The original concept of “strain clusters” for pressure ulcer prevention was presented by Bucki *et al.* [31]. The authors call “cluster” a group of adjacent elements that are subject to a strain that is above a specific selected threshold. This term is introduced for the analysis of the results from simulations to have a clearer understanding of the regions that could be the starting point of a pressure ulcer. In fact, monitoring only the maximum strains could be misleading as this solution is strongly influenced by the numerical “outliers”: singular strain concentrations due to the geometry of the mesh, which can be generated by FE when subject to high loads. On the other hand, strain clusters highlight areas where groups of elements are all under high strain, meaning that a relevant portion of tissue is in danger. The concept is relatively new, and therefore its implementation for pressure ulcer prevention is still scarce. Such a solution could give the possibility for new considerations in this aspects.

2.11.5. FEM Validations

As computational models become more sophisticated, a consistent and robust methodology for model validation through rigorous experimental measurements is requited [10]. Even if the prospect of using simulations in clinical applications seems giving encouraging results, caution must be exercised. Many studies that use FE analysis have not looked enough into establishing the validity of their methods via thorough experimentation. Instead, indirect validation (data from existing literature) is commonly used to compare the contact pressure and stress/strain results of specific tissues. Since all the published studies suffer from the same limitations, this does not provide any really meaningful validation of the results. New validation techniques are required in order to be confident that FE models can predict the risk of pressure injury. This could be done by comparison with medical imaging data or other experimental methods of measuring tissue strains.

2.12. Conclusion

Computational simulations are among the most promising techniques for pressure ulcer prevention. Therefore, the current process for the development of computational models of the human heel was presented. Emphasis was given to describe the challenges and the current techniques to perform each step required in the modeling process. In the last decade, the number of FE models for addressing pressure

ulcers on the heel region have strongly increased compared with the previous times. However, results are still not satisfactory and more investigation, especially in terms of validation, is required. The main objective of this thesis is to propose a new validation technique to evaluate FE models of the human heel. This technique will be used to evaluate existing FE models of the literature on one hand, and to propose a new set of constitutive properties that will best describe experimental data on the other hand.

Hopefully this work will provide a better understanding of how can FE models help to prevent pressure ulcers. This should allow for the development of concrete solutions implementable in a clinical environment. Next chapter will describe the development of a MR compression device to study the internal deformations of the soft tissues of the heel under normal and shearing loading. This will allow to have a complete dataset in terms of geometry, boundary conditions and displacements. This information will be used to generate and evaluate the FE model of the heel.

3. Chapter 3

MR-compatible loading device for assessment of heel pad internal tissue displacements under shearing load.

From the literature review of the previous chapter it was deduced the importance of defining new techniques for the evaluation FE models of the human heel. To this respect, is was considered to be crucial to be able to work in a simulation environment where most of the key variables, as applied loads and internal displacements, are known. To this respect, in this chapter, the design of an experiment to define a dataset for FE model generation of the heel will be described. Initially, the steps to realize a MR compatible device to apply normal and shearing loadings on the plantar region of the human heel are proposed. The MR experiment is then described and the dataset including geometry, boundary conditions and internal tissues displacement is presented.

This chapter was adapted from the related published article:

Alessio Trebbi, Antoine Perrier, Mathieu Bailet, Yohan Payan.
MR-compatible loading device for assessment of heel pad internal tissue displacements under shearing load.
Medical Engineering & Physics, Vol. 98, pp. 125–132.

3.1. Introduction

Despite being the second most common type of pressure ulcers, heel ulcers are considerably understudied compared to the rest of the ulcer literature, having a relative low number of groups actively investigating in this area [33][32][8]. Most loadings applied to the human heel are localized in two regions, namely the posterior and the plantar regions of the heel. The plantar region is subject to repetitive normal and shearing loads generated by gait or standing positions [92][93]. It can also be subject to a constant load generated by the weight of the leg when a patient is sitting on a wheelchair [94]. On the other hand, the posterior region of the heel is subject to constant normal and shearing loads generated by the contacts and friction with the mattress in patients that are bedridden [33]. Despite the higher load intensity that is applied on the plantar region, ulceration has a much higher incidence on the posterior part of the heel [39][95]. This is due to a fatty layer, called the fat pad, which covers the lower part of the heel. This structure is able to absorb impacts and redistribute the external loads to the internal tissues in order to prevent internal damage during gait. The fat pad is composed of adipose tissue for shock absorption and of a stiffer connective tissue (the septa) to maintain the pad structural integrity [53]. Currently, very few researchers are investigating the protective properties of the fat pad and analyzing the different roles of the materials it is made of [8].

Measuring *in vivo* the deformations of deep tissue is a complex procedure. Magnetic Resonance (MR) Imaging can be a solution for such a measurement as soon as an image is successively collected first with soft tissue at rest and second with the tissue deformed by an external loading device. These two images, if they are transformed into a common coordinate system using a 3D image registration technique, can provide a quantitative measurement of deep tissue displacement [96][97]. The main challenge to collect the two MR images involves designing a loading device that is fully non-magnetic and that is able to quantitatively measure the applied load. Indeed, forces cannot be measured by conventional load cells that would disturb the magnetic field of the MR machine. Various solutions to overcome this problem have been described in the literature. Chatzistergos et al. [98] used the gravitational force of a known MR-compatible mass to generate a specific load on the forefoot. Other applications used an optical sandwich [65], or a strain gauge placed sufficiently far from the region of interest (ROI) to measure the applied load [99]. However, with these solutions, the applied forces were limited to 5 Newtons (N) which is considerably lower than the forces observed during gait [92]. Devices that were capable of applying higher loads used pistons actuated by hydrostatic pressure that was remotely controlled outside the MR room [64]. Among these solutions, the device proposed by Petre et al. [100] was the only one designed to apply and to

measure shearing loads on the metatarsal region. However, to the best of our knowledge, this functionality of the device was never used in practice; in subsequent works, only the normal loads have been applied [90].

At this point, it is possible to list the requirements that an MR compatible device should have in order to address the matters described above. First of all, it is important to state that the device should provide a dataset (in terms of 3D images and boundary conditions) that will allow a complete FE analysis of heel pad internal tissue deformations. Therefore, the device should be able to apply loadings on the skin's surface (with a quantitative measurement of these loads) and to measure the generated internal tissue displacements. The type of applied loading should be both with normal and shearing forces since shear forces have been increasingly suspected to play a determinant impact in the formation of deep pressure ulcers [101]. This chapter aims at providing a response to such requirements, with the design of an MR compatible device able to apply calibrated shearing and normal loads and with the use of a non-rigid image-based registration method that provides a quantitative measurement of internal tissue displacements.

3.2. Methods

3.2.1. MR-compatible loading device

The loading device consists of two main parts: the foot fixation and the mechanics of the loading plate. A schematic diagram of the loading device is shown in *Figure 10* and photographs in *Figure 11*. This device consists of two parts: the foot fixation and the loading plate. These two components are held together by an external frame made in polyvinyl chloride (PVC). The loading mechanics are based on the compression of two sets of polylactide (PLA) springs respectively oriented to generate a normal and shearing load. These springs were printed using conventional 3D printers with 100% infill. The printing orientation was set in order to have the spring axis orthogonal to the printing plane. Table 2 gives an overview of the springs implemented in the loading device.

	Configuration	Coil Diameter	Length	Spring Diameter	No. of coils
Normal load set	4 parallel	5.0	55.0	25.0	4
Shear load set	2 parallel	3.0	43.0	20.0	4

Table 2: *Parameters of springs implemented in the loading device. Dimensions are given in [mm]*

By rotating a handle connected to a nylon screw (in grey color on *Figure 10*) the operator is able to displace one extremity of the springs. The other extremity is directly connected to the loading plate. By displacing the extremity connected to the nylon screw, the spring compresses and exerts a force on the plate that delivers the load on the heel. *Figure 10* shows a comparison of the device for an unloaded configuration (Load 0) and a loaded configuration where the plate is applying a normal and a shearing load (Load N). The directions of the loads are shown in the *Figure 10* from the green and orange arrows, respectively representing the shearing Fs and normal Fn forces.

To reduce friction, the plates connected to the spring extremities are constrained by guides made in Teflon which respectively allow one degree of freedom. Double-sided tape was used to adhere the heel to the loading plate and to ensure no sliding while applying the shearing loads. The foot casing (in blue in (*Figure 10*) was used to hold the heel in a fixed position by blocking the rotation of the ankle and limiting any additional displacement of the foot with respect to the MR machine. This component was designed to incorporate a negative of the foot surface, which was obtained in a previous MR acquisition and manufactured in PLA with the use of a 3D printer (see *Figure 11* for a view of this foot casing). The casing was printed in order to allow 1 mm of margin with the foot while the sharp edges in contact with the skin were filleted in order to make the device more comfortable to wear. The external frame and foot casing were held together by screws made of nylon.

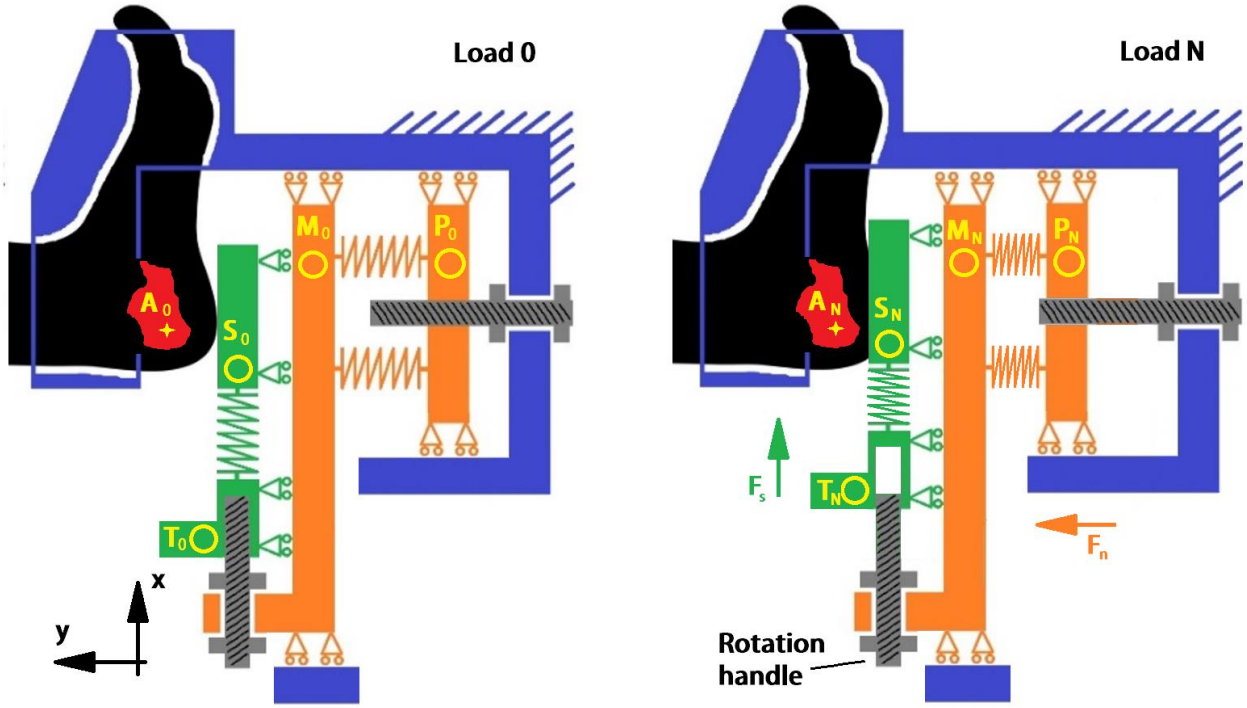

Figure 10: Schematic diagram of the MR-compatible compression device. The human heel (in black) is deformed by a loading plate (in green) that exerts normal and shearing forces (resp. Fn and Fs when Load N is applied). External fixed frame is colored in blue. The mechanism to apply normal loading Fn is shown in orange while the mechanism to apply shearing loading Fs is shown in green. The handles and respective screws to displace the spring extremities are shown in gray. Calcaneus bone is drawn in red. MR markers are plotted as yellow circles. From the MR acquisition, only components colored in red, yellow and black are visible in the images. However, thanks to the MR markers, it is still possible to deduce the position of every component at the time of the acquisition. Coordinate frame is set in order to make the subsequent analysis more intuitive.

MR markers, illustrated with yellow circles in *Figure 10*, were glued on the key components of the device to measure the level of compression of the springs during acquisition. The image of the calcaneus, captured in the acquisition allows for the identification of key points (landmarks like small holes in the bone, illustrated as point A in *Figure 10*) that permit to identify the internal displacement of the calcaneus between two images. The position of the calcaneus together with the position of the plate enables the calculation of the compression of the fat pad soft tissues. Spring compressions and tissue indentations were calculated from the positions (in the x-y sagittal plane) of the MR markers with the following formulas:

$$Spring\ normal\ deflection = \left(M_{0y} - P_{0y}\right) - \left(M_{Ny} - P_{Ny}\right)$$
$$Spring\ shear\ deflection = \left(S_{0x} - T_{0x}\right) - \left(S_{Nx} - T_{Nx}\right)$$
$$Soft\ tissue\ compressive\ displacement = \left(A_{0y} - S_{0y}\right) - \left(A_{Ny} - S_{Ny}\right)$$
$$Soft\ tissue\ shear\ displacement = \left(A_{0x} - S_{0x}\right) - \left(A_{Nx} - S_{Nx}\right)$$

Measuring for how long the springs were compressed during the experiment allows to reproduce *a posteriori* the compression time history of the springs during the experiment. The compression timings can then be reproduced later, in a compression test machine, by applying the same compressions captured in the MR images for the same time frame of the experiment. This gives an estimation of the forces that the device applied on the soft tissues across the MR acquisition.

3.2.2. Experimental protocol

A volunteer (male, 40 years old) agreed to participate in an experiment part of a pilot study approved by an ethical committee (MammoBio MAP-VS pilot study N°ID RCB 2012-A00340-43, IRMaGe platform, Univ. Grenoble Alpes). He gave his informed consent to the experimental procedure as required by the Helsinki declaration (1964) and the local Ethics Committee. The volunteer was placed in a supine position with his right foot inserted into the compression device and fixed inside the foot casing. A proton density MR machine was used to collect 512 consecutive 0.3125 mm thick sagittal slices (MRI system Achieva 3.0T dStream Philips Healthcare). Each slice had a field of view of 160 × 160 mm and a resolution of 512 × 428 for a total scanning time of 7 minutes.

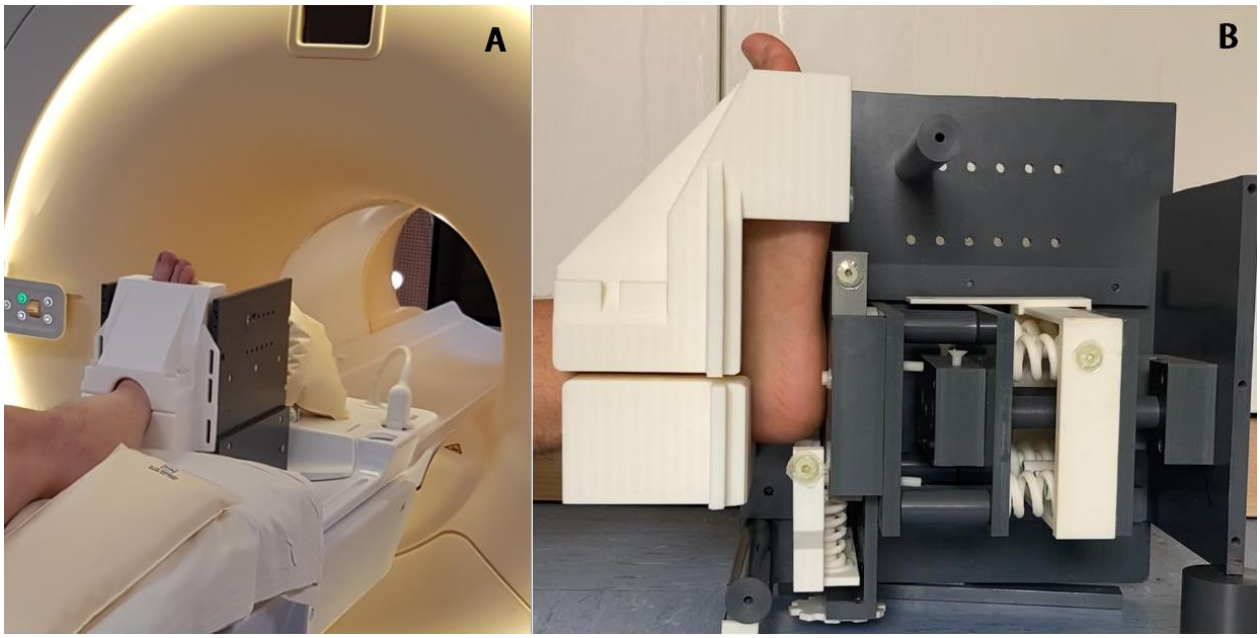

Figure 11: A) Loading device attached to the foot of the subject entering the MR machine. The white part is the 3D printed foot casing used to hold the heel in a fixed position. B) Internal view of the MR compatible device showing the springs and their orientation. The white gear wheel that can be seen in the lower part of the image is the rotating handle through which the user can displace one extremity of the springs. The circles of around 2 cm in diameter attached on the components are the MR markers.

The imaging acquisition protocol was divided into five stages in order to capture images for five different loading configurations. The first acquisition, Load 0, was taken in a resting configuration with the indenting plate in a tangent position with respect to the plantar skin of the heel but without any contact with the heel. This step was also used to identify the proper region of interest (ROI) and to make sure all the MR

markers, together with the relevant part of the heel, were present in the 3D images. Then, four successive load configurations were applied by rotating the handles of the device to displace the internal springs:

- Load 0 – No load applied
- Load 1 – High normal load
- Load 2 – Low normal load
- Load 3 – Low normal load and high shearing load
- Load 4 – Low normal load and low shearing load

This was chosen in order to capture the non-linear mechanical properties of the soft tissues; stiffer for higher loads and more compliant for lower loads. For the high loads, the subject gave feedback according to the highest magnitude he could comfortably handle for the duration of the acquisition. The same lower normal force was kept through the application of the shearing loads in order to ensure good contact between the indenting plate and the plantar skin of the heel.

3.2.3. Force measurements

The MRI acquisitions were analyzed using Amira software. Image segmentations of the heel at rest were carried out in order to define regions corresponding to bone, muscle, tendon, fat and skin. In order to align all 3D images, a rigid registration (rotation + translation) was implemented using the publicly available registration package Elastix [102]. Images were aligned with respect to the position and orientation of the calcaneus. For this purpose, a mask hiding soft tissues around the calcaneus was implemented. This was done in order to concentrate the registration capabilities on the alignment of the calcaneus that is considered to be undeformed in all the loading configurations. The Load 0 configuration is chosen as the "fixed image" and the other loads (Load 1-4) to be "moving images". This was chosen in order to get all the displacement fields starting from the same initial configuration (Load 0).

Once images were aligned, the locations of the MRI markers were considered. By comparing the respective positions of these markers in the images, the compressions of the springs were calculated for each loading configuration (Equations 1 and 2). In order to estimate the applied forces during the acquisitions, the spring compressions for the normal and shearing load were *a posteriori* reproduced in a compression test machine (MTS Criterion Model 41); the compression plates deflected the sets of springs for the same amount displayed in MR images and for the time frame noted during the session. The same compression test was repeated 8 times for each set of springs in order to analyze possible stiffness changes across subsequent compressions.

3.2.4. Internal tissue displacement

In order to measure the tissue internal displacements, a non-rigid image registration method using the Elastix package was implemented with the Normalized Correlation Coefficient [102] used as the similarity measure between images. The aligned set of images obtained by the previous rigid registration were implemented as inputs for this non-rigid registration in order to have the volume of the calcaneus aligned in the images. The Load 0 configuration was imposed to be the fixed image and the others (Load 1-4) to be moving ones (see [102] for a description of these notions of fixed and moving images in Elastix). This allowed the respective displacement fields to be obtained for each loaded configuration.

3.3. Results

3.3.1. MRI acquisition

The developed MR-compatible loading device allowed high quality MR measurements of the heel before and during the application of loads by means of the indenting plate. A good fixation of the ankle and the metatarsal part of the foot allowed the heel to be maintained in position for well-defined consecutive MR measurements and image comparisons. No image artifacts were detected in the ROI (Figure 12). The MR acquisitions had enough quality to clearly distinguish the different tissues that compose the human heel; specifically the bone, muscle, tendons, fat and skin. This allowed for a semiautomatic segmentation of the respective tissues. In the following images the result of the segmentation of the heel at rest (in red on Figure 12) are superposed in order to help the comparison between the loading configurations. To analyze the effect of the shear loading, we will focus on Loads 2 and 3 as their conditions are the same, apart for the addition of the shearing component in Load 3. The superposition of the red continuous line with the calcaneus can be used to evaluate the result of the alignment process.

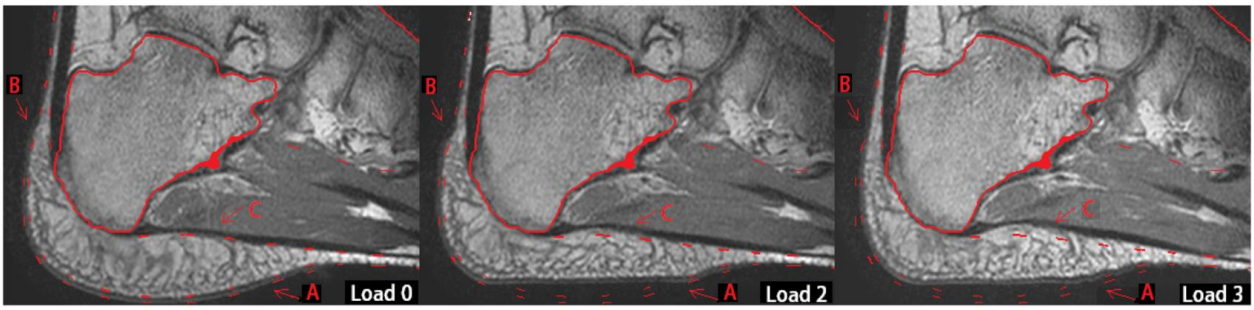

Figure 12: Sagittal MRI sequence of loading configurations in order to compare the effects of normal and shearing loadings. The red contours represent the segmentation of Load 0. Arrows A, B and C are placed in locations where the most clear impacts of the applied loads are visible. Load 0: no load ; Load 2: Fn as a normal load ; Load 3: Fn + Fs as a normal and shearing load.

The effects of the applied loads can be inspected visually in Figure 12. Arrow A points to the location where the plate was applying the loading. As can be seen for Load 2, the normal load dislocates the adipose tissue of the fat pad from the lower part of the calcaneus to the sides and the posterior part of the heel, as pointed by arrow B. Once the shearing load is added (Load 3), the fat is moved from the posterior part to the lower part of the calcaneus close to where the plantar fascia is connected to the calcaneus (arrow C).

3.3.2. Force measurement

The MR images show the position of the MR markers needed to reconstruct the amount of compression of the springs and the position of the indenting plate during the experiment. Figure 13 illustrates heel deformations due to Load 1 with a superposition of the spring as represented in *Figure 10*. The components that were not captured in the MR acquisition are the loading plate in green and the springs in red. These were added for clarification.

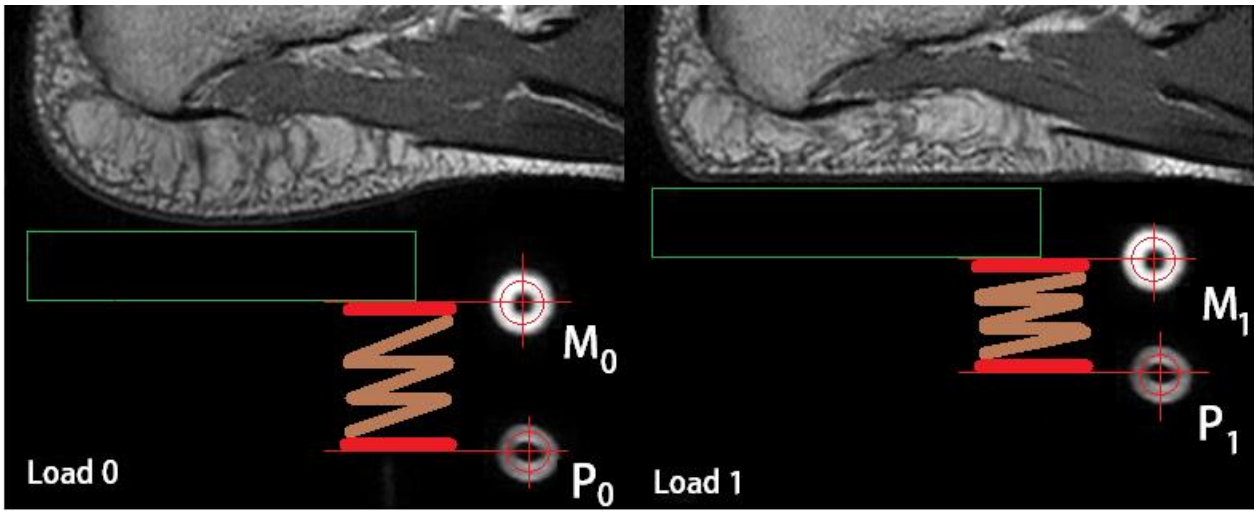

Figure 13 Process of tracking the positions of the MR markers in order to calculate the level of compression of the springs. This figure is the actual result of Figure 1 for Load 1. The MR markers represented by yellow circles in Figure 1 are the only components of the device that can be seen in the images, together with the biological tissues. The two circles represent the spring extremities. In Load 0 the spring is in a relaxed position with the markers far apart. For load 1, the circles are close to each other showing that the spring was compressed. The upper marker is also closer to the foot sole, showing that the indenting plate moved upwards to compress the heel.

Figure 14 plots the results of the four loading configurations measured from the springs' compressions and reproduced in the compression test machine. The 3D printed springs implemented in this study showed a viscoelastic behavior that reduced the reaction force of the spring over time. In order to reduce the force drop, the MR acquisitions were performed 3 minutes after compressing the springs. Areas highlighted in green show the time frames in which the machine was acquiring the images. The respective shaded areas in blue and red show the standard deviations (S.D.) across the 8 compression trials. *Table 3* summarizes the measured forces for each loading configuration.

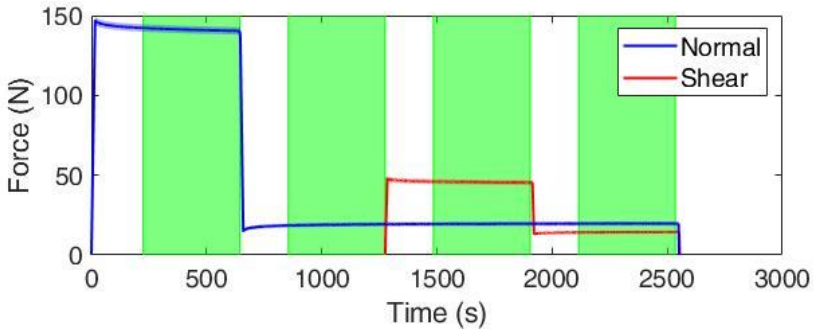

Figure 14 A posteriori reproduction of the spring loading configurations in the compression test machine. Green regions show when the MR machine was acquiring images. Load 1 is related to the first green area, Load 2 to the second and so on.

	Normal force [N]	S.D.	Normal force drop [N]	Shear force [N]	S.D.	Drop [N]
Load 1	140.35	2.34	-1.63	0	0	0
Load 2	14.86	1.33	+0.80	0	0	0
Load 3	15.85	1.33	+0.20	45.05	1.55	-0.40
Load 4	16.15	1.33	+0.10	11.87	1.00	+0.23

Table 3 Values resulting from the reproduction of spring loading configurations in the compression test machine. The force drop refers to the reduction in force over the green areas due to the viscoelastic behavior of the springs.

3.3.3. Plate force/displacement pseudo-curves

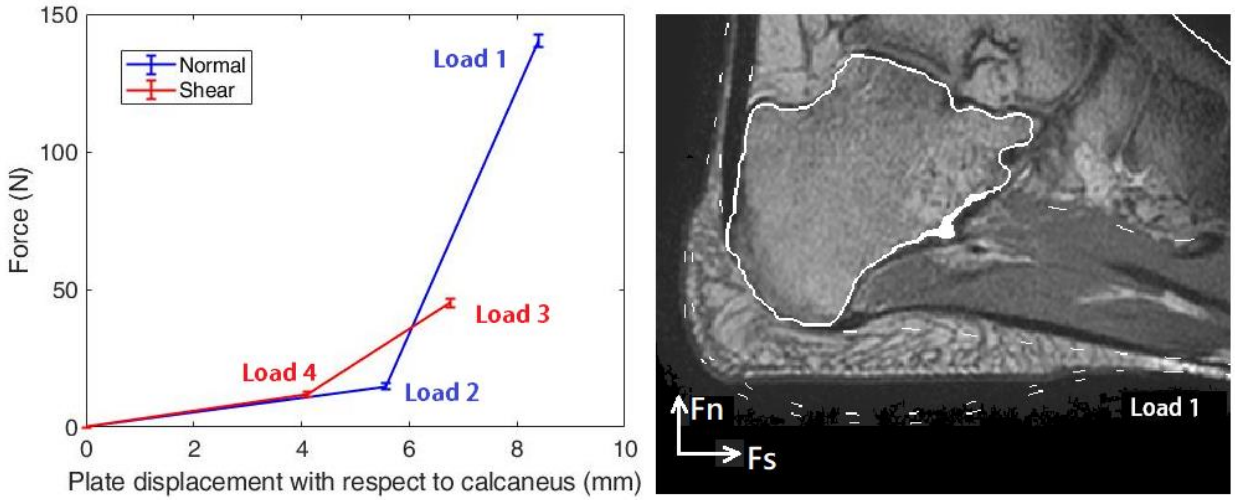

Figure 15: A) Plots the loading configurations on a force/displacement plane. The blue points only refers to the normal forces applied by the normal set of springs and the respective displacement of the plate with respect to the calcaneus. The red points only refer to the shearing forces applied by the springs. B) Slice from the Load 1 configuration that had the highest normal load applied in the experiment: 140 N. The two arrows Fn and Fs show the direction of the applied loads.

Figure 15 plots in 2D the four loading configurations applied during the experiment with the forces generated by the springs on the vertical axis and the displacement of the indenting plate with respect to the calcaneus on the horizontal axis. In this figure we want to distinguish the behavior of the soft tissues under normal load and shearing load. With this regard, the blue line of the graph is only related to load 1 and 2 and to the forces and displacements applied in the direction normal to the heel sole surface (i.e. the y direction as represented in *Figure 10*). On the other hand, the red line focuses on Load 3 and 4 that applied the shearing loads and only account for forces and displacements applied in the direction tangential to the heel sole surface (i.e. the x direction as represented in *Figure 10*). Values are obtained from the data in Figure 14 and *Table 2*. As can be seen in Figure 15, both the normal and shearing loadings elicited a non-linear response of the plantar tissues: initial low stiffness followed by a higher stiffness when the applied force increases (which is coherent with what is known as concerns the non-linear constitutive behavior of most human soft tissue [76][103]).

3.3.4. Internal tissue displacements

This section aims at analyzing the displacements of fat pad internal tissues due to the applications of normal and shearing loads. The presented results are obtained from the non-rigid image registration performed between Load 0 and over the other loading configurations (Load 1-4). Since the images were already aligned with respect to the calcaneus bone, the displacement of the points located inside that bone are expected to have a displacement close to zero. In order to compare tissue displacements due to normal loads versus displacements due to shearing loads, we show the respective slice of Load 2 and 3 previously presented in Figure 3.

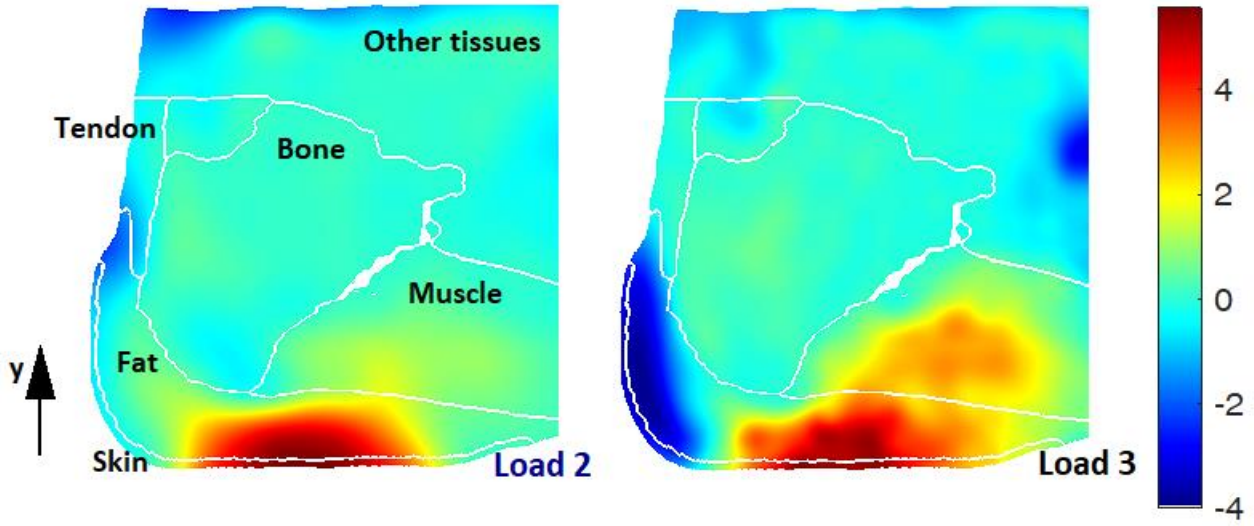

Figure 16 Sagittal view of the internal tissues displacement map (in mm) obtained from the non-rigid image registration. Note that only the components of the displacements (in mm) along the direction normal to the heel sole surface (y axis) are plotted. White lines mark the boundaries of the biological tissues. Note that the displacement map is plotted in the heel geometrical configuration that corresponds to the undeformed state (as collected for Load 0). Load 2: mild normal load ; Load 3: mild normal load + high shearing load

Figure 16 plots a sagittal view of the internal displacements (in mm) with respect to the calcaneus along the direction normal to the heel sole surface (i.e. the y direction as represented in *Figure 10*) for Loads 2 (left panel) and 3 (right panel). Results between Load 2 and 3 are similar in the lower part of the heel (arrow A in Figure 12) as the amount of normal load is the same, but some relevant differences appear when the shearing force is applied (Load 3). As previously noted by the arrow B in Figure 12, the shearing

load is pulling downwards the posterior tissues of the heel. The effects of the shearing load can also be analyzed in the plantar aponeurosis region (Arrow C in Figure 12), where the tissues are pushed upwards.

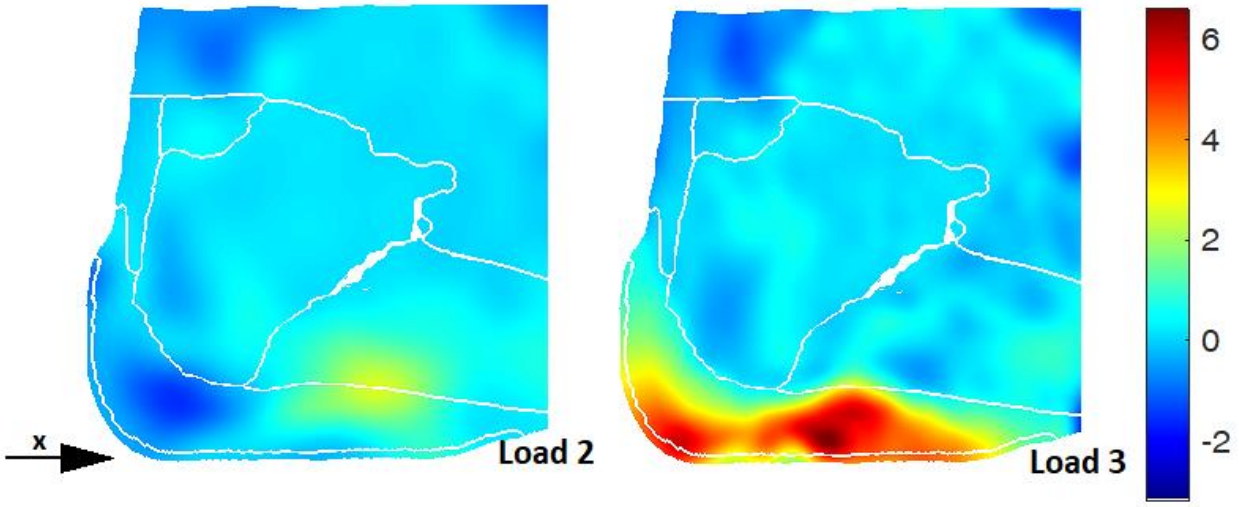

Figure 17: Analogous plot to Figure 16 but, in this case, only the displacement component along the direction tangential to the heel sole surface (i.e. the x direction as represented in Figure 1) are plotted.

Figure 17 is the analogous version of Figure 16 but with respect to the displacements along the direction tangential to the heel sole surface (i.e. the x axis). In this case, plots look different since no shearing force in the x direction is exerted by the plate for Load 2. For that load, the calcaneus is acting as a watershed pushing the fat towards the back or the front according to its initial location (the dark blue spot towards the left part of the bone surface and the yellow spot towards the right part). Displacements become significantly higher looking at Load 3, where the shearing load is clearly pushing all the tissues towards the frontal part of the foot.

3.4. Discussion

A MR-compatible loading device was developed to permit the simultaneous application of normal and shearing loadings on the plantar part of the human heel while acquiring MR images. A rigid and non-rigid image-based registration method was then used to align the images and to quantitatively measure the internal tissue displacements. The quality of the MR acquisitions and the absence of artifacts is enough for a semi-automatic segmentation process that defines surfaces delimiting the internal anatomical components of the heel; specifically the bone, muscle, tendon, fat and skin. The quality of the images enabled the calcaneus bone surfaces in each image to be successfully aligned, thus providing a rigid

registration of the different loading configurations between each other. This can be seen in Figure 12 where the calcaneus bone surface segmented from Load 0 perfectly fits the calcaneus frontiers as shown in the images related to Load 2 and 3.

The application of shearing and normal loads generated considerable displacements in the fat pad of the subject that can be visually identified in the MR images (Figure 12). The applied force was estimated considering the compression of 3D PLA springs. The force drop due to the viscoelastic properties of the PLA springs had a maximal impact in Load 1 configuration with a drop in force of 1.63 N from 140 N. Repeating the same compression test for the springs has shown not significant changes in stiffness of the 3D springs across subsequent usages. The highest standard deviation was found in Load 1 with 140 N ± 2 N (i.e. an accuracy of 1.6%). Information about force accuracy of other MR-compatible loading devices is scarce and is mostly presented in terms of pressure. In the works of Stekelenburg et al. [99] and Tokuno et al. [104], force accuracy is less than 1%. However, it must be considered that these devices are capable of measuring forces that do not reach values higher than 5 N and therefore are not suitable for applications related to the plantar pressures that have a consistent higher value. Thanks to the ease of 3D printing various sets of springs with different parameters can be adapted to reach different levels of stiffness. However, it must be taken into consideration that for in vivo human experiments, the magnitude of the load will always be limited by the tolerance of the subject in supporting the applied load for the duration of the acquisition (with actual force magnitudes applied by our device that are far below the magnitudes of typical ground reaction forces during gait). The main limitation of this device is the impossibility to apply dynamic loadings and to directly control during the MR acquisition the amount of force applied. The level of force can indeed only be estimated *a posteriori* with an analysis of the MR images and a compression test of the relative springs. This limitation, however, is common in devices of this kind due to the limited allowed materials in the MR environment [99][100]. A possibility to overcome this limitation would be to *a priori* mechanically characterize the set of springs and to calibrate them in order to know the exact amount of force exerted by the plate for any compressions of the springs measured during the MR session. This would however not be a straightforward task as it would require an on-line segmentation of the MR images to track the MR markers or, as an alternative, it would require to design a mechanical system to accurately measure the springs compressions during the MR session (like for example a 3D printed caliper attached to the moving parts of the device). This could be explored as an extension of this study.

Displacements computed from the Elastix non-rigid image registration are in line with what was expected looking at Figure 12. First, loads applied in a direction normal to the heel sole surface compress tissues against the calcaneus frontier and push some tissue at the back of the foot, in the region of the Achilles

tendon. Second, shearing loads mainly moved the soft tissues towards the frontal part of the foot. It is also interesting to note that the higher displacement values at the external skin surface as plotted for Figure 16 load 2 and Figure 17 load 3 match with the values reported in the plot of Figure 15 (and measured from the location of MR markers). This is reasonable as we expect that the displacement of the outermost layer of skin would match the displacement of the indenting plate (as the skin is fixed to the plate with two-sided tape).

3.5. Conclusion

This chapter has described the design and use of a MR-compatible device capable of applying shearing and normal loadings on the human heel and of quantitatively measuring the corresponding force and internal displacement values. The device is based on the compression of 3D printed springs. The imaging process produced a valid data set for the analysis of displacements of the internal components of the fat pad. The outcomes of this study are multiple. Firstly, the possibility to apply shearing loads and to observe the corresponding tissue deformations provide insights concerning the impact that these loads can have on the biological tissues in the development of pressure ulcers. Secondly, the displacement of internal soft tissues generated by the high loadings is crucial for understanding the roles of the fat pad sub-components in mitigating the formation of pressure ulcers in the plantar part of the heel. Thirdly, the load/displacement pseudo-curves can be used for the estimation of the biomechanical properties of the heel pad subcomponents, especially for FE models that require constitutive parameters. Finally, the data relating to the deformations of internal soft tissues can be used to validate the simulations provided by such FE foot models to reproduce gait or configurations related to wheelchair or bedridden patients.

The pilot study described here indicates that the crucial elements of the experimental procedure are feasible to be implemented in a wider study. Further research will include analysis on more subjects and with different loading configurations, together with the adaptation of the device to apply loadings on different parts of the body to gain insight into the relative mechanical soft tissue properties.

The next chapter will describe the calculation of strain maps from the displacement fields obtained in the registration process. A special focus will be given in the evaluation of these results in terms of accuracy.

4. Chapter 4

MR-based quantitative measurement of human soft tissue internal strains for pressure ulcer prevention

From the MR experiment of the previous chapter was obtained a dataset including a complete definition of the geometry, boundary conditions and internal displacements of the human heel. As described in chapter 2, the most important index for pressure ulcer prevention from a biomechanical aspect is the intensity of tissue internal strains. This chapter will focus on the estimation of shear strains from the displacement fields obtained from the MR experiment. A special emphasis will be given in analyzing the errors of this technique in relation to strain calculations.

This chapter was adapted from the related published article:

Alessio Trebbi, Ekaterina Mukhina, Pierre-Yves Rohan, Nathanaël Connesson, Mathieu Bailet, Antoine Perrier, Yohan Payan.
MR-based quantitative measurement of human soft tissue internal strains for pressure ulcer prevention. Medical Engineering & Physics, Volume 108, 2022, 103888, ISSN 1350-4533.

4.1. Introduction

A common methodology to estimate internal tissue strains relies on Finite Element (FE) modeling, with simulations that reproduce the body part morphology, tissue biomechanical parameters and the type of loading [105][106][107]. However, validation of FE simulations of the mechanical response of *in vivo* biological tissues to external mechanical loads has always been problematic. Keenan et al. report that none of the current heel models have been properly validated against independent experimental measurements and that further work is needed to develop models that are well validated to draw reliable clinical conclusions [105]. Regarding the buttock region, Savonnet et al. reached a similar conclusion stating that only few models were validated with experimental observations [106]. Because direct validation of internal mechanical strains is a challenging problem, many research works proposed to evaluate FE models of the foot in terms of their capacity to predict interface plantar pressure by comparing the contact pressure predicted by the FE model with the measurements from pressure mattresses [76]. Yet, as observed in Macron et al. [108] on data from 13 healthy volunteers, interface pressure distributions do not correlate with internal strains and one cannot be used to predict the other. This issue was partially addressed by Linder-Granz et al. [28] for a buttock FE model in a study where the authors compared contours of the computational domain in the deformed configuration predicted by the simulations to the ground truth segmented contours obtained from MR images. This comparison, however, considers only the external shape and not the quantity of interest, which is the local internal tissue displacement and associated tissue strains.

In an original contribution, Stekelenburg et al. [109] proposed to use MR tagging and phase contrast sequences on a rat leg model under indentation to assess local tissue displacements and compute the associated tissue strains. The main restriction of this approach is that the indenter (used inside the MR machine to deform the tissue) has to be applied rapidly and repetitively as the tagging grid fades within 1 s because of MR relaxation. This requirement can be complex to overcome with an MR compatible device. Moreover, this constraint does not allow for conventional control systems for the application of loads such as gravity, hydrostatic pressure or compression springs [98][100][110]. Additionally, with dynamic loads applied, the viscoelastic properties of the biological tissues could have an impact on the mechanical response, thus increasing the complexity to estimate the tissues passive mechanical properties from the experimental measurements.

Digital Volume Correlation (DVC) is an emerging non-invasive technique that allows to characterize experimentally material mechanical response to external loadings by tracking the displacement of natural

patterns. From the displacement field, local strains can be computed. Combined with 3D MR images, DVC can, for example, be used to estimate human tissue internal strains [111]. From two MR datasets, one collected in an arbitrary undeformed configuration and another in a deformed configuration, the non-linear transformations that will align the MR volume at rest to the deformed one can be computed using a procedure call Image Registration. To illustrate the process, a graphical summary of the procedure is proposed based on data collected by the authors on the foot (*Figure 18*). DVC has previously been used in for *in vivo* strain estimation in human intervertebral discs, brain and leg muscles under external mechanical loading [112][113][114].

Our group has recently developed an MR-compatible device for applying controlled shearing and normal loads to the human heel pad [16]. With such a device, 3D MR volumes of the heel pad soft tissue can be imaged under various loads applied on the foot sole. This chapter aims at describing the methodology proposed by our group to implement DVC on human soft tissues and at estimating the internal strains from the DVC-derived 3D displacement field. The long-term objective is to validate a FE model, in terms of its capacity to predict the localization and the intensity of the strain field in the soft tissues.

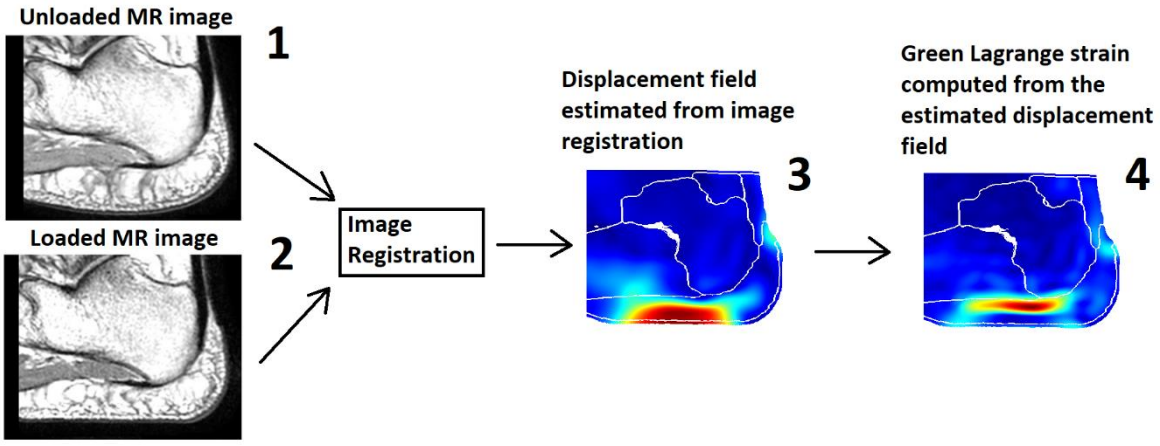

Figure 18: Scheme of quantitative measurement of soft tissue internal strains obtained from image registration. Image 1: unloaded configuration. Image 2: Loaded configuration. The image registration estimates the displacement field (Image 3) that transforms the unloaded image into the loaded configuration. The strain field can then be derived from the displacement field (Image 4).

4.2. Materials

4.2.1. Materials: heel and sacrum MR datasets previously collected on one healthy volunteer

The MRI datasets used in this study have been collected in a previous study [110]. For the sake of clarity, the main details regarding the experimental setup, protocol and participant are summarized in the following paragraph. For more details, the reader is referred to the associated publication.

A healthy volunteer (male, 40 years old) gave his informed consent to participate in the experimental part of a pilot study approved by an ethical committee (MammoBio MAP-VS pilot study N°ID RCB 2012-A00340-43, IRMaGe platform, Univ. Grenoble Alpes).

For the heel MR image datasets, the volunteer was placed in a supine position with his right foot locked in a MR compatible device designed to apply both a normal force (15 N) or a combined normal-and-shearing force (15 N normal + 45 N shearing) on the heel pad by means of an indenting platform. The setup is illustrated in *Figure 19* A. A proton density MR sequence was used to collect 3D images composed of 512x428x512 voxels with voxel size of 0.3125 mm x 0.375 mm x 0.3125 mm (MRI system Achieva 3.0T dStream Philips Healthcare). Two acquisitions of the same unloaded configuration allowed to avoid having the same noise pattern between equivalent images in the subsequent image registration process in order to test the repeatability of strain calculation.

For the sacrum images, the subject was placed in the MR bed in a prone position. An indenter actuated by gravity applied a normal load (12 N) on the sacrum region. The 3D images were composed by 800×800×240 voxels with a dimension of 0.5×0.5×0.5 mm (*Figure 19* B). Likewise, two acquisitions were collected in the unloaded configuration to test the repeatability of strain calculation.

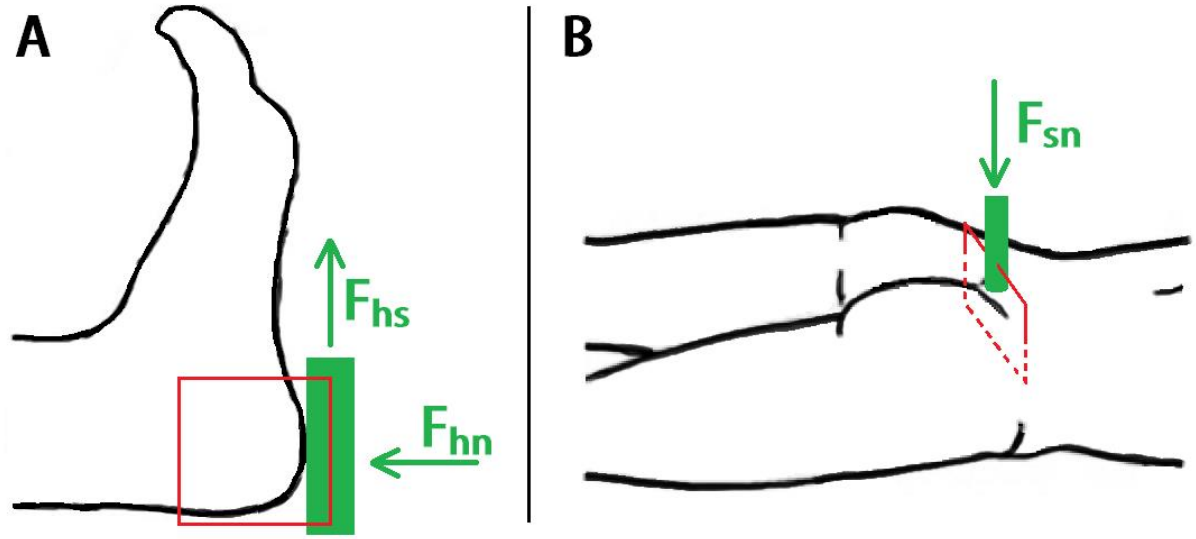

Figure 19: (A) Scheme of the heel configurations during the MR acquisitions. The green rectangle represents the plate applying the loads. Direction of the loads is represented by the green arrows Fhn (Force heel normal) and Fhs (Force heel shear). The red rectangle shows the orientation of the MRI slice that will be shown in the rest of the chapter. (B) Scheme for the sacrum configuration (Analogous to A). The green block represents the indenter with the respective Fsn (Force sacrum normal) applied. The indenter has the external shape of an ultrasound probe, 10-2 linear probe transducer developed by (Aixplorer, SuperSonic Imagine, France).

Four 3D MR images of the heel and three 3D MR images of the sacrum region were considered in this contribution and were referred to using a unique name as listed in *Table 4*.

Name	Description	Load
Heel01	Unloaded heel – Acquisition 1	0 N
Heel02	Unloaded heel – Acquisition 2	0 N
Heel1	Heel with normal load	15 N normal
Heel2	Heel with normal and shearing load	15 N normal and 45 N shear
Sacrum01	Unloaded Sacrum – Acquisition 1	0 N
Sacrum02	Unloaded Sacrum – Acquisition 2	0 N
Sacrum1	Sacrum with normal load	12 N normal

Table 4 List of MR acquisitions. The first name indicates the body location of the image. The unloaded configurations are indicated by the initial number 0 (01, 02). The loaded configurations are indicated by the integer positive numbers (1,2).

A 2D snapshot of each MR volume (presented as the red rectangle in *Figure 19*).

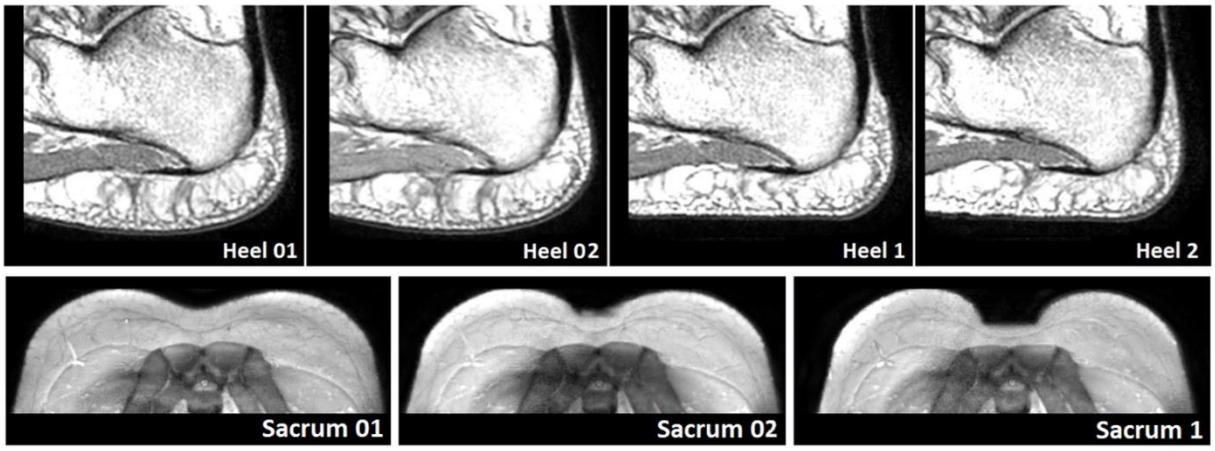

Figure 20: Slices of the heel and the sacrum unloaded and loaded configurations described in Table 4. The respective region is indicated in Figure 19 by the red rectangle.

4.2.2. Rigid registration

The four MR volumes of the heel and the three MR volumes of the sacrum were rigidly registered to align the calcaneus bone and the sacrum bone respectively using the publicly available registration package Elastix [102].

4.2.3. Digital Volume Correlation between the loaded and the unloaded MR images

The registration package Elastix [102] was then used to perform Digital Volume Correlation. Two images are involved in this registration process: the reference image $I_0(x)$ (unloaded configuration: Heel/Sacrum 01/02, called "fixed image" in the Elastix library) and the deformed image, $I_Q(x)$ (loaded configuration: Heel 1 and 2 and Sacrum 1, called "moving image" in the Elastix library), where x represents the position of a point in the images. The registration between these two images defines a non-rigid deformation field $u_Q(x)$, which describes how the reference unloaded image transforms into the deformed image. Applying the deformation field to the reference image creates a transformed-deformed image $I_0\left(x + u_Q(x)\right)$ that aims to look identical to the deformed image.

The optimal deformation field was estimated by minimizing a cost function by means of an iterative optimization method (adaptive stochastic gradient descent) embedded in a hierarchical (multiresolution)

scheme. The cost function relates to the similarity between the two images (*i.e.* the reference image and its transformation) using image features and was based on the Normalized Correlation Coefficient (NCC). During the optimization step, the value of the cost function was evaluated at non-voxel positions, for which intensity interpolation with cubic B-Spline was used.

4.2.4. Computing mechanical strains from the DVC-derived displacement fields

From the displacement fields obtained by the registrations, strain maps were calculated as follows: The relation between the position X of a material point in the undeformed configuration and its position x in a deformed configuration Q is described by the spatial displacement vector $u_Q(x)$ which consists of 3 components u_{Qx} , u_{Qy} , u_{Qz} :

$$u_Q(x) = \left[u_{Qx}\,, u_{Qy}\,, u_{Qz}\right]^T$$

From these, the deformation gradient F can be computed:

$$F = I + \frac{\partial u}{\partial X}$$

And the right Cauchy-Green deformation tensor C deduced:

$$C = F^T F$$

The Green Lagrange (GL) principal strains:

$$E_p = eig\left(\frac{1}{2}\,(C - I)\right)$$

The maximum GL shear strains are defined as:

$$E_s = \frac{1}{2} * \max(|E_1 - E_2|, |E_1 - E_3|, |E_2 - E_3|)$$

4.2.5. Uncertainty of the Image registration procedure

To evaluate the uncertainty of the DVC we consider six evaluation Cases A to F. The first three cases are related to the repetition of the same strain measurement and to the analysis of the differences between the respective results (reproducibility of the registration). The last three cases focus on the ability of DVC to estimate a known a priory strain field (trueness of the registration).

Reproducibility

Reproducibility refers to the closeness of agreement between test results. In this section, we propose to evaluate the reproducibility of strain calculation through image registration. Two acquisitions of the unloaded configurations of the heel and sacrum (namely Heel01 and Heel02 and sacrum01 and sacrum02 respectively) were registered to the same moving image (Heel1 and Sacrum1 respectively). The corresponding strain maps are computed from the two estimated deformation fields. The reproducibility is then inspected by analyzing the differences between these two strain maps. Three cases, summarized in *Table 5*, are considered: heel under normal load (A), heel under normal+shearing load (B) and sacrum under normal load (C).

Fixed image	Moving image	Case	Displacement field	Shear strain field
Heel 01	Heel 1	A	DA_{011}	SA_{011}
Heel 02	Heel 1		DA_{021}	SA_{021}
Heel 01	Heel 2	B	DB_{012}	SB_{012}
Heel 02	Heel 2		DB_{022}	SB_{022}
Sacrum 01	Sacrum 1	C	DC_{011}	SC_{011}
Sacrum 02	Sacrum 1		DC_{021}	SC_{011}

Table 5 List of image registrations to evaluate the reproducibility of strain calculation from image registration. Each line represents an image registration composed by its fixed and moving image. The tests are grouped in three Cases: A) Heel with normal load, B) Heel with normal+shearing load, C) Sacrum with normal load. The resulting displacement fields and shearing strain field are respectively denoted with the letters D and S. The second letter in the field nomenclature reports the respective case of the registration. The numbers report the name of the fixed and moving images.

Accuracy

Trueness reflects how close a data is to a known or accepted value. In this section, we propose to evaluate the trueness of our image registration procedure to identify a known *a priori* strain field. We focus specifically here on the images of the heel. Two different displacement fields are considered:

1. For the first case, an artificial displacement field D_{DEM} is generated from a Finite Element (FE) simulation. A rectangular parallelepiped volume with the same size of the 3D MR images is first generated in ANSYS 19.2 APDL (ANSYS, Inc., Canonsburg, PA). This volume is then meshed with 8-

nodes hexahedral elements and a linear elastic material model is implemented. The 3D mesh is composed of 24389 hexahedral elements. The nodes on the sides of the parallelepiped are fixed in order to avoid any displacements outside of the defined volume. A set of 196 internal central nodes located on the same XZ plane are then submitted to a prescribed displacement boundary condition in a normal (Y) and in a tangent (X) direction (Figure 21). The displacement field computed by ANSYS is then extracted for all the nodes of the parallelepiped and interpolated to fit the resolution of the MR images. The corresponding displacement field is applied to the unloaded image (Heel 01) to generate a new artificially loaded image of the heel, named Heel FEM (Table 6 and Figure 22). It is worth noting that the objective of the FE method is mainly to produce a known a priori displacement filed. This displacement filed will be subsequently estimated through the image registration technique. The simulation itself, and the artificially generated image Heel FEM, do not have any real physical meaning. The main benefit of using such an FE solver is the possibility to get a ground-truth strain field that can be compared to values estimated from image registration.

2. For the second case, the previously computed displacement field DA_{011} is applied to the unloaded image (Heel 01) to generate a new artificially loaded image of the heel, named Heel TRA (from the word transformed) (Table 6 and Figure 22).

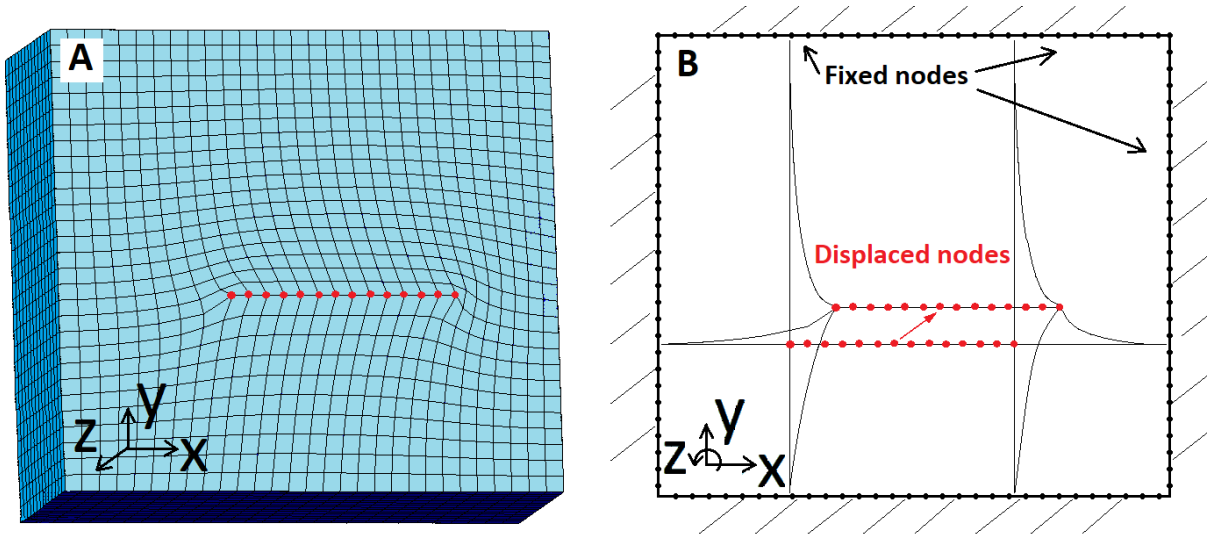

Figure 21: Generation of an artificial displacement field from a Finite Element simulation generated by Ansys. The size of the cube matches with the size of the MR images of the heel. A selection of nodes (red dots) on a plane orthogonal to the y axis was displaced as boundary conditions. (A) Section of the simulated cube along a plane orthogonal to the z axis. (B) schematization of the boundary conditions imposed. The external nodes were fixed, and the selection of red nodes was displaced.

Image	Applied displacement field	Artificial image	Shear strain field
Heel 01	D_{FEM}	Heel FEM	S_{FEM}
Heel 01	DA_{011}	Heel TRA	SA_{011}

Table 6 : List of transformations to create the artificial images to test the trueness of strain calculation through image registration. The image column lists the images to be transformed. The displacement field column lists the transformation to be applied to generate the artificially deformed image.

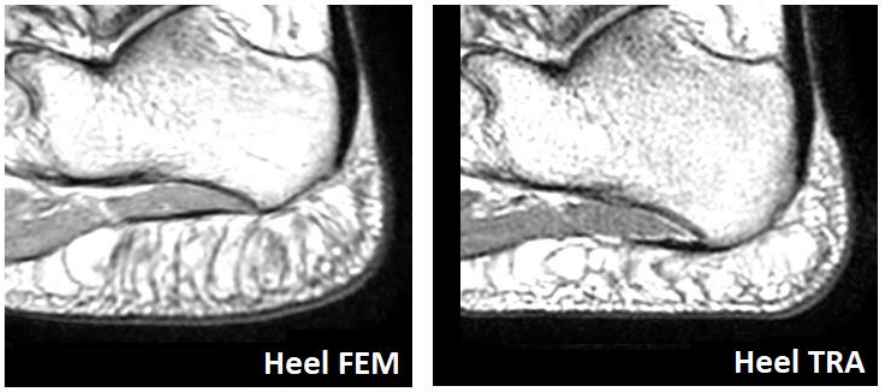

Figure 22: Artificial images obtained once the displacement fields D_{FEM} and DA_{011} are applied to the unloaded image Heel 01.

Image registration was then computed between Heel 02 and the two artificially deformed images Heel FEM and Heel TRA. Note here that having two acquisitions of the same unloaded configuration (Heel 01 and Heel 02) allowed to implement different noise patterns during the registration process in the fixed and moving image (Cases D and F of Table 7). On the other hand, to show the impact of having the same noise pattern between the fixed and the moving image the image Heel 01 was also considered for Case E (Table 7).

Fixed	Moving	Case	Displacement field	Shear strain field
Heel 02	Heel FEM	D	DD	SD
Heel 01	Heel FEM	E	DE	SE
Heel 02	Heel TRA	F	DF	SF

Table 7 : Following cases A, B and C mentioned in *Table 5*, cases D, E and F relate to the estimation of the trueness of strain calculation through image registration. The shear strain fields SD and SE will be compared with S_{FEM}. The shear strain fields SF will be compared with SA_{011}.

4.2.6. Error quantification

The error estimation was performed analyzing the obtained strain fields with a Bland–Altman plot. This representation is a method of data plotting used in analyzing the agreement between two different set of data corresponding to the same measurement. The plotted graph shows the error distribution throughout the whole range of measured strain values.

4.3. Results

4.3.1. Strain measurements for heel under normal load (case A, *Table 5*)

The distribution of the DVC-derived displacement field in the heel domain under normal load is given in the sagittal slice containing the highest shear strains (*Figure 23* A). The highest displacements are uniform in the area where the plate was in contact with the plantar skin of the heel. *Figure 23* B shows the corresponding maximal Green Lagrange shear strains computed from the displacement field. Shear strains are concentrated around the lower part of the calcaneus bone propagating towards the plantar fascia and the flexor digitorium brevis.

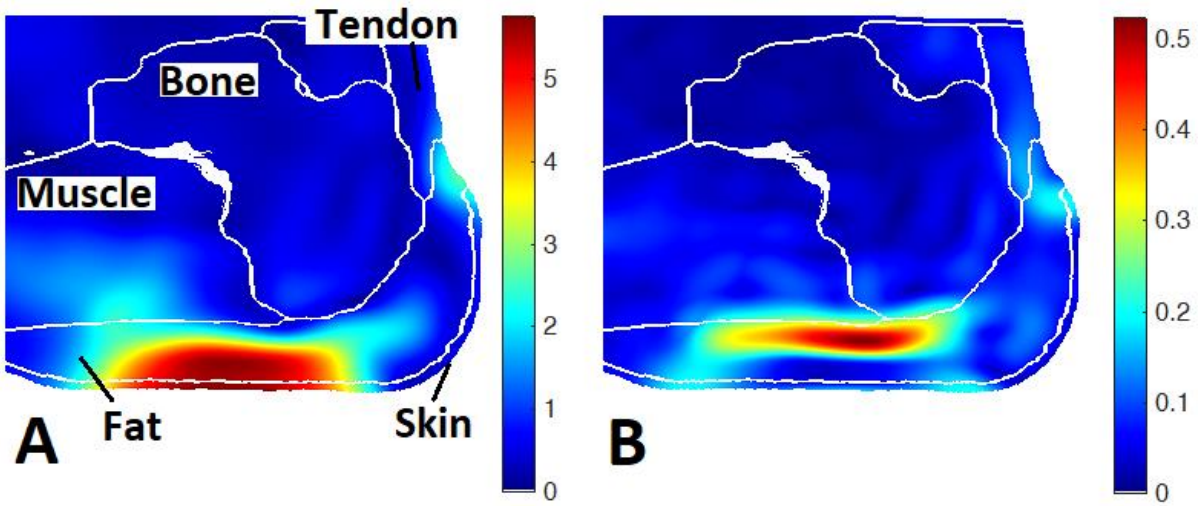

Figure 23: Case A. Biological tissues are delimited by white lines. A slice from the MR volume is shown from the sagittal plane corresponding to the location of the highest shear strain. (A) Visual representation of

DA_{011}. Modulus of displacement field [mm] for heel under normal load. (B) Visual representation of SA_{011}. Max GL shear strain field for heel under normal load (0.5 corresponds to 50% of deformation).

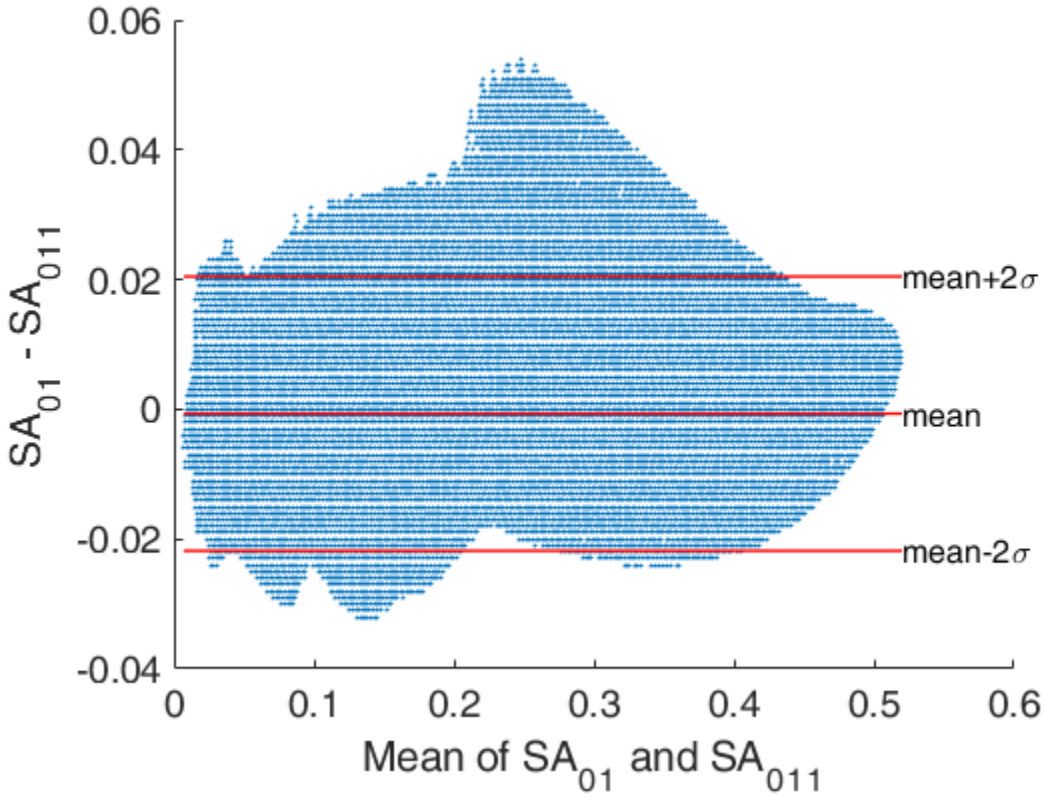

Figure 24: Bland-Altman plot referring to the strain estimation computed from Case A: heel under normal load. The upper and lower red line correspond the 95% confidence interval, meaning that 95% of the values have an error lower than 0.02 strain. The most relevant part of the plot is the region with the highest values of the strains 0.4-0.5 as these can represent the threat for tissue damage.

The agreement between SA_{011} and SA_{021} was described graphically with a Bland-Altman plot (*Figure 24*) with mean of differences, reported with corresponding 95% confidence interval (CI), and lower and upper limits of agreement, calculated as mean ± 2σ (where σ represents the standard deviation SD). Differences were assessed using a Wilcoxon-Signed-Rank Test (paired data) at the default 5 % significance level.

1.1. Strain measurements for heel under normal+shearing load (case B, *Table 5*)

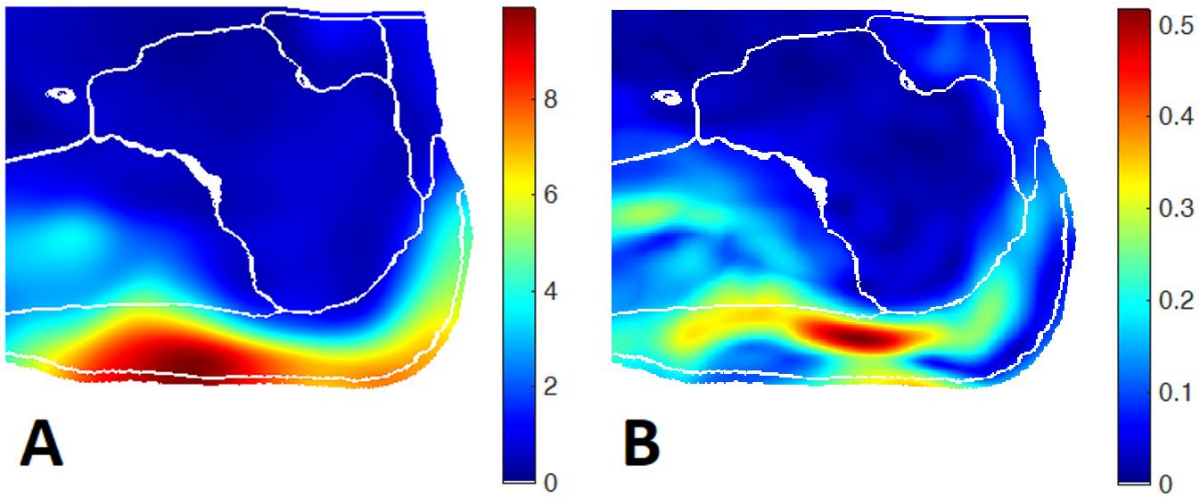

Figure 25: Modulus (in mm) of displacement field for heel under shearing load DB_{012}. (B) Max GL shear strain field for heel under shearing load SB_{012}.

The application of the shearing load had a relevant impact on the soft tissue displacements. The plate moved the posterior and the plantar regions of the heel skin towards the forefoot. This caused the shear strains to propagate on a wider region of the fat pad and the muscle (Figure 25). A concentration of high levels of strains is found in the fat pad under the flexor digitorium brevis.

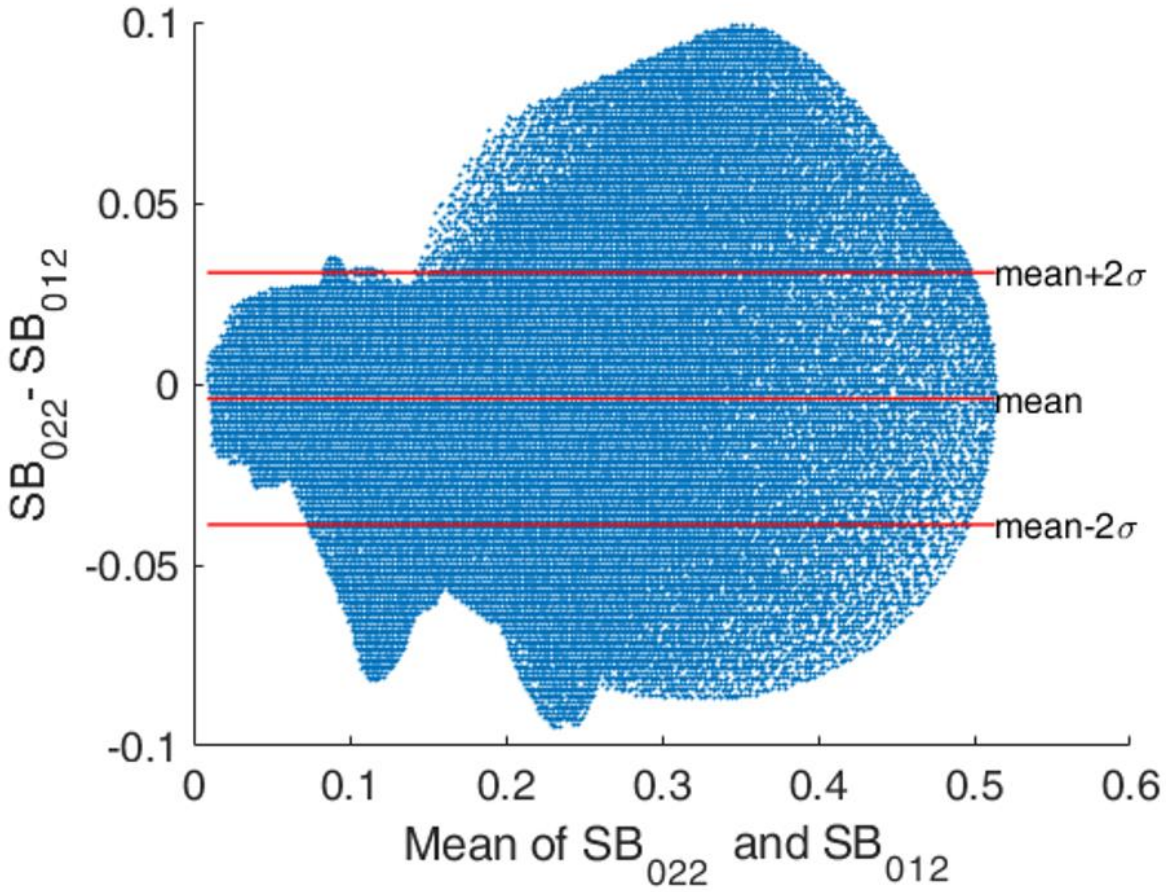

Figure 26: Bland-Altman plot referring to the strain estimation computed from Case B: heel under normal+shearing load.

Figure 26 shows the correlation between the strain measurements of the heel under normal+shearing loads (Case B of *Table 5*). Errors of 0.1 are observed across most of the strain intensities even for the highest strains (around 0.5). These errors tend to narrow down for the peak values. The SD shows that 95% of voxels have a strain error lower than 0.04. In general, this shearing configuration (Case B) shows errors with a double intensity and twice the propagation with respect to the normal load configuration (Case A).

4.3.2. Strain measurements for sacrum under normal load (case C, *Table 5*)

For the sacrum loading configuration (*Figure 27*), the highest levels of displacements are found around the edges of the indenter. Shear strains are concentrated on the soft tissues around the contact area between the indenter and the skin. Adipose tissue and skin are subject to the highest levels of strains.

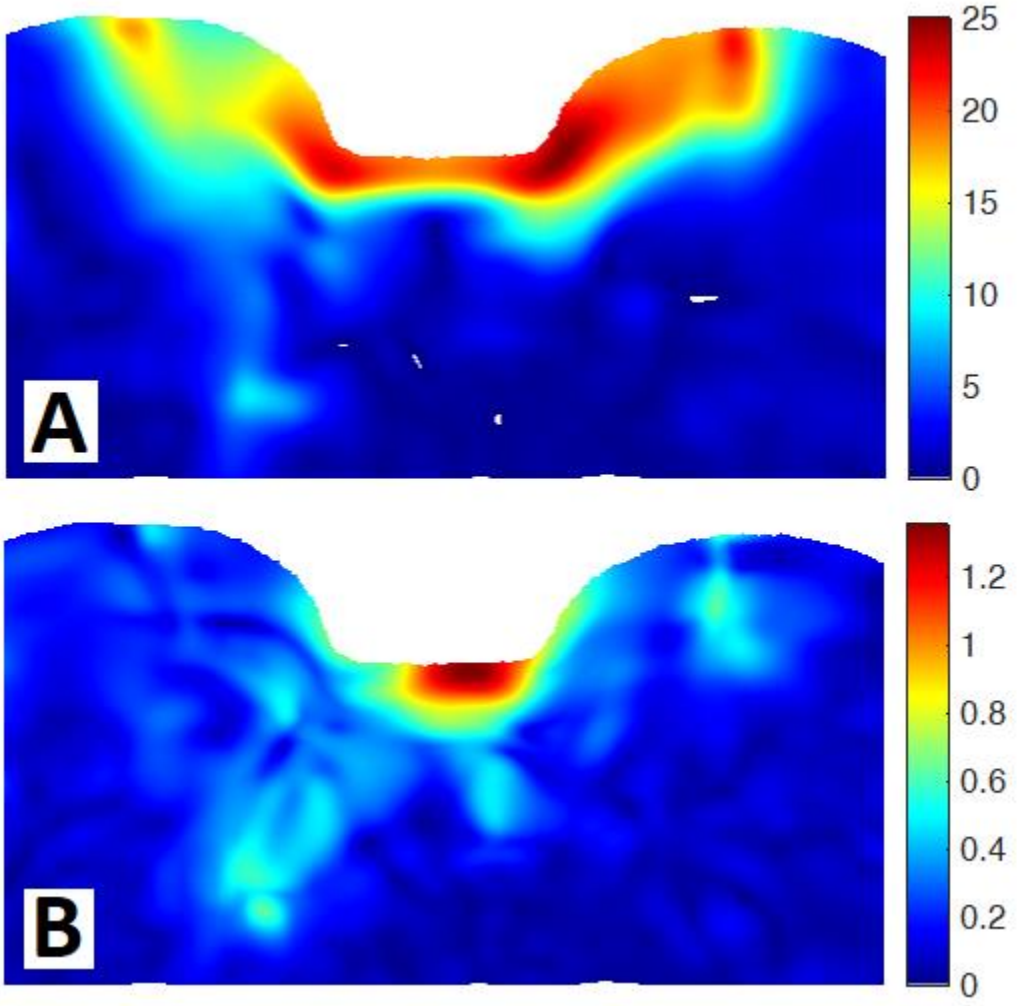

Figure 27: (A) Modulus (in mm) of displacement field for sacrum under normal load DC_{011}. (B) Max GL shear strain field for sacrum under normal load SC_{011}.

Figure 28 presents the Bland-Altman plot between the shear strain measurements produced by an indenter on the sacrum region (Case C of *Table 5*). In this case, the errors are considerably higher than what was observed for the heel application. Errors of 0.3 are spread throughout the image and the SD describes an error distribution where 95% of the voxels have an error that is lower than 0.15.

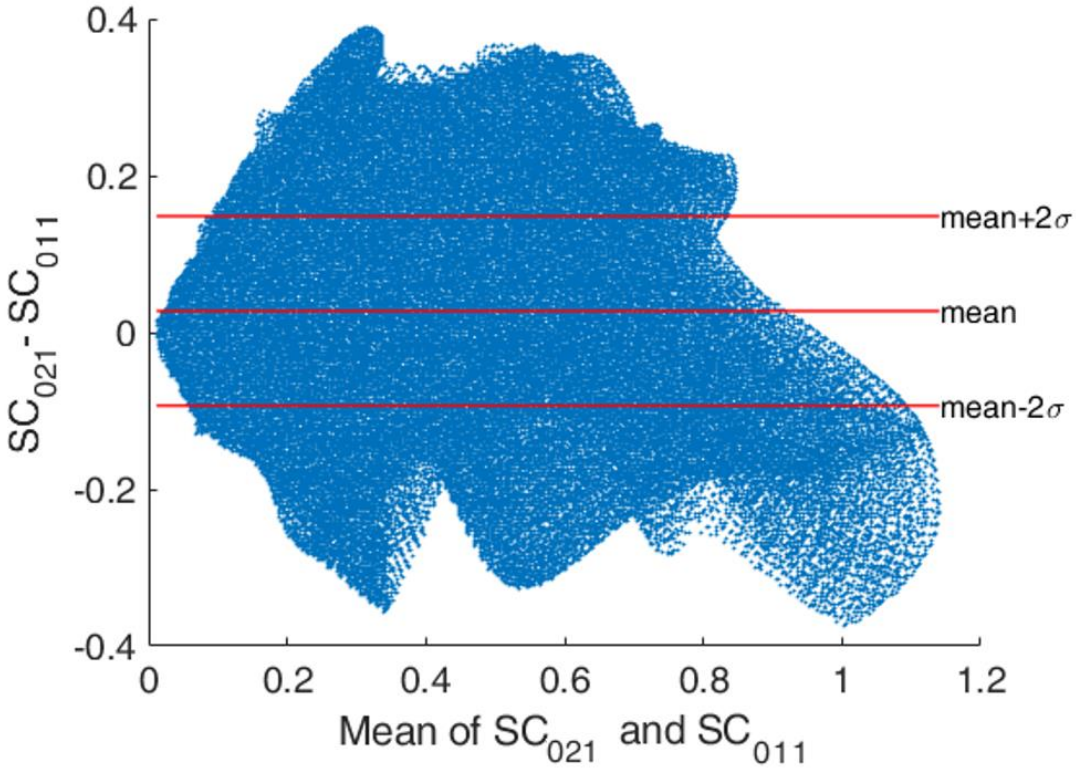

Figure 28: Bland-Altman plot referring to the strain estimation computed from Case C: sacrum under normal load.

4.3.3. Estimation of strain field generated by the FE model (case D, Table 7)

Figure 29 shows the results of image registration in the estimation of the artificial displacement field generated by Ansys (*Figure 21*). Magnitudes of displacements were selected in order to generate strains comparable with Cases A and B.

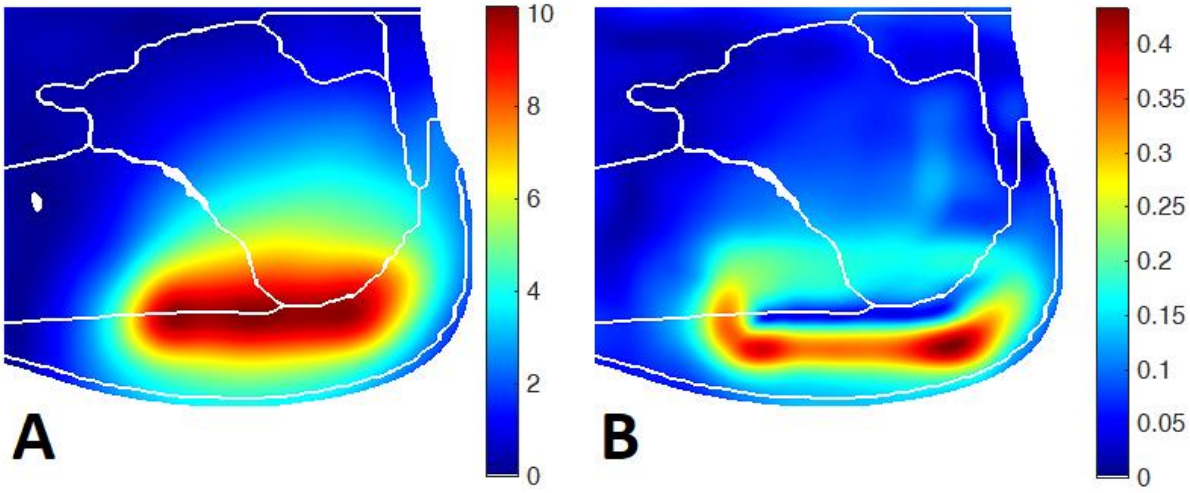

Figure 29: (A) Estimation of the displacement field (mm) generated by Ansys DD. (B) Estimation of GL max shear strain generated by Ansys SD.

Figure 30 presents the correlation between the strain field calculated by Ansys and the corresponding measurements obtained by image registration (Case D of Table 7). The error distribution is comparable to Case A. For the regions with the highest levels of strains, the measurements slightly underestimate the strains since the points distribution shows an inclination that is higher than the red line. This artifact could be a result of the transformation step described in Table 6. In this process, some details of the original displacement field could have been lost in the image reconstruction after the application of the displacement to the respective voxels.

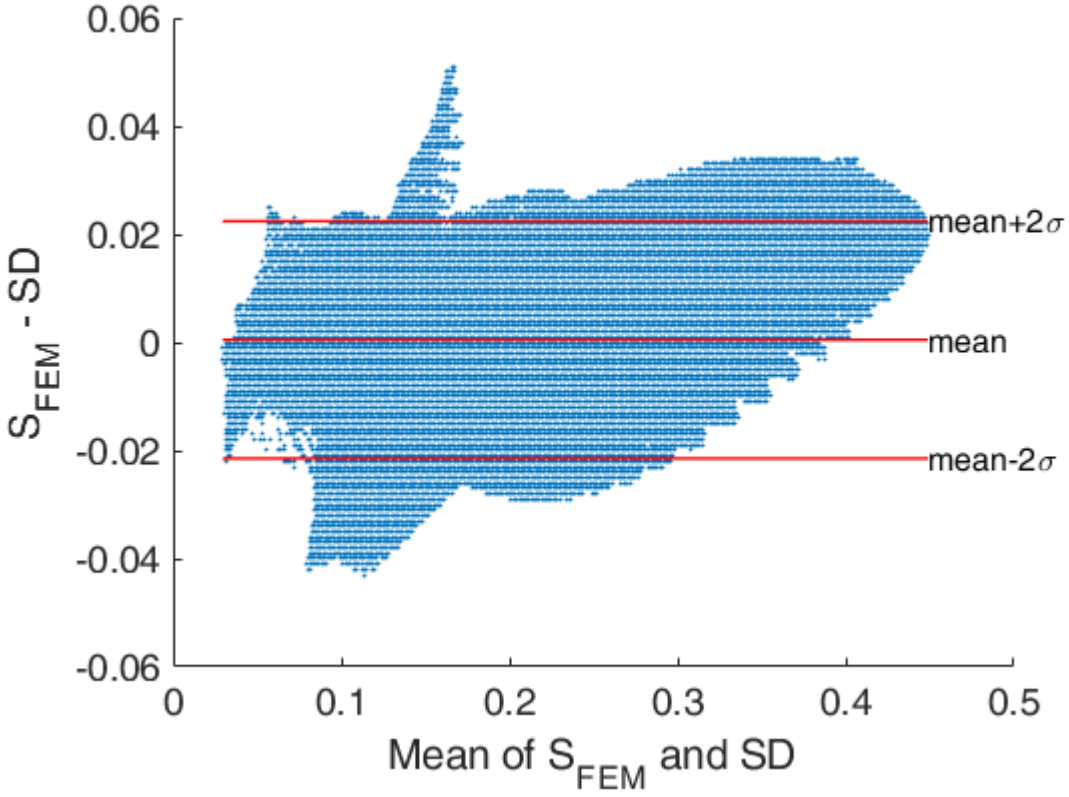

Figure 30: Bland-Altman plot referring to the strain estimation computed from Case D: Displacement field generated by Ansys.

4.3.4. Deformation field from Ansys – Same noise pattern (case E, Table 7)

This case is running the registration between two images with the same noise pattern, undeformed (Heel 01), and artificially deformed (Heel FEM). Using the same image helps considerably the algorithms of the image registration process since the noise pattern present in the unloaded image matches the one of the unloaded image. This allows to easily identify the respective deformation matching the voxels with their equivalent copy in the respective deformed image. Results in terms of error distribution are as expected very precise showing a relevant strain field estimation (*Figure 31*). This reflects the described facilitations in terms of using an image and its deformed version in the registration process.

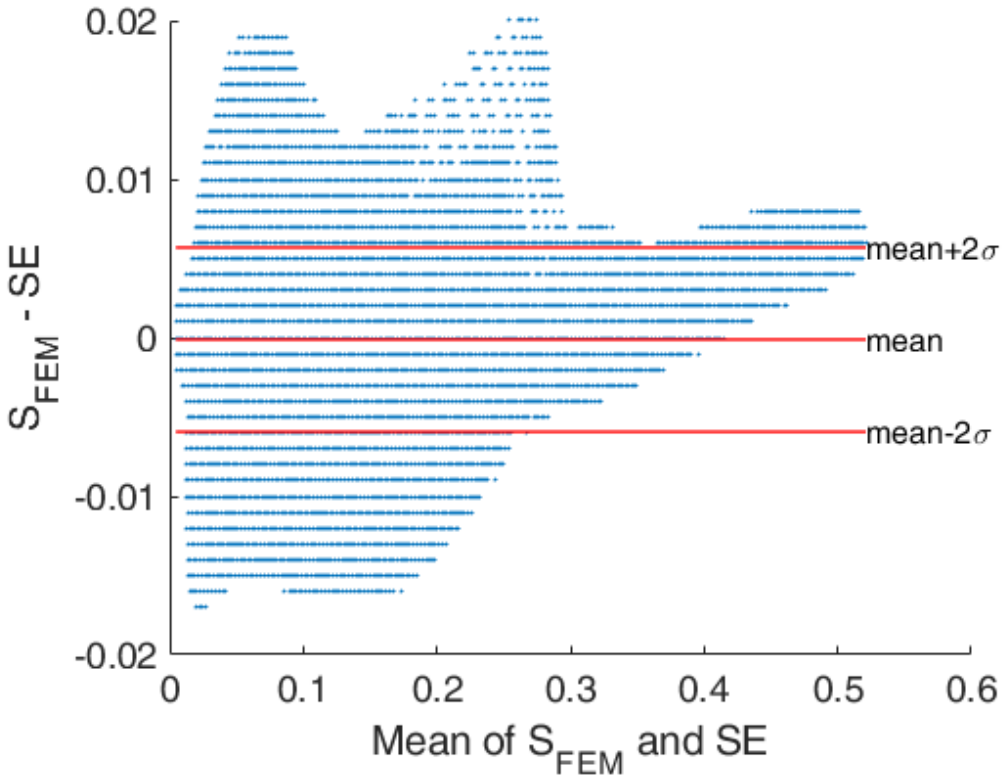

Figure 31: Bland-Altman plot referring to the strain estimation computed from Case E: Displacement field generated by Ansys.

4.3.5. Deformation field from Elastix (case F, Table 7)

Case F is analogous to Case D with the main difference that the considered displacement field is not generated by Ansys but is taken from the image registration computed in Case A. The error distribution in terms of maximal error and SD is comparable to Case A (*Figure 32*). For the regions with the highest levels of strains, as detected also in case D, the measurements slightly underestimate the strains. In this case, the deformed image is also the result of an image transformation reported in Table 6.

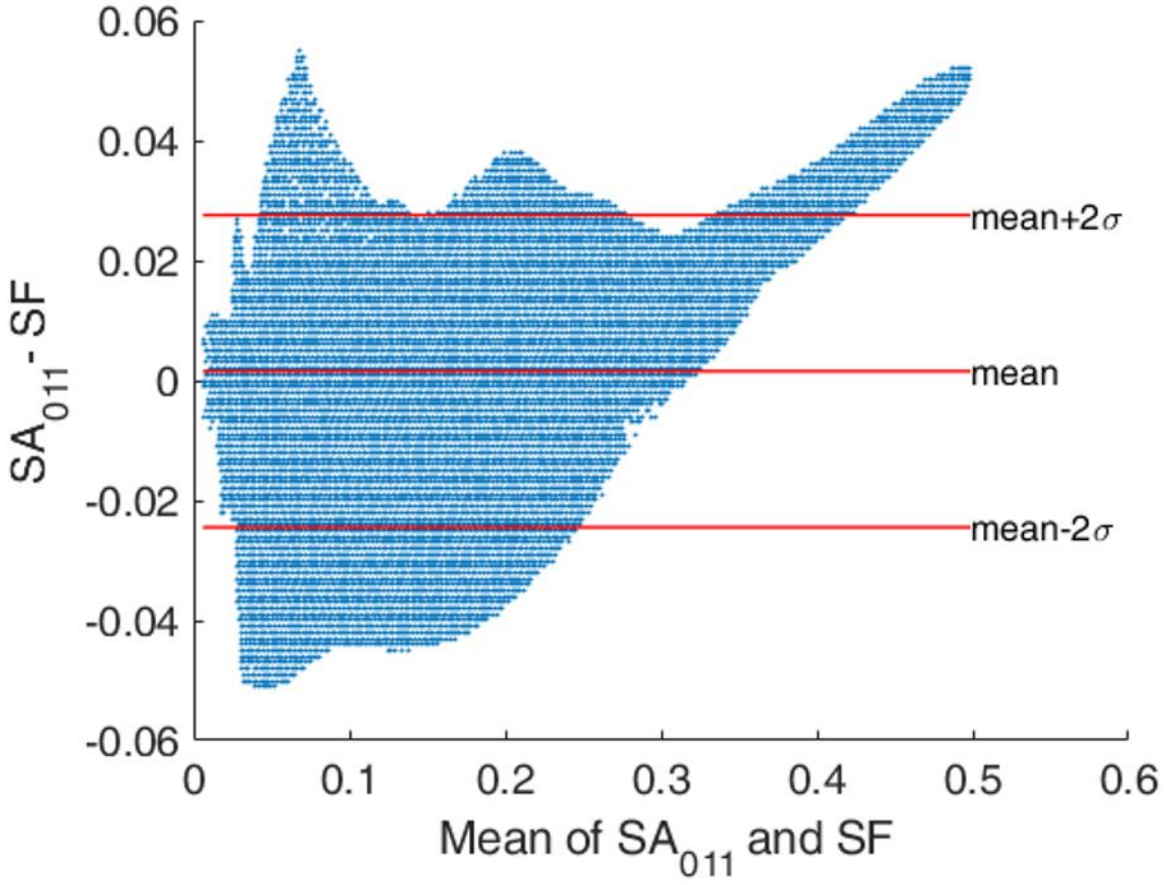

Figure 32: Bland-Altman plot referring to the strain estimation computed from Case F: Displacement field generated by Elastix in Case A.

4.4. Discussion

In this study, a method to estimate 3D internal tissue strains in the heel and sacrum regions based on DVC-derived displacement fields was developed in the context of pressure ulcers etiology. The methodology to implement DVC between two MR exams of human soft tissues (one at rest and the other one deformed) and to estimate the internal strains from the DVC 3D displacement field was first described. The implemented methodology requires a MR compatible device to apply loading on the skin surface during the acquisition of MR images. The obtained acquisitions was then used as input for 3D image registration. Images were first aligned based on the fixed body part (like bones) and then the non-rigid transformation was calculated. This transformation consists of a displacement field mapping every voxel between its initial position in the unloaded image and its final position in the loaded image. The Green Lagrange shear strains

are then computed from this displacement field. This methodology was implemented to analyze strain propagation in body regions that are critical in terms of pressure ulcer development: heel and sacrum.

For the results related to the heel pad, the calculated strain maps show as expected shear and compressive strain concentrations around the bony prominences of the calcaneus. This is coherent with the study of Luboz et al. which highlighted that strains generated around the calcaneus head strongly depended on the shape of this calcaneus bone [32]. Strains values in the deep tissues of the human heel were considerably higher than those in superficial tissue layers (*Figure 23*B). This is consistent with previous findings listing the strain concentration in deep tissues as a key aspect in the etiology of ulceration [115]. The strains were concentrated in the fat pad region and propagating towards the interface with the muscular region. Oomens et al. identified skeletal muscle and fat as the two main biological tissues where pressure ulcers could develop [27]. The application of a shearing load pushing the first layer of skin towards the forefoot generated significantly higher shearing loads in the anterior region of the fat pad compared with the configuration with only normal plantar pressure. Shear loadings can therefore impact significantly wider regions with higher levels of shear strains compared with normal loads of comparable intensity. This confirms what Ceelen et al. stated, namely (1) that shearing loads are more dangerous to treat than normal loadings, in terms of shear strain concentrations, and (2) that they must be taken into consideration for an effective pressure ulcer prevention [116].

For the results related to the sacrum, the calculated displacement and strain maps have values that are significantly higher than the results from the heel. The application of a load by means of an indentation device with a small contact area is probably more likely to generate higher shear strains right on the contact surface between the skin and the indenter [116].

The second objective of this article was to evaluate in a general way the reproducibility and the trueness of strain calculation through image registration. Respectively, two main methodologies were presented: one related to the repetition of the same strain measurement from an equivalent set of images, and the other one to the calculation of a known *a priory* displacement field.

Concerning reproducibility as how much two equivalent measurement match, *Figure 24*,*Figure 26*,*Figure 28* are considered. Comparing the strain error distribution between image registrations of the heel related to Case A and Case B, we found that errors are twice higher and more distributed in the case where the shearing load is applied. This suggests that strain measurement from image registration is affected by the type of deformation applied on the soft tissues. A possible explanation for this effect can be related to the fact that a normal load displaces the skin in a normal direction generating a clear displacement of the edge between the portion of image representing the biological tissues and the dark background (see *Figure 20*

Heel 01 and Heel 1). On the other hand, a shear load displaces the skin only in a tangent direction to the surface of the skin without generating any clear movement of the edge between the skin and the background (see *Figure 20* Heel 1 and Heel 2).

The image registration related to the sacrum has a much wider strain error distribution and values compared to the examples of the heel. This implies that strain measurement from image registration strongly depends on the image characteristics. To explain the reasons behind this we can try to analyze how image registration works. The first steps in the algorithms of image registration are feature detection and feature matching [117]. Salient and distinctive objects as edges, regions are considered as features. The trueness of image registration therefore directly depends on the quality of the acquired images [118]. The main parameters that characterize the quality of digital images are related to resolution and noise [119]. Noise is generated by the statistical fluctuation of the value from voxel to voxel. A common measurement of noise is the standard deviation, a measure of how spread out the values of the pixels are. The lower the standard deviation, the higher the accuracy of the average voxel value [120]. Spatial resolution is the ability of the imaging system to detect small objects that are close to each other [121]. The size of the voxels defines the maximum spatial resolution. However, image resolution is also influenced by other parameters such as blur factors. The most common blur factor is motion blur: when motion occurs during acquisition, the boundaries of patient structures will move from their initial position, making the boundaries blurred in the image [122]. The motion can in general be reduced by fixing the body part with heavy MR-compatible pillows or casts [100]. These solutions, however, are ineffective when motions are generated by physiological movements such as breathing, peristalsis or heart beats. The line spread function (LSF) can be used to evaluate and quantify spatial resolution [123][124]. From this parameter, it was calculated that in the more crucial region of the images, the MR image of the heel had a quality parameter related to the spatial resolution that was 4.5 time higher than the one calculated for the sacrum images. It is possible therefore that this aspect played a crucial role in the strain estimation through image registration, thus decreasing significantly its reproducibility.

Concerning trueness as how close a measurement is to a known or accepted value, Cases D and F were considered. These cases report errors of shearing strains around 0.02. This value can be compared to the level of strains that is considered to be sufficient to generate significant tissue damage. According to Ceelen et al., this value is around 0.65 for the shearing strain [125].

An interesting aspect is related to Case E, which uses the same image Heel 01 and its transformed version (Heel TRA) for the estimation of the displacement field. In this case, the strain errors are much less distributed (with a 95% confidence value below 0.007 error). This is due to the fact that any variability due

to noise, or other artifacts, present in both images will have an impact on the strain estimation. This implies that for images with appropriate quality levels, this methodology can reach high trueness.

The diversity of results obtained between the heel and sacrum applications implies that crucial further research is therefore required in finding the relation between specific image quality parameters and the respective error distribution in the strain calculation. This would permit in fact to select the image acquisition protocols in order to obtain the type of images to minimize errors in the registration process.

An advantage of the proposed methodology to calculate strains is that no additional tool to perform the error estimation is required. Considering Case E, the error estimation can be performed just with an additional image transformation (Table 6) and the respective image registration.

It is clear that the trueness of the results is strongly related to the image registration process and to the selected parameters to perform it. By tuning the respective parameters of the registration process, it is possible to identify smaller deformations or to select the amount of volume compression and expansion. An optimization for the selection of the ideal parameters of the registration for the related application will be considered in the future steps to improve the accuracy of this methodology.

It must be considered that this work was based on specific mechanical configurations of a single subject meaning that results obtained are to be considered specific to this application. Fat and muscle biomechanical properties can change significantly as a consequence of diseases (for example, diabetes) and chronic immobilizations [8][126]. This inter-subject variability may introduce significant variations in the strain calculations making imperative to analyze each subject specifically.

4.5. Conclusion

The results obtained from the practical application on the heel and sacrum, in terms of location and magnitude of strains, are in line with the literature. This technique of calculating strains offers broad new possibilities to analyze the impact of external loads on the internal state of the soft tissues. The standard technique of FE is a very complex and time-consuming task involving segmentations, meshing and selections of proper constitutive laws. The possibility of strain calculation through image registration can provide results in terms of strain propagation in a significantly faster framework and offer the possibility for comparison and validation with results obtained from FE simulations. The present study proposed to quantify subdermal tissue strain distributions on the heel and sacrum from image registrations based on MR-acquisitions. This data is crucial for understanding the etiology of pressure ulcers that occur in the deep tissues of the heel pad.

The pilot study described here indicates that the crucial steps for computing strains from image registration are feasible to be implemented in a wider study. Further research will include analysis on more subjects and with different loading configurations, together with the adaptation of this methodology to different parts of the body to gain insight into the relative mechanical soft tissue properties.

The next chapter will describe the generation of a Finite Element model of the human heel and its validation with the described DVC technique. Secondly, this validation will be extended to compare various constitutive materials from the literature, implemented in our heel FE geometry. The constitutive models that best approximate the data obtained from our experiment are then discussed.

5. Chapter 5

Definition and validation of a finite element model of the human heel for diabetic foot ulcer prevention under shearing loads

The previous chapters have allowed us to complete our dataset to provide the full simulation environment in which the FE model will be developped. From the MR experiment, the geometry and boundary conditions, in terms of applied loads, were defined. From the operations performed in chapter 3 with image transformations, the strains and their error magnitudes where calculated. In this chapter, we will finally use this dataset to define and evaluate the FE model of the heel for the prevention of diabetic foot ulcers. A special emphasis will be given to the shearing strains generated by the shearing loads as these are considered to be the most dangerous.

This chapter was adapted from an article recently submitted to Journal of Biomechanics:

Alessio Trebbi, Nolwenn Fougeron, Yohan Payan.
Definition and evaluation of a finite element model of the human heel for diabetic foot ulcer prevention under shearing loads, *Journal of Biomechanics*.
(under review).

5.1. Introduction

Finite Element (FE) modelling is a technique that is considered to have the potential to assist the prevention of diabetic foot ulcers either as a tool for preclinical testing of support interfaces and/or identifying anatomical risk factors [29][108]. This solution is a conventional computational technique for estimating internal stress and strains derived by the application of a surface loading. This information can then be used to predict tissue damage where these exceed appropriate thresholds [116]. However, the link between mechanical loading and tissue damage is still not completely understood which hindered the diffusion of FE models in the clinical routine.

Soft tissues can be loaded perpendicularly, described clinically as pressure, or in a direction parallel to the skin surface, described as shear. Nowadays it is considered that a combination of these two loadings could result (I) in occlusion of blood and lymphatic vessels which is suspected to be very damaging [127] and (II) the weakening of the cellular membrane of the soft tissues cells [128]. In the last decade, attention has been drawn on the role that shear strains could play in the development of deep tissue injuries [129][130]. It is therefore nowadays believed that a FE model should properly simulate the behavior of soft tissues under shearing loads, in order to successfully predict the formation of PUs. A common methodology to simulate the heel in a loaded configuration is to apply an imposed displacement on the skin surface and analyze the resulting strains [33][131]. Injury criteria include maximum values of strains, averaged over a volume (called “cluster” [31]) in which a specific threshold is exceeded. In general, peak stress and strain values tend to be strongly mesh dependent and can become unrealistically high when a specific element is squeezed in the mesh. Therefore, a solution that gives a quantitative estimation of the tissue cluster under a specific strain threshold is recommended [27].

Experimental data on injury thresholds was reported by Ceelen et al. which demonstrated that the Green-Lagrange maximal shear strain was the best predictor of pressure injury [125]. In a subsequent study, the team demonstrated that these strains could be estimated with FE modelling [132]. However, the design of personalized FE model is still an open challenge, more particularly considering the characterization of the constitutive behavior of each soft tissue included in the model, such as skin, fat, muscles [105].

As the boundary conditions implemented in the models published in the literature are different, the results provided by such models are difficult to compare [61][82]. When considering studies involving FE models of the heel, researchers adopt stiffness parameters from curve fitting data from cadavers or animals [7][81], inverse modelling [133], or values extracted from other published papers [134]. Data on soft tissue mechanical properties is very diverse and strongly depends on the considered tissue. For the same

material, it is possible to find studies reporting stiffness parameters that differ of several orders of magnitude [134][135]. This can be misleading and confusing when researchers have to select a specific set of constitutive laws and parameters for a FE model to simulate a specific configuration. At this point, it is clear that new tools are required to evaluate these FE models.

FE analyses require a consistent and robust methodology for evaluation, involving rigorous experimental measurements [10]. In the literature, most studies establish the validity of FE models via experimental measurements. Concerning foot modeling, researchers proposed to evaluate FE models in terms of their capacities to predict interface plantar pressure (by comparing the contact pressure predicted by the model with the measurements from pressure mattresses) [76]. Yet, as observed in Macron et al. on data from 13 healthy volunteers, interface pressure distributions do not correlate with internal strains [108]. Therefore, pressures cannot be used to predict the internal strains. Linder-Granz et al. compared soft tissue contours provided by the simulation in the deformed configuration to the segmented contours obtained from MR images [28]. This comparison, however, considers only the external geometry and not the quantity of interest, which are the local internal tissue displacement and the associated strains. Probably the most crucial aspect is that, to the best of our knowledge, none of these models were evaluated with any technique to analyze specifically their performances under shearing load conditions.

In a recent work, Trebbi et al. proposed a Digital Volume Correlation (DVC) technique based on volumetric Image Registration (IR) of Magnetic Resonance (MR) images to calculate internal strains from the application of shearing loads [136]. This solution is based on finding the non-rigid transformation that matches two MR images of the same body part, one in an unloaded configuration and one in a mechanically loaded configuration [110]. Tissue strains in the loaded deformed configuration are then computed from that non-rigid transformation field. This solution offers a methodology to quantitatively evaluate the strains that are simulated from a FE model deformed with the same loading configuration.

The objective of this chapter is to define and evaluate a FE model of the human heel for diabetic foot ulcer prevention. To this purpose, a 3D subject-specific FE model of the human heel is elaborated. We propose to derive the constitutive laws for the soft tissues, from experimental data published in the literature. For each tissue (skin, fat and muscle) the experiment curve (such as the stretch/stress curve from an uniaxial tensile test done on ex vivo specimen) is fitted to optimize a constitutive law and its corresponding parameters values. Regarding the evaluation, it is believed to be crucial to analyze the behavior of soft tissues under shearing loads configurations, as these are considered the most dangerous for triggering PU. The strains computed by the FE simulations under shearing loads configurations are compared with the strains measured by the IR methodology proposed by Trebbi et al [136]. In parallel, another type of analysis

is developed by comparing the simulation results with other constitutive laws proposed in the literature for the definition of heel FE models. This is done to analyze the constitutive behavior of the proposed model with respect to the other ones already published in the literature.

5.2. Methods

5.2.1. Imaging

A healthy volunteer (male, 40 years old) gave his informed consent to participate in the experimental part of a pilot study approved by an ethical committee (MammoBio MAP-VS pilot study N°ID RCB 2012-A00340-43, IRMaGe platform, Univ. Grenoble Alpes).

For that heel MR image datasets, the volunteer was placed in a supine position with his right foot locked in a MR compatible device designed to apply both a normal force or a combined normal-and-shearing force on the heel pad by means of an indenting platform. Two different amounts were selected for each type of load in order to account for the hyperelasticity of the tissues. The setup is illustrated in Figure *33*. A double face tape was applied on the plate surface to allow the application of the shearing load without any slipping. A proton density MR sequence was used to collect 3D images composed of 512x428x512 voxels with voxel size of 0.3125 mm x 0.375 mm x 0.3125 mm (MR system Achieva 3.0T dStream Philips Healthcare).

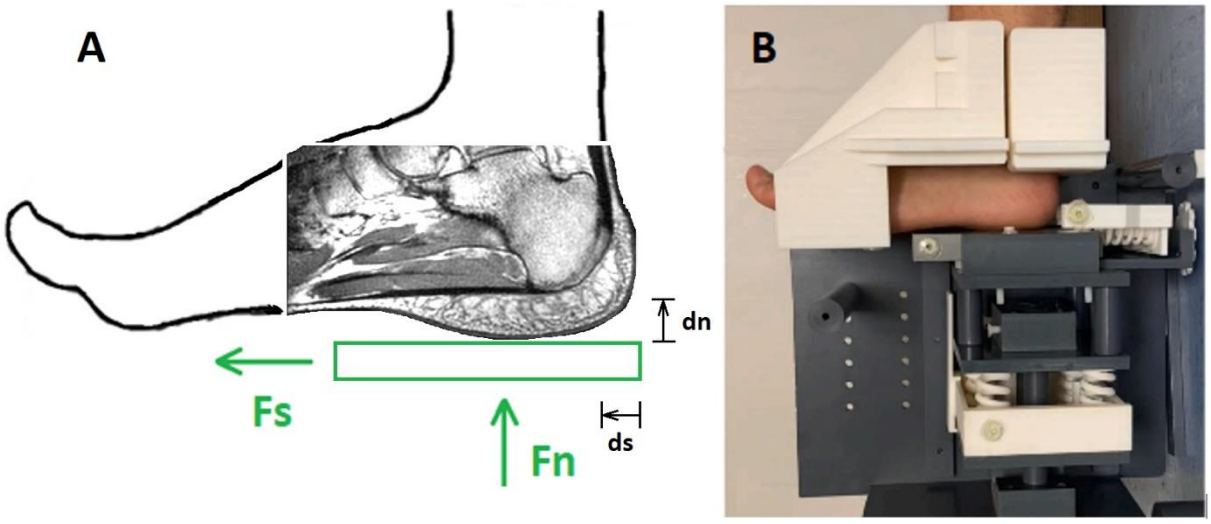

Figure 33: A) Schematic representation of load application on the heel in the MR acquisition. The green rectangle represents the loading platform and the respective arrows show the application of forces (Fn normal force, Fs shearing force). The plate displacements (dn normal displacement, ds shear displacement) are shown in black. B) Internal view of the MR compatible device described by Trebbi et al. [110].

Five 3D MR images of the heel were considered in this contribution and were referred to using a unique name as listed in Table 8.

Name	Description	Load
Load0	Unloaded heel	0 N
Load1	Heel with high normal load	140 N
Load2	Heel with normal load	15 N normal
Load3	Heel with normal and high shearing load	15 N normal and 45 N shear
Load4	Heel with normal and shearing load	15 N normal and 12 N shear

Table 8 : List of lading configurations

A 2D sagittal snapshot of the MR volume of Load0, Load1 and Load3 is provided in *Figure 34*.

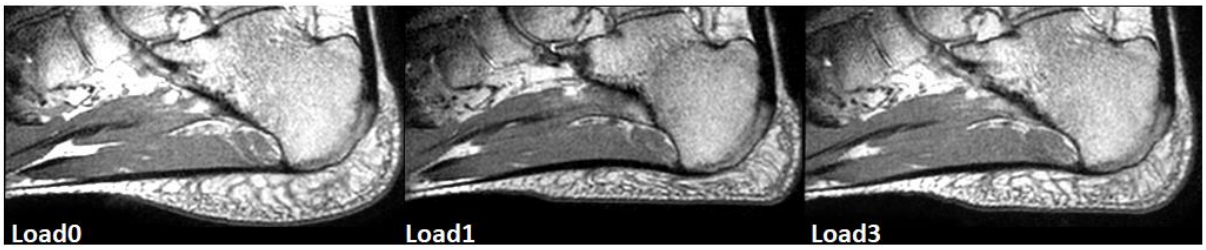

Figure 34: Sagittal MR slices for the loading configurations Load0-unloaded, Load1-normal load, Load3-shering load.

5.2.2. Generation of the heel 3D FE mesh

Manual segmentation of MR images was performed using Amira 6.5.0 (Thermo Fisher Scientific Inc.). The unloaded Load0 acquisition was used to segment the calcaneus, fat pad, muscle and skin. The resulting surface files were imported in HyperMesh 2019 (Altair Engineering, Inc.) for FE mesh generation. This 3D mesh (*Figure 35*) was composed by 80,000 linear tetrahedral elements (with a mesh size of 2 mm). The 3D mesh was then imported into ANSYS 19.2 APDL (ANSYS, Inc., Canonsburg, PA). A rectangular platform was created underneath the FE model of the heel representing the plate of the loading device. A mesh convergence study was performed to verify the consistency of the simulations for the adopted mesh density.

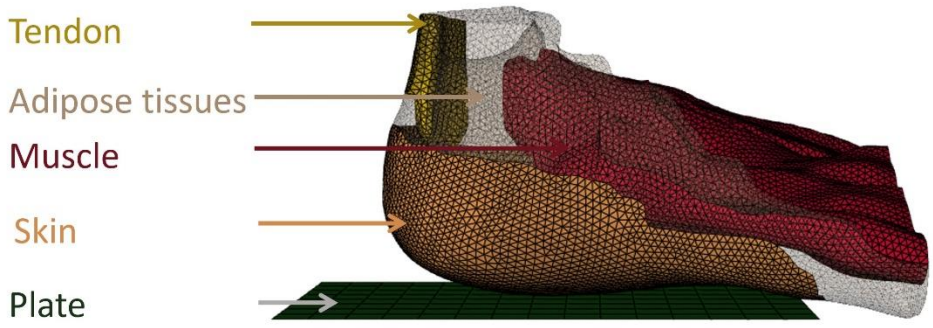

Figure 35: Finite element mesh of the heel generated from MR image segmentation

5.2.3. Material properties

The calcaneus bone was assumed to be rigid [137]. The boundary between the bones and soft tissues were modeled as a rigid surface. The skin was modelled with an Isihara's et al. law (equivalent to a Yeoh constitutive law with the parameter C_{30} equals to zero) [138]. Material parameters were optimized using a curve fitting method with Matlab (MathWorks Inc, USA) from the skin experimental data of Annaidh et al. [139]. Muscles were modeled using a Yeoh constitutive law with the same procedure using the data of uniaxial tensile test from Gras et al. [140]. Considering the fat pad, a first order Ogden constitutive law was chosen as proposed by Moerman et al. [141]. Material parameters were optimized using the same procedure according to the quasi-static experimental data from Miller-Young et al. who performed several compression tests on the foot fat tissues [69] *Table 9* (Figure 36).

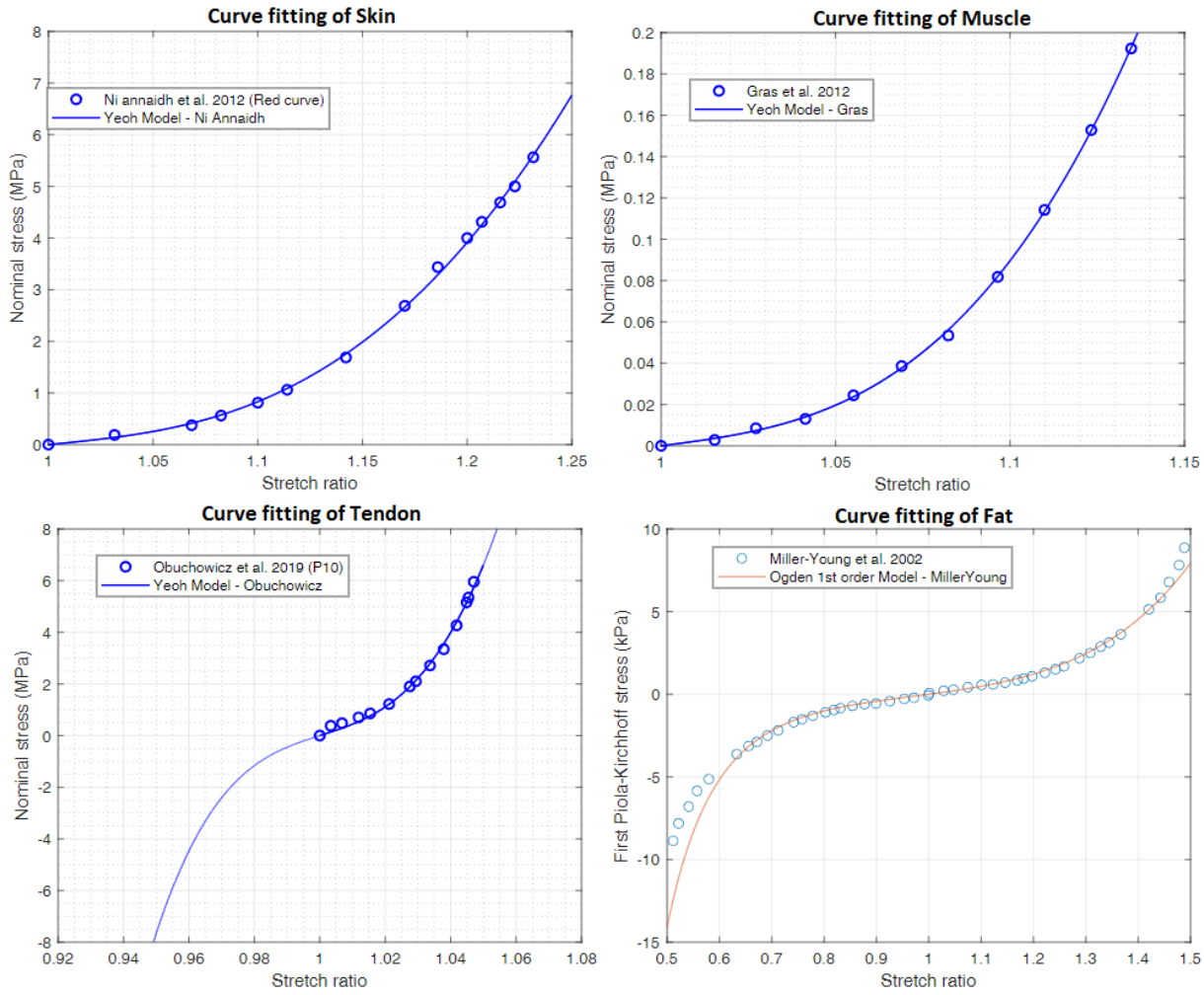

Figure 36: Curve fitting process to define the constitutive laws obtained from experimental data in literature (This step was performed in collaboration with my colleague Nowlenn Fougeron).

Incompressibility parameters in all directions were supposed equal and were computed from the formula provided in Mott et al. [142] for each material, assuming a Poisson ratio ν of 0.4999:

$$D_1 = D_2 = D_3 = \frac{3(1-2\nu)}{2C_{10}(1+\nu)}$$

Tissue	ν	μ (MPa)	α	C_{10} (MPa)	C_{20} (MPa)	C_{30} (MPa)	D_1 (MPa^{-1})	D_2 (MPa^{-1})	D_3 (MPa^{-1})
Fat	0.4999	0.0034	6.2				0.1177	-	-
Skin	0.4999			0.2650	1.9230	-	0.0008	0.0008	-
Muscle	0.4999			0.0050	0.0690	1.9670	0.0400	0.0400	0.0400
Tendon	0.4999			9.6540	189.7000	78 950	$2.1\ 10^{-5}$	$2.1\ 10^{-5}$	$2.1\ 10^{-5}$

Table 9 : Set of constitutive laws implemented in the FE model of the heel. With ν, the Poisson's ratio, set to 0.4999, to account for the nearly incompressibility of soft tissues.

In parallel, isotropic constitutive laws from the literature related to FE heel models were implemented in the heel FE mesh to compare the results of the corresponding simulations. Table 10 lists the six hyper-elastic material laws and their respective parameters that are compared here.

Study	Tissue	Method	Model	ν	α	μ (kPa)
Akrami [143]	Homogeneous	Average	LE	0.49		385.9
Edemir [133]	Homogeneous	Inverse modeling	OG	0.49	6.82	16.45
Friedman [134]	Skin	Literature [144]	NH	0.495		324.7
	Fat	Literature [145]	NH	0.495		0.290
Luboz [32]	Skin	Average	NH	0.495		66.89
	Fat	Average	NH	0.49		10.07
	Muscle	Average	NH	0.495		20.07
Spears [145]	Skin	Inverse modeling	OG	0.49	6.80	640
	Fat	Fitted	OG	0.495	8.80	0.290
Zwam [135]	Skin	Literature [32]	OG	0.49	2.3	50
	Fat	Literature [133]	OG	0.49	6.82	16.45
	Muscle	Literature [32]	LE	0.49		20.07

Table 10: List of constitutive models presented in the literature for the soft tissues of the human heel. LE = Linear elastic, OG = Ogden, NH =Neo-Hookean. The coloring on the tissue column are made in order to facilitate comparisons between the same tissues.

5.2.4. Mesh convergence study

Some preliminary simulations were performed in order to check the convergence of the results related to the mesh size. The same simulation was performed with six new meshes which elements sizes ranged between 1.5 and 5.5mm. Results in terms of soft tissue volume subject to a specific amount of strain are shown in Figure 37. From the plot, we can see that by varying the mesh size around the selected size (2mm), the results in terms of shear strain do not change a lot. This validates the implemented mesh size.

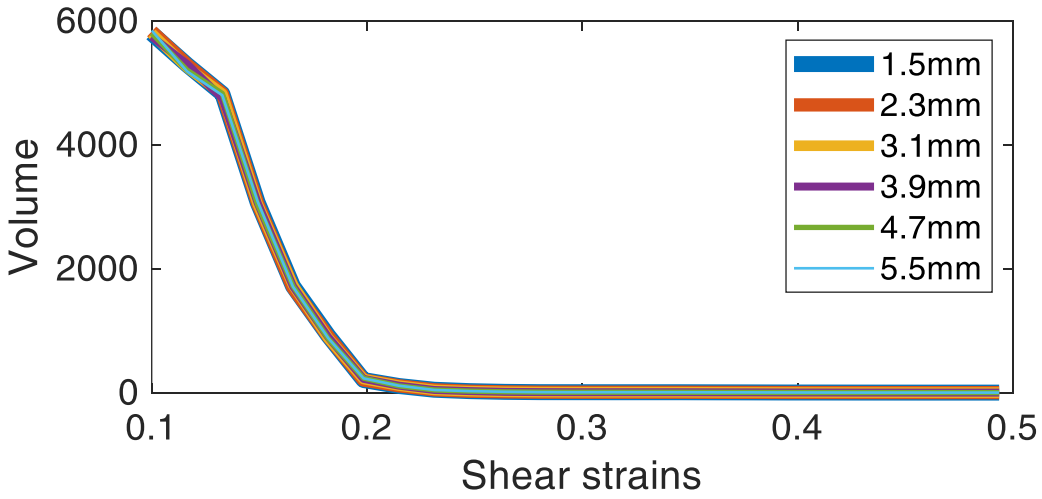

Figure 37 Mesh convergence study showing the results in terms of volume of tissue subject to a specific amount of shear strain. The considered meshes ranged from the thinnest 1.5 mm to the coarsest 6mm.

5.2.5. Boundary conditions

Boundary conditions were defined based on the MR load configurations. The FE model was fixed on the rigid bone boundaries while the rectangular plate was actuated to apply the respective loads. The simulations were divided in three steps: I) the plate was displaced by 3 mm to get in contact with the meshed skin, II) the normal load was applied on the plate, III) the shearing load was added. Contacts between soft tissue components (skin, fat, muscle) were assumed without sliding. The contact between the plate and the skin was also assumed as bounded since a tape was placed at this interface during the MR acquisitions (*Figure 35*).

5.2.6. Image Registration

The MR image registration technique presented in this chapter has been developed in a previous study [136]. The main details regarding the steps to perform the IR analysis are summarized in the following paragraph. For additional details concerning the trueness and repeatability of the measurements, the reader is referred to the associated publication.

DVC was implemented using the publicly available Elastix package used to non-rigidly register 3D MR images [102]. The four MR loaded images (Load1-Load4) of the heel were first rigidly registered to align the calcaneus bone with the unloaded image (Load0). Then, the image-based non-rigid registration was used to estimate the displacements and strains fields. Two images are involved in this registration process: the reference image, unloaded configuration (Load0), and the deformed image, loaded configuration (Load1-Load4). The registration between these two images defines a non-rigid deformation field, which describes how the reference unloaded image transforms into the deformed image. From the displacement fields obtained by the registrations, Green Lagrange maximal shear strain maps were calculated as described by Ceelen et al. [116].

5.3. Results

In order to evaluate each FE model (the one we propose and the six other models built with constitutive laws from the literature), the results from the simulations are compared with the outputs from the IR that are considered as a reference. First, the intensity of strains is discussed by analyzing the volume of tissue subjected to a specific amount of strain; this type of representation is indeed used in strain analysis for PU prevention [146][147]. Second, the location of strain concentrations is analyzed by inspecting sagittal sections that show the levels of strains in the internal layers.

5.3.1. Strain intensity

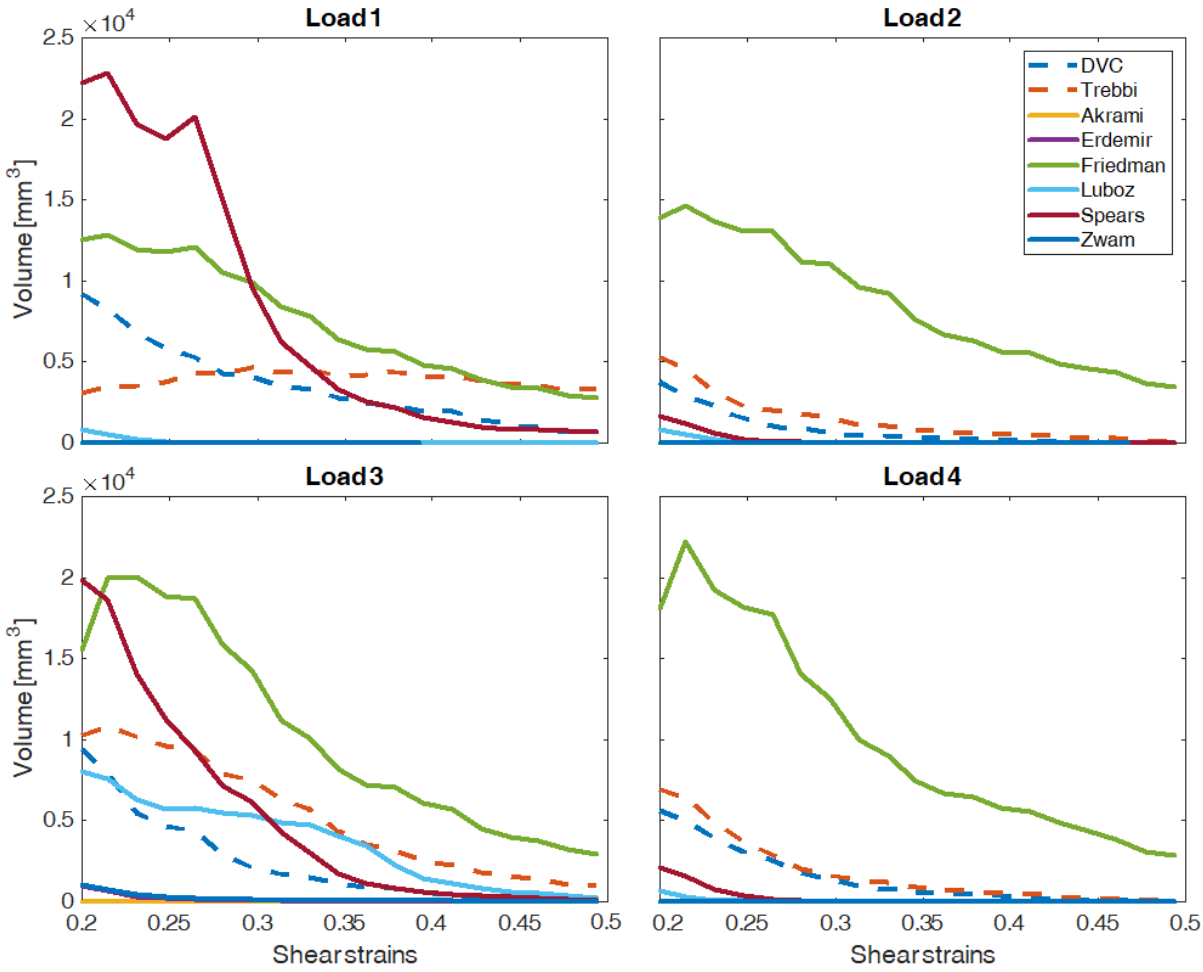

Figure 38: Volume of soft tissue subject to a specific amount of Green Lagrange shear strain intensity.

Model (10^5)	Trebbi	Luboz	Eedemir	Zwam	Akrami	Spears	Friedman
Load1	0.42	0.65	0.59	0.66	0.66	0.91	-
Load2	0.05	0.20	2.17	0.21	0.21	0.18	1.40
Load3	0.55	0.27	0.41	0.40	0.44	0.20	1.52
Load4	0.07	0.26	0.27	0.27	0.27	0.22	1.63
Total	1.11	1.39	1.50	1.57	1.60	1.51	>4.55

Table 11 : For each curve plotted on figure 4 and representing a given constitutive model, the area located between this curve and the reference DVC curve is computed. The higher the area is, the larger is the error. Constitutive models are ordered from the lowest total error to the highest one.

In this section, the amount of tissue under a specific intensity of strain is considered. The focus is given for strain levels comprised between 0.2 and 0.5. This was chosen for two reasons. First, the intensity of strains falls in this range for most of the configurations. Second, these values are the base levels of strain considered to be possible cause of tissue damage [116]. As proposed by Grigatti & Gefen [147], the volume of tissue subject to a specific amount of strain is plotted on *Figure 38* for the seven constitutive models studied here, as well as for the reference data measured with DVC. For each curve plotted on this figure and representing a given constitutive model, the area located between this curve and the reference DVC curve is computed. The higher the area is, the larger is the error. Table 11 summarizes the errors for each constitutive model and for each load configuration.

With this criteria, the constitutive law proposed in this chapter (called *Trebbi* here) seems to be the best to describe the strain intensities across the considered loading configurations (Table 11). The best fits are related to the configurations with the lower amount of load, namely Load2 and Load4. This emphasizes the complexity of modeling hyperplastic tissues that vary significantly their stiffness in relation to the amount of strain they experience.

The model of Friedman showed high levels of strains distributed in a large amount of volume. This is due to the low value of shear modulus implemented for the fat 0.290 kPa (*Table 10*). The same value was used by Spears, but in this case, a significant higher stiffness for the skin was selected. This resulted in a significant reduction of the strains for the lower loading configurations Load2 and Load4. The impact of shearing loads can be seen in the results from the model of Luboz. For Load3 (with 45 N of shearing load) the model had a considerable higher amount of shearing strains compared with Load1 (140 N of normal load). The models of Zwam, Erdemir and Akrami showed a stiff behavior that maintained the strain propagation low compared from the DVC results.

5.3.2. Strain location

In this section, the location of strain concentrations is analyzed by looking at a sagittal slice passing through the lowest point of the calcaneus. This slice was selected as experiments have shown that the highest values of strains are mainly located in this area. Results are plotted in Figure 39.

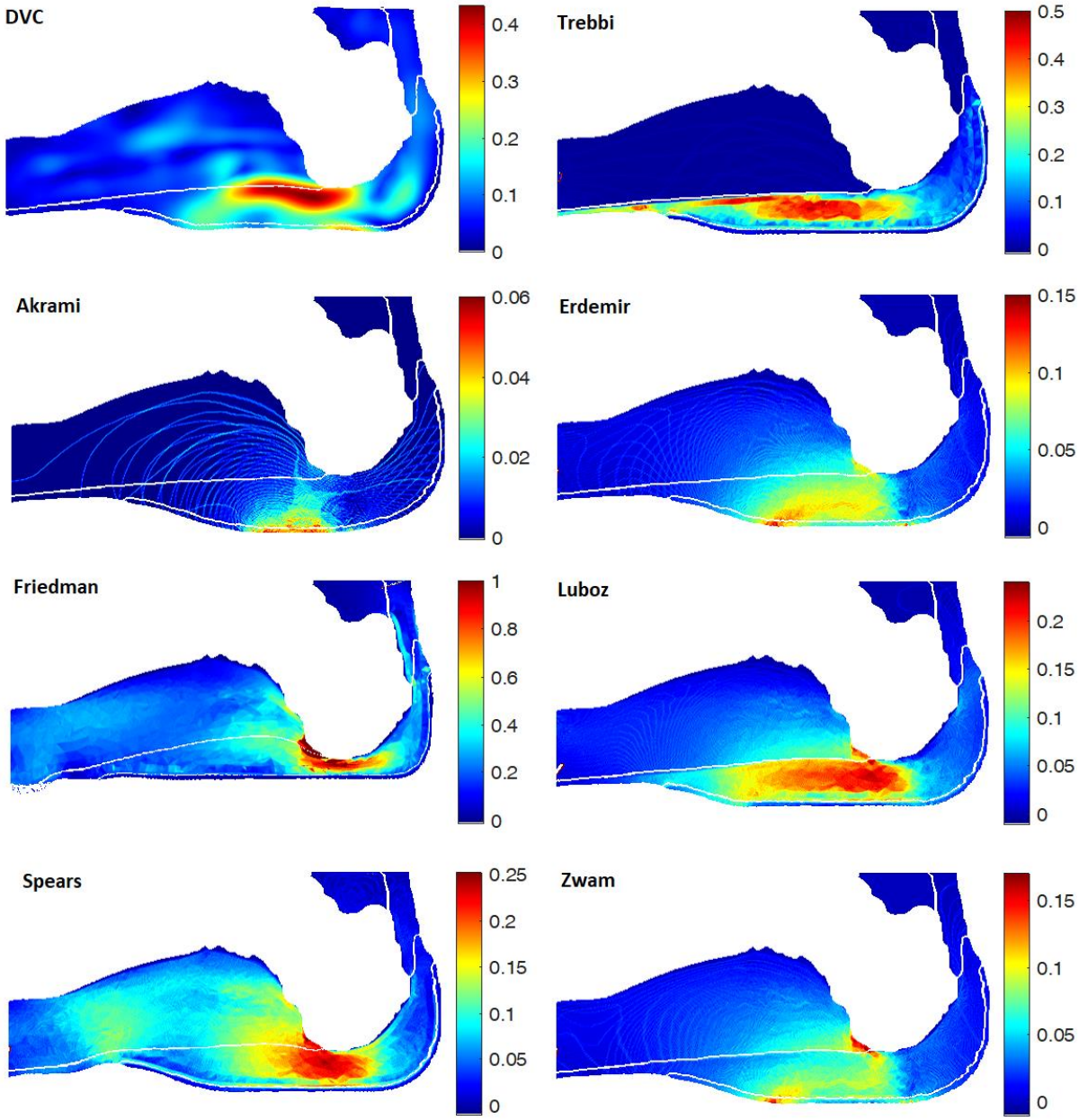

Figure 39: Green Lagrange strains propagation for all the constitutive models in loading configurations Load4 (15 N normal and 12 N shear forces).

The comparison shows that Luboz, Spears and Trebbi models provide strain concentrations in comparable locations with the DVC, namely in the fat pad around the calcaneus head with a propagation towards the forefoot under the aponeurosis.

Considered the proposed model (Trebbi) the strains keep propagating in the interface between the muscle and the fat. This is due to the different compliance between the constitutive laws of these two tissues.

With this respect, the muscle appears probably to be too stiff considering the uniform low levels of strains in the muscular region.

The selection of a stiffer behavior for the skin can be clearly seen in the models of Spears and Trebbi as there is a sudden change in the strain propagation in the interface between the fat and the adipose tissue. From the deformed shapes of the image, it is possible to have an idea of the amount of plate displacement resulted from the simulation, with Trebbi and Spears models that seem the closest to the current plate displacement. The overall stiffness of the tissues has relevant effects in the strain locations as in the cases of Akrami and Friedman. For Akarmi (too stiff) strains are concentrated on the contact region between the plate and the skin. The amount of displacement applied by the plate is low with the skin being almost in its undeformed configuration. On the other hand, in Friedman's model (too compliant), the strains are unrealistically high and strongly concentrated around the head of the calcaneus. In that case, the fat pad is completely flattened by the load applied by the plate.

It must be noted that the intensity of strain shown in the considered slice can be misleading as this representation is showing the values of this slice only (Figure 39). Strain values can vary significantly between the slices. Therefore, in relation to the magnitude of strains, the reader is addressed to the strain intensity paragraph.

5.4. Discussion

The objective of this chapter was to define and evaluate a FE model of the heel for foot ulcer prevention under shearing loads. To this account, a FE mesh was generated from a MR image and a set of constitutive equations was derived from curve fitting experimental results from the literature. To evaluate the model, the results from the simulations were compared with data obtained from an MR experiment applying different intensities of normal and shearing loads. IR was used in combination with the MR images of loaded tissues to estimate the generated internal displacements and strains. This technique allowed to gain insights on the location of the shear strain clusters and their intensity. It allowed also a quantitative comparison with the strains computed by the FE simulation. The FE results obtained with the selected constitutive equations were compared with other constitutive laws reported in the literature for other FE heel models. Six sets of material models from the literature were therefore considered to run simulations with the same boundary conditions as for our FE model. The differences in terms of strain intensity and propagation were analyzed.

Results showed larger discrepancies between data and FE simulations for high loads (Load1, Load3). This is probably due to the hyperelastic behavior and heterogeneous/anisotropic structure of the fat pad, which stiffness varies significantly in relation to the amount of load applied. The constitutive laws proposed in this chapter and fitted from tissue experimental stretch/stress curves published in the literature, provided the best results as compared to the strains measured by DVC. This is particularly encouraging since we know that some improvements should be done to better fit the current subject-specific constitutive parameter, which would probably require the use of in vivo measurements such as elastography [148] or local aspiration [149].

As concerns the comparison with other literature constitutive models, results show that the choice of the material properties is critical for the analysis as it may provide highly different strains patterns among models. The constitutive parameters have also a significant impact on the location and the intensity of the strain concentrations. This confirms the fact that it is crucial to implement constitutive laws that refer specifically to the considered subject when building a subject-specific FE model. MR compatible experiments such as the ones presented in Gefen et al. [65], Spears et al. [145] or the one introduced in this chapter, offer space to estimate in vivo material properties.

It is important to note that the methodology introduced in this chapter, to compare strains computed by FE models and strains measured by DVC, is quite new. It is therefore difficult to compare such a methodology with other methods proposed in the literature. However, some considerations can be made on strain intensities and locations found in previous studies. Zwam et al. looked at strains generated into the deep tissues of the heel for a subject laying in a supine position. The analyzed Green Lagrange strains reached a level of 0.4 that is comparable with what was observed in the FE simulations [135]. As concerns strain locations, our results are in line with what was found in previous studies, namely high strains located in the fatty region, close to the bony prominence [74], [134].

The current work still suffers from some limitations. First, the DVC and all the FE models were defined from the MR images of a single subject. This limits the implemented geometry of the FE models to a single case without account for the impact of morphological variability. Second, the proposed FE model did not consider specific interfaces between each soft tissues (skin, fat, muscles). It is believed that analyzing specific features such as sliding and friction could improve the results in terms of strain propagation. Third, the implemented constitutive laws were obtained from ex vivo experiments proposed in the literature. It is clear that to increase the correlation between the strains measured from the DVC and the ones computed by the FE model, such constitutive parameters should be estimated in vivo from the same subject that performed the MR experiment. Finally, it is important to note that our model does not include

the plantar fascia. This thick connective aponeurosis tissue supports the arch on the bottom plantar side of the foot and plays an important role in foot biomechanics. We decided however not to include such a structure in the model since its role during hell fat pad compression and shearing is probably limited.

5.5. Conclusion

This chapter introduced an original methodology to compare tissue strains computed by various FE constitutive models of the human heel with strains estimated from MR-based DVC. This comparison showed that fitting the constitutive parameters from ex vivo tensile and compression tests is probably a good approach when no in vivo subject-specific measurement such as elastography or local indentation/aspiration is available. This methodology could easily be implemented in other body locations such as sacrum or buttocks where strain propagation is fundamental to understand PU risks. The results provided in this chapter should also be considered as an illustration of the importance for choosing the constitutive equation for each tissue implemented in the FE models, especially for larger strains when hyperplastic laws are considered. This is of crucial importance as material parameters proposed in the literature can range over several orders of magnitude for the same tissue. The future steps of our work will have to face the challenge concerning the capability of these FE models to actually predict PU risks. This final goal will presumably require extensive clinical trials.

6. Chapter 6

General conclusion

In this thesis the biomechanical heel modeling and its evaluation have been extensively developed with the objective to gain insight in pressure ulcer prevention of the diabetic foot. The contributions, results, limitations and perspectives of the various performed studies have been already discussed in the corresponding chapters, each of them being adapted from published or submitted journal articles. In the following section, the main findings and contributions of the PhD thesis are summarized.

In the first and the second chapters of this manuscript, a review on the biomechanical heel modeling for pressure ulcer prevention was presented. One of the main outcomes was the complexity of tools to compare the various models and constitutive laws presented in the literature. Additionally, the lack of evaluation techniques to validate soft tissues FE models was highlighted. This PhD thesis has tried to address and to solve these issues.

The third chapter described a MR compatible device designed to collect good quality MR acquisitions and to meet various requirement. First, this device had to be MR compatible without any component made in a material that could alter the magnetic field. Second, to prevent any blur in the images and to ensure a high definition, the device had to be capable to fix the subject's foot from any involuntary movements for all the duration of the scans. Finally, the device should apply known normal and shearing loads by means of a compression platform in contact with the plantar region of the heel. These objectives were accomplished by using a 3D printer to create the main components of the device. The forces were delivered through the compression of springs made in polylactide. They were measured by using MR markers that track the springs level of compression. The obtained images showed good quality. This allowed from one side to distinguish the internal components of the fat pad: skin, fat, muscle, tendons and bones, and from the other side, to identify the location of the MR makers for the force calculation. In total, six acquisitions were taken: two in an unloaded configuration, two with a normal load applied, and two with a shearing load applied.

There are two main implications of this successful design. First, it offers a new solution to apply a load and to track the tissue internal displacements. Second, the realization of the device is cheap and easy to be modified and implemented in different parts of the human body. Therefore, this adds a useful and versatile tool to investigate the constitutive behavior of various soft tissues that are close to the skin surface.

The forth chapter focused on the implementation of DVC through image registration performed on the MR images. From an unloaded and a loaded image, the registration provided the transformation between both images and therefore computed the displacement field. From that displacement field, the Green Lagrange strain maps were computed. The corresponding results showed that the repeatability and the accuracy of calculating strains from image registration depends on the image quality and on the type of deformation applied. The main implication of this methodology is the possibility to track soft tissues internal displacements with high precision. This technique, combined with the application of a known load, provides all the required information to propose a constitutive model for the soft tissues of that body part.

In the fifth chapter of the thesis, the generation of a FE model of the human heel was described, to simulate the compression test performed in the MR machine. One of the two unloaded images of the heel was used

to perform a segmentation and obtain the related surfaces defining the internal components of the subject's heel. After a meshing process, the simulations reproducing the plate compression applied in the MR scan were computed. Constitutive laws of the current heel models published in the literature were implemented in our FE mesh to simulate the corresponding stiffness properties. The results, interms of tissues displacements and strains, were compared with the ones obtained from the DVC. Different aspects were considered for the evaluation of the FE simulations: plate displacements, locations of the strain concentrations, and strain intensities. The results showed a relevant correlation between DVC and predictions of the FE model, thus providing a credibility in the implementation of FE models for estimating the strain propagation in soft tissues. However, all the constitutive models taken from the literature lacked to successfully simulate all the considered aspects. For this reason, a set of constitutive equations was proposed in this PhD, to generate a model that better matched the data from DVC.

The main implication of this comparison between FE models and DVC is the possibility to clearly gain insight in how a specific model, with its own set of parameters, relates to others models published in the literature and approximates a concrete experiment.

Finite element modeling is a hard task. There are so many variables involved in every simulation. Geometry, stiffness parameters, internal frictions, boundary conditions are only some of them. This becomes even more challenging when applying FE modeling to the human body. The aspects that could make an impact here grow exponentially: ageing, body location, hydration, blood flow, temperature or even the mood of the subject in that moment could change the material properties of some specific related organs. To make things even more complex, the whole process of FE modeling is completely intangible, confined in the computer algorithms. The selection of material properties and the analysis in terms of strain and stress are concepts that are very far from what our senses are capable of appreciating. However, despite all of these complications that seem to define a mission impossible, humans managed to define models that correctly simulate the required aspects of a body part making their impact by improving the life of many people.

Finite element modeling of the human heel seems on its good way to have one day an impact in successfully contributing to pressure ulcer prevention. Despite this, the way to go is still long, having still many aspects to investigate and understand. A successful technique, when dealing with something complex and unknown, is to proceed with tiny steps, one at a time, and making sure that each of these steps is based on a solid background. The objective of this thesis was to define a solid background on which the future steps for the FE modeling of the human heel will be based.

The possibility of measuring applied forces in the MR environment and to track precisely every local displacement in the soft tissues gives an inestimable tool to validate a FE model of that part. A comparison between the various models published in literature and the DVC measurements offers another useful tool to have a more concrete idea on what the stiffness parameters in the constitutive equations actually mean from a more practical point of view.

Sometimes, to propose more sophisticated assumptions, it is important to take a step back, and to focus on validating the concepts on which we are basing. This allows to increase the trust on the current ground, to tighten the grip, and to prepare for the next leap.

References

[1] J. Kottner, J. Black, E. Call, A. Gefen, and N. Santamaria, “Microclimate: A critical review in the context of pressure ulcer prevention,” *Clin. Biomech.*, vol. 59, pp. 62–70, Nov. 2018, doi: 10.1016/j.clinbiomech.2018.09.010.

[2] C. V. Bouten, C. W. Oomens, F. P. Baaijens, and D. L. Bader, “The etiology of pressure ulcers: Skin deep or muscle bound?,” *Archives of Physical Medicine and Rehabilitation*. 2003, doi: 10.1053/apmr.2003.50038.

[3] E. Linder-Ganz, S. Engelberg, M. Scheinowitz, and A. Gefen, “Pressure–time cell death threshold for albino rat skeletal muscles as related to pressure sore biomechanics,” *J. Biomech.*, vol. 39, no. 14, pp. 2725–2732, Jan. 2006, doi: 10.1016/J.JBIOMECH.2005.08.010.

[4] N. Shoham, L. Mor-Yossef Moldovan, D. Benayahu, and A. Gefen, “Multiscale modeling of tissue-engineered fat: Is there a deformation-driven positive feedback loop in adipogenesis?,” *Tissue Eng. - Part A*, 2015, doi: 10.1089/ten.tea.2014.0505.

[5] A. Gefen, “Reswick and Rogers pressure-time curve for pressure ulcer risk. Part 1.,” *Nurs. Stand.*, vol. 23, no. 45, 2009, doi: 10.7748/NS2009.07.23.45.64.C7115.

[6] A. Macron, H. Pillet, J. Doridam, A. Verney, and P. Y. Rohan, “Development and evaluation of a new methodology for the fast generation of patient-specific Finite Element models of the buttock for sitting-acquired deep tissue injury prevention,” *J. Biomech.*, vol. 79, pp. 173–180, Oct. 2018, doi: 10.1016/J.JBIOMECH.2018.08.001.

[7] E. Linder-Ganz and A. Gefen, “Stress analyses coupled with damage laws to determine biomechanical risk factors for deep tissue injury during sitting,” *J. Biomech. Eng.*, vol. 131, no. 1, Jan. 2009, doi: 10.1115/1.3005195/440453.

[8] C. G. Fontanella, F. Nalesso, E. L. Carniel, and A. N. Natali, “Biomechanical behavior of plantar fat pad in healthy and degenerative foot conditions,” *Med. Biol. Eng. Comput.*, 2016, doi: 10.1007/s11517-015-1356-x.

[9] I. R. Spears and J. E. Miller-Young, “The effect of heel-pad thickness and loading protocol on measured heel-pad stiffness and a standardized protocol for inter-subject comparability,” *Clin. Biomech.*, 2006, doi: 10.1016/j.clinbiomech.2005.09.017.

[10] H. B. Henninger, S. P. Reese, A. E. Anderson, and J. A. Weiss, “Validation of computational models in biomechanics,” *Proceedings of the Institution of Mechanical Engineers, Part H: Journal of*

Engineering in Medicine. 2010, doi: 10.1243/09544119JEIM649.

[11] D. Beeckman *et al.*, "EPUAP classification system for pressure ulcers: European reliability study," *J. Adv. Nurs.*, 2007, doi: 10.1111/j.1365-2648.2007.04474.x.

[12] A. N. Pressure, "European Pressure Ulcer Advisory Panel and National Pressure Ulcer Advisory Panel . Treatment of pressure ulcers : Quick Reference Guide .," *Natl. Press. Ulcer Advis. Panel*, 2009.

[13] T. V. Perneger, C. Héliot, A. C. Raë, F. Borst, and J. M. Gaspoz, "Hospital-acquired pressure ulcers: Risk factors and use of preventive devices," *Arch. Intern. Med.*, 1998, doi: 10.1001/archinte.158.17.1940.

[14] V. R. Driver, M. Fabbi, L. A. Lavery, and G. Gibbons, "The costs of diabetic foot: The economic case for the limb salvage team," *J. Vasc. Surg.*, vol. 52, no. 3, pp. 17S-22S, Sep. 2010, doi: 10.1016/J.JVS.2010.06.003.

[15] J. APELQVIST, J. LARSSON, and C. -D AGARDH, "Long-term prognosis for diabetic patients with foot ulcers," *J. Intern. Med.*, vol. 233, no. 6, pp. 485–491, 1993, doi: 10.1111/J.1365-2796.1993.TB01003.X.

[16] G. Bennett, C. Dealey, and J. Posnett, "The cost of pressure ulcers in the UK," *Age Ageing*, vol. 33, no. 3, pp. 230–235, May 2004, doi: 10.1093/AGEING/AFH086.

[17] K. B. Al Mutairi and D. Hendrie, "Global incidence and prevalence of pressure injuries in public hospitals: A systematic review," *Wound Med.*, vol. 22, pp. 23–31, Sep. 2018, doi: 10.1016/J.WNDM.2018.05.004.

[18] S. M. Dinsdale, "Decubitus ulcers: role of pressure and friction in causation," *Arch. Phys. Med. Rehabil.*, 1974.

[19] J. B. Reuler and T. G. Cooney, "The pressure sore: Pathophysiology and principles of management," *Ann. Intern. Med.*, 1981, doi: 10.7326/0003-4819-94-5-661.

[20] R. K. Daniel, D. L. Priest, and D. C. Wheatley, "Etiologic factors in pressure sores: An experimental model," *Arch. Phys. Med. Rehabil.*, 1981.

[21] G. M. Yarkony, "Pressure ulcers: A review," *Archives of Physical Medicine and Rehabilitation*. 1994, doi: 10.1016/0003-9993(94)90117-1.

[22] G. T. Nola and L. M. Vistnes, "Differential response of skin and muscle in the experimental production of pressure sores," *Plast. Reconstr. Surg.*, 1980, doi: 10.1097/00006534-198011000-00008.

[23] M. R. Bliss, "Acute pressure area care: Sir James Paget's legacy," *Lancet*, 1992, doi: 10.1016/0140-

6736(92)90016-V.

[24] E. C. Herrman, C. F. Knapp, J. C. Donofrio, and R. Salcido, “Skin perfusion responses to surface pressure-induced ischemia: Implication for the developing pressure ulcer,” *J. Rehabil. Res. Dev.*, 1999.

[25] N. P. Reddy, G. V. B. Cochran, and T. A. Krouskop, “Interstitial fluid flow as a factor in decubitus ulcer formation,” *J. Biomech.*, 1981, doi: 10.1016/0021-9290(81)90015-4.

[26] S. M. Peirce, T. C. Skalak, and G. T. Rodeheaver, “Ischemia-reperfusion injury in chronic pressure ulcer formation: A skin model in the rat,” *Wound Repair Regen.*, 2000, doi: 10.1046/j.1524-475X.2000.00068.x.

[27] C. W. J. Oomens, D. L. Bader, S. Loerakker, and F. Baaijens, “Pressure Induced Deep Tissue Injury Explained,” *Ann. Biomed. Eng.*, 2015, doi: 10.1007/s10439-014-1202-6.

[28] E. Linder-Ganz, N. Shabshin, Y. Itzchak, and A. Gefen, “Assessment of mechanical conditions in sub-dermal tissues during sitting: A combined experimental-MRI and finite element approach,” *J. Biomech.*, 2007, doi: 10.1016/j.jbiomech.2006.06.020.

[29] C. W. J. Oomens *et al.*, “A numerical study to analyse the risk for pressure ulcer development on a spine board,” *Clin. Biomech.*, 2013, doi: 10.1016/j.clinbiomech.2013.07.005.

[30] M. B. Silver-Thorn, J. W. Steege, and D. S. Childress, “A review of prosthetic interface stress investigations,” *J. Rehabil. Res. Dev.*, 1996.

[31] M. Bucki *et al.*, “Clinical workflow for personalized foot pressure ulcer prevention,” *Med. Eng. Phys.*, 2016, doi: 10.1016/j.medengphy.2016.04.017.

[32] V. Luboz *et al.*, “Influence of the Calcaneus Shape on the Risk of Posterior Heel Ulcer Using 3D Patient-Specific Biomechanical Modeling,” *Ann. Biomed. Eng.*, 2015, doi: 10.1007/s10439-014-1182-6.

[33] A. Levy, M. B. O. Frank, and A. Gefen, “The biomechanical efficacy of dressings in preventing heel ulcers,” *J. Tissue Viability*, 2015, doi: 10.1016/j.jtv.2015.01.001.

[34] K. Vanderwee, M. Clark, C. Dealey, L. Gunningberg, and T. Defloor, “Pressure ulcer prevalence in Europe: A pilot study,” *J. Eval. Clin. Pract.*, 2007, doi: 10.1111/j.1365-2753.2006.00684.x.

[35] M. Makhsous, D. Lim, R. Hendrix, J. Bankard, W. Z. Rymer, and F. Lin, “Finite element analysis for evaluation of pressure ulcer on the buttock: Development and validation,” *IEEE Trans. Neural Syst. Rehabil. Eng.*, 2007, doi: 10.1109/TNSRE.2007.906967.

[36] E. Linder-Ganz, G. Yarnitzky, Z. Yizhar, I. Siev-Ner, and A. Gefen, “Real-time finite element monitoring of sub-dermal tissue stresses in individuals with spinal cord injury: Toward prevention

of pressure ulcers," *Ann. Biomed. Eng.*, 2009, doi: 10.1007/s10439-008-9607-8.

[37] R. Katzengold and A. Gefen, "What makes a good head positioner for preventing occipital pressure ulcers," *Int. Wound J.*, 2018, doi: 10.1111/iwj.12857.

[38] W. J. Jeffcoate and K. G. Harding, "Diabetic foot ulcers," *Lancet*. 2003, doi: 10.1016/S0140-6736(03)13169-8.

[39] W. R. Ledoux, J. B. Shofer, M. S. Cowley, J. H. Ahroni, V. Cohen, and E. J. Boyko, "Diabetic foot ulcer incidence in relation to plantar pressure magnitude and measurement location," *J. Diabetes Complications*, 2013, doi: 10.1016/j.jdiacomp.2013.07.004.

[40] H. M. Rathur and A. J. M. Boulton, "The diabetic foot," *Clin. Dermatol.*, 2007, doi: 10.1016/j.clindermatol.2006.09.015.

[41] J. A. Mayhfield, G. E. Reiber, L. J. Sanders, D. Janisse, and L. M. Pogach, "Preventive foot care in people with diabetes," *Diabetes Care*. 1998, doi: 10.2337/diacare.21.12.2161.

[42] K. Kirby and A. Calabro, "Foot Strike Patterns Study Ignites Barefoot Running Debate Foot Strike Patterns Study Ignites Barefoot Running Debate Page 2 of 3," *Business*, 2010.

[43] O. Swensson *et al.*, "Specialized keratin expression pattern in human ridged skin as an adaptation to high physical stress," *Br. J. Dermatol.*, 1998, doi: 10.1046/j.1365-2133.1998.02499.x.

[44] J. L. Rinn *et al.*, "A dermal HOX transcriptional program regulates site-specific epidermal fate," *Genes Dev.*, 2008, doi: 10.1101/gad.1610508.

[45] N. Singh, D. G. Armstrong, and B. A. Lipsky, "Preventing foot ulcers in patients with diabetes," *Journal of the American Medical Association*. 2005, doi: 10.1001/jama.293.2.217.

[46] M. J. Mueller, D. Zou, and D. J. Lott, "'Pressure gradient' as an indicator of plantar skin injury," *Diabetes Care*, 2005, doi: 10.2337/diacare.28.12.2908.

[47] A. Gefen, "Plantar soft tissue loading under the medial metatarsals in the standing diabetic foot," *Med. Eng. Phys.*, 2003, doi: 10.1016/S1350-4533(03)00029-8.

[48] E. Atlas, Z. Yizhar, S. Khamis, N. Slomka, S. Hayek, and A. Gefen, "Utilization of the foot load monitor for evaluating deep plantar tissue stresses in patients with diabetes: Proof-of-concept studies," *Gait Posture*, 2009, doi: 10.1016/j.gaitpost.2008.10.055.

[49] A. J. M. Boulton, "The Pathway to Ulceration: Aetiopathogenesis," *Foot Diabetes*, pp. 19–31, Apr. 2003, doi: 10.1002/0470846399.CH3.

[50] G. E. Reiber *et al.*, "Causal pathways for incident lower-extremity ulcers in patients with diabetes from two settings," *Diabetes Care*, vol. 22, no. 1, pp. 157–162, Jan. 1999, doi: 10.2337/DIACARE.22.1.157.

[51] A. I. Adler, E. J. Boyko, J. H. Ahroni, and D. G. Smith, “Lower-extremity amputation in diabetes: The independent effects of peripheral vascular disease, sensory neuropathy, and foot ulcers,” *Diabetes Care*, vol. 22, no. 7, pp. 1029–1035, Jul. 1999, doi: 10.2337/DIACARE.22.7.1029.

[52] A. N. Natali, C. G. Fontanella, and E. L. Carniel, “Constitutive formulation and numerical analysis of the heel pad region,” *Comput. Methods Biomech. Biomed. Engin.*, 2012, doi: 10.1080/10255842.2010.539561.

[53] K. Rome, “Mechanical properties of the heel pad: Current theory and review of the literature,” *Foot*. 1998, doi: 10.1016/S0958-2592(98)90026-8.

[54] R. F. Ker, “The design of soft collagenous load-bearing tissues,” *J. Exp. Biol.*, 1999.

[55] C. C. Hsu, W. C. Tsai, C. L. Wang, S. H. Pao, Y. W. Shau, and Y. S. Chuan, “Microchambers and macrochambers in heel pads: Are they functionally different?,” *J. Appl. Physiol.*, 2007, doi: 10.1152/japplphysiol.01137.2006.

[56] Y. N. Wang, K. Lee, and W. R. Ledoux, “Histomorphological evaluation of diabetic and non-diabetic plantar soft tissue,” *Foot Ankle Int.*, 2011, doi: 10.3113/FAI.2011.0802.

[57] A. N. Natali, C. G. Fontanella, and E. L. Carniel, “A numerical model for investigating the mechanics of calcaneal fat pad region,” *J. Mech. Behav. Biomed. Mater.*, 2012, doi: 10.1016/j.jmbbm.2011.08.025.

[58] A. N. Natali, C. G. Fontanella, and E. L. Carniel, “Constitutive formulation and analysis of heel pad tissues mechanics,” *Med. Eng. Phys.*, 2010, doi: 10.1016/j.medengphy.2010.02.018.

[59] C. G. Fontanella, A. Forestiero, E. L. Carniel, and A. N. Natali, “Analysis of heel pad tissues mechanics at the heel strike in bare and shod conditions,” *Med. Eng. Phys.*, 2013, doi: 10.1016/j.medengphy.2012.06.008.

[60] W. R. Buschmann, M. H. Jahss, F. Kummer, P. Desai, R. O. Gee, and J. L. Ricci, “Histology and histomorphometric analysis of the normal and atrophic heel fat pad,” *Foot Ankle Int.*, 1995, doi: 10.1177/107110079501600502.

[61] C. G. Fontanella *et al.*, “Investigation on the load-displacement curves of a human healthy heel pad: In vivo compression data compared to numerical results,” *Med. Eng. Phys.*, 2012, doi: 10.1016/j.medengphy.2011.12.013.

[62] K. H. Herrmann, C. Gärtner, D. Güllmar, M. Krämer, and J. R. Reichenbach, “3D printing of MRI compatible components: Why every MRI research group should have a low-budget 3D printer,” *Med. Eng. Phys.*, 2014, doi: 10.1016/j.medengphy.2014.06.008.

[63] L. Filli *et al.*, “Metal-induced artifacts in computed tomography and magnetic resonance imaging:

comparison of a biodegradable magnesium alloy versus titanium and stainless steel controls," *Skeletal Radiol.*, 2015, doi: 10.1007/s00256-014-2057-5.

[64] E. D. Williams *et al.*, "The design and validation of a magnetic resonance imaging-compatible device for obtaining mechanical properties of plantar soft tissue via gated acquisition," *Proc. Inst. Mech. Eng. Part H J. Eng. Med.*, 2015, doi: 10.1177/0954411915606150.

[65] A. Gefen, M. Megido-Ravid, M. Azariah, Y. Itzchak, and M. Arcan, "Integration of plantar soft tissue stiffness measurements in routine MRI of the diabetic foot," *Clin. Biomech.*, 2001, doi: 10.1016/S0268-0033(01)00074-2.

[66] S. Matteoli *et al.*, "Investigations on the viscoelastic behaviour of a human healthy heel pad: In vivo compression tests and numerical analysis," *Proc. Inst. Mech. Eng. Part H J. Eng. Med.*, 2013, doi: 10.1177/0954411912465061.

[67] Y. Gu, J. Li, X. Ren, M. J. Lake, and Y. Zeng, "Heel skin stiffness effect on the hind foot biomechanics during heel strike," *Ski. Res. Technol.*, 2010, doi: 10.1111/j.1600-0846.2010.00425.x.

[68] E. D. Williams *et al.*, "A preliminary study of patient-specific mechanical properties of diabetic and healthy plantar soft tissue from gated magnetic resonance imaging," *Proc. Inst. Mech. Eng. Part H J. Eng. Med.*, 2017, doi: 10.1177/0954411917695849.

[69] J. E. Miller-Young, N. A. Duncan, and G. Baroud, "Material properties of the human calcaneal fat pad in compression: Experiment and theory," *J. Biomech.*, 2002, doi: 10.1016/S0021-9290(02)00090-8.

[70] A. Gefen, M. Megido-Ravid, and Y. Itzchak, "In vivo biomechanical behavior of the human heel pad during the stance phase of gait," *J. Biomech.*, 2001, doi: 10.1016/S0021-9290(01)00143-9.

[71] W. S.C., S. J.E., Y. B., U. S.R., and D. P., "Bulk compressive properties of the heel fat pad during walking: A pilot investigation in plantar heel pain," *Clinical Biomechanics*. 2009.

[72] J. B. Weaver *et al.*, "Imaging the shear modulus of the heel fat pads," *Clin. Biomech.*, 2005, doi: 10.1016/j.clinbiomech.2004.11.010.

[73] Y. Y. Cheung *et al.*, "Magnetic resonance elastography of the plantar fat pads: Preliminary study in diabetic patients and asymptomatic volunteers," *J. Comput. Assist. Tomogr.*, 2006, doi: 10.1097/00004728-200603000-00031.

[74] V. Luboz, M. Petrizelli, M. Bucki, B. Diot, N. Vuillerme, and Y. Payan, "Biomechanical modeling to prevent ischial pressure ulcers," *J. Biomech.*, 2014, doi: 10.1016/j.jbiomech.2014.05.004.

[75] S. Chokhandre, J. P. Halloran, A. J. Van Den Bogert, and A. Erdemir, "A three-dimensional inverse

finite element analysis of the heel pad," *J. Biomech. Eng.*, 2012, doi: 10.1115/1.4005692.

[76] A. Perrier, V. Luboz, M. Bucki, F. Cannard, N. Vuillerme, and Y. Payan, "Biomechanical Modeling of the Foot," in *Biomechanics of Living Organs: Hyperelastic Constitutive Laws for Finite Element Modeling*, 2017.

[77] A. Perrier, V. Luboz, M. Bucki, N. Vuillerme, and Y. Payan, "Conception and evaluation of a 3D musculoskeletal finite element foot model," *Computer Methods in Biomechanics and Biomedical Engineering*. 2015, doi: 10.1080/10255842.2015.1069606.

[78] Y. Gu, J. Li, X. Ren, M. J. Lake, and Y. Zeng, "Heel skin stiffness effect on the hind foot biomechanics during heel strike," *Ski. Res. Technol.*, vol. 16, no. 3, pp. 291–296, Aug. 2010, doi: 10.1111/J.1600-0846.2010.00425.X.

[79] G. Chagnon, M. Rebouah, and D. Favier, "Hyperelastic Energy Densities for Soft Biological Tissues: A Review," *J. Elast. 2014 1202*, vol. 120, no. 2, pp. 129–160, Dec. 2014, doi: 10.1007/S10659-014-9508-Z.

[80] C. C. Hsu *et al.*, "Diabetic effects on microchambers and macrochambers tissue properties in human heel pads," *Clin. Biomech.*, 2009, doi: 10.1016/j.clinbiomech.2009.06.005.

[81] A. N. Natali, C. G. Fontanella, E. L. Carniel, and J. M. Young, "Biomechanical behaviour of heel pad tissue: Experimental testing, constitutive formulation, and numerical modelling," 2011, doi: 10.1177/09544119JEIM851.

[82] R. Sopher, J. Nixon, E. McGinnis, and A. Gefen, "The influence of foot posture, support stiffness, heel pad loading and tissue mechanical properties on biomechanical factors associated with a risk of heel ulceration," *J. Mech. Behav. Biomed. Mater.*, 2011, doi: 10.1016/j.jmbbm.2011.01.004.

[83] A. Ruggiero, R. D'Amato, and S. Affatato, "Comparison of meshing strategies in THR finite element modelling," *Materials (Basel).*, 2019, doi: 10.3390/ma12142332.

[84] J. E. Lloyd, I. Stavness, and S. Fels, "ArtiSynth: A Fast Interactive Biomechanical Modeling Toolkit Combining Multibody and Finite Element Simulation," in *Studies in Mechanobiology, Tissue Engineering and Biomaterials*, 2012.

[85] A. Bijar, P. Y. Rohan, P. Perrier, and Y. Payan, "Atlas-Based Automatic Generation of Subject-Specific Finite Element Tongue Meshes," *Ann. Biomed. Eng.*, vol. 44, no. 1, pp. 16–34, Jan. 2016, doi: 10.1007/S10439-015-1497-Y/FIGURES/9.

[86] D. De Clercq, P. Aerts, and M. Kunnen, "The mechanical characteristics of the human heel pad during foot strike in running: An in vivo cineradiographic study," *J. Biomech.*, 1994, doi: 10.1016/0021-9290(94)90275-5.

[87] P. Aerts and D. De Clercq, “Deformation characteristics of the heel region of the shod foot during a simulated heel strike: The effect of varying midsole hardness,” *J. Sports Sci.*, 1993, doi: 10.1080/02640419308730011.

[88] J. R. Mackey and B. L. Davis, “Simultaneous shear and pressure sensor array for assessing pressure and shear at foot/ground interface,” *J. Biomech.*, 2006, doi: 10.1016/j.jbiomech.2005.10.001.

[89] N. A. Lahmann, A. Tannen, T. Dassen, and J. Kottner, “Friction and shear highly associated with pressure ulcers of residents in long-term care - Classification Tree Analysis (CHAID) of Braden items,” *J. Eval. Clin. Pract.*, 2011, doi: 10.1111/j.1365-2753.2010.01417.x.

[90] M. Petre, A. Erdemir, V. P. Panoskaltsis, T. A. Spirka, and P. R. Cavanagh, “Optimization of nonlinear hyperelastic coefficients for foot tissues using a magnetic resonance imaging deformation experiment,” *J. Biomech. Eng.*, 2013, doi: 10.1115/1.4023695.

[91] D. B. Bogy, “Two edge-bonded elastic wedges of different materials and wedge angles under surface tractions,” *J. Appl. Mech. Trans. ASME*, 1971, doi: 10.1115/1.3408786.

[92] T. Marasovič, M. Cecič, and V. Zanchi, “Analysis and interpretation of ground reaction forces in normal gait,” *WSEAS Trans. Syst.*, 2009.

[93] A. Gefen, “The biomechanics of heel ulcers,” *J. Tissue Viability*, 2010, doi: 10.1016/j.jtv.2010.06.003.

[94] C. Tavares, M. F. Domingues, T. Paixão, N. Alberto, H. Silva, and P. Antunes, “Wheelchair pressure ulcer prevention using FBG based sensing devices,” *Sensors (Switzerland)*, 2020, doi: 10.3390/s20010212.

[95] M. J. Mueller *et al.*, “Total contact casting in treatment of diabetic plantar ulcers. Controlled clinical trial,” *Diabetes Care*, 1989, doi: 10.2337/diacare.12.6.384.

[96] A. I. Veress, G. T. Gullberg, and J. A. Weiss, “Measurement of Strain in the Left Ventricle during Diastole with cine-MRI and Deformable Image Registration,” *J. Biomech. Eng.*, vol. 127, no. 7, pp. 1195–1207, Dec. 2005, doi: 10.1115/1.2073677.

[97] M. R. Hardisty, M. K. Akens, S. P. Hojjat, A. Yee, and C. M. Whyne, “Quantification of the effect of osteolytic metastases on bone strain within whole vertebrae using image registration,” *J. Orthop. Res.*, vol. 30, no. 7, pp. 1032–1039, Jul. 2012, doi: 10.1002/JOR.22045.

[98] P. E. Chatzistergos, R. Naemi, and N. Chockalingam, “An MRI compatible loading device for the reconstruction of clinically relevant plantar pressure distributions and loading scenarios of the forefoot,” *Med. Eng. Phys.*, 2014, doi: 10.1016/j.medengphy.2014.06.006.

[99] A. Stekelenburg, C. W. J. Oomens, G. J. Strijkers, L. De Graaf, D. L. Bader, and K. Nicolay, “A new

MR-compatible loading device to study in vivo muscle damage development in rats due to compressive loading," *Med. Eng. Phys.*, 2006, doi: 10.1016/j.medengphy.2005.07.005.

[100] M. Petre, A. Erdemir, and P. R. Cavanagh, "An MRI-compatible foot-loading device for assessment of internal tissue deformation," *J. Biomech.*, 2008, doi: 10.1016/j.jbiomech.2007.09.018.

[101] K. K. Ceelen *et al.*, "Validation of a numerical model of skeletal muscle compression with MR tagging: A contribution to pressure ulcer research," *J. Biomech. Eng.*, 2008, doi: 10.1115/1.2987877.

[102] S. Klein, M. Staring, K. Murphy, M. A. Viergever, and J. P. W. Pluim, "Elastix: A toolbox for intensity-based medical image registration," *IEEE Trans. Med. Imaging*, 2010, doi: 10.1109/TMI.2009.2035616.

[103] J. M. Gerard, J. Ohayon, V. Luboz, P. Perrier, and Y. Payan, "Non-linear elastic properties of the lingual and facial tissues assessed by indentation technique: Application to the biomechanics of speech production," *Med. Eng. Phys.*, vol. 27, no. 10, pp. 884–892, Dec. 2005, doi: 10.1016/J.MEDENGPHY.2005.08.001.

[104] T. Tokuno, M. Tada, and K. Umeda, "High-precision MRI-compatible force sensor with parallel plate structure," 2008, doi: 10.1109/BIOROB.2008.4762897.

[105] B. E. Keenan, S. L. Evans, and C. W. J. Oomens, "A review of foot finite element modelling for pressure ulcer prevention in bedrest: Current perspectives and future recommendations," *J. Tissue Viability*, Jun. 2021, doi: 10.1016/J.JTV.2021.06.004.

[106] L. Savonnet, X. Wang, and S. Duprey, "Finite element models of the thigh-buttock complex for assessing static sitting discomfort and pressure sore risk: a literature review," *https://doi-org.sid2nomade-1.grenet.fr/10.1080/10255842.2018.1466117*, vol. 21, no. 4, pp. 379–388, Mar. 2018, doi: 10.1080/10255842.2018.1466117.

[107] A.-D. Rma and P. G. Affiliations, "A Comprehensive Literature Review of the Pelvis and the Lower Extremity FE Human Models under Quasi-static Conditions," 2012, doi: 10.3233/WOR-2012-1039-4218.

[108] A. Macron *et al.*, "Is a simplified Finite Element model of the gluteus region able to capture the mechanical response of the internal soft tissues under compression?," *Clin. Biomech.*, vol. 71, pp. 92–100, Jan. 2020, doi: 10.1016/J.CLINBIOMECH.2019.10.005.

[109] A. Stekelenburg, G. J. Strijkers, H. Parusel, D. L. Bader, K. Nicolay, and C. W. Oomens, "Role of ischemia and deformation in the onset of compression-induced deep tissue injury: MRI-based studies in a rat model," *J. Appl. Physiol.*, 2007, doi: 10.1152/japplphysiol.01115.2006.

[110] A. Trebbi, A. Perrier, M. Bailet, and Y. Payan, “MR-compatible loading device for assessment of heel pad internal tissue displacements under shearing load.,” *Med. Eng. Phys.*, vol. 98, pp. 125–132, Dec. 2021, doi: 10.1016/J.MEDENGPHY.2021.11.006.

[111] S. Tavana *et al.*, “Quantifying deformations and strains in human intervertebral discs using Digital Volume Correlation combined with MRI (DVC-MRI),” *J. Biomech.*, vol. 102, p. 109604, Mar. 2020, doi: 10.1016/J.JBIOMECH.2020.109604.

[112] J. H. Yoder *et al.*, “Internal three-dimensional strains in human intervertebral discs under axial compression quantified noninvasively by magnetic resonance imaging and image registration,” *J. Biomech. Eng.*, vol. 136, no. 11, Nov. 2014, doi: 10.1115/1.4028250/371076.

[113] G. Schulz, H. J. A. Crooijmans, M. Germann, K. Scheffler, M. Müller-Gerbl, and B. Müller, “Three-dimensional strain fields in human brain resulting from formalin fixation,” *J. Neurosci. Methods*, vol. 202, no. 1, pp. 17–27, Oct. 2011, doi: 10.1016/J.JNEUMETH.2011.08.031.

[114] A. Yaman, C. Ozturk, P. A. Huijing, and C. A. Yucesoy, “Magnetic resonance imaging assessment of mechanical interactions between human lower leg muscles in vivo,” *J. Biomech. Eng.*, vol. 135, no. 9, Sep. 2013, doi: 10.1115/1.4024573/370990.

[115] A. Stekelenburg, D. Gawlitta, D. L. Bader, and C. W. Oomens, “Deep Tissue Injury: How Deep is Our Understanding?,” *Arch. Phys. Med. Rehabil.*, vol. 89, no. 7, pp. 1410–1413, Jul. 2008, doi: 10.1016/J.APMR.2008.01.012.

[116] K. K. Ceelen *et al.*, “Compression-induced damage and internal tissue strains are related,” *J. Biomech.*, vol. 41, no. 16, pp. 3399–3404, Dec. 2008, doi: 10.1016/J.JBIOMECH.2008.09.016.

[117] F. P. M. Oliveira and J. M. R. S. Tavares, “Medical image registration: a review,” *https://doi-org.sid2nomade-1.grenet.fr/10.1080/10255842.2012.670855*, vol. 17, no. 2, pp. 73–93, 2013, doi: 10.1080/10255842.2012.670855.

[118] A. J. Nederveen, S. Avril, and L. Speelman, “MRI strain imaging of the carotid artery: Present limitations and future challenges,” *J. Biomech.*, vol. 47, no. 4, pp. 824–833, Mar. 2014, doi: 10.1016/J.JBIOMECH.2014.01.014.

[119] L. W. Goldman, “Principles of CT: Radiation Dose and Image Quality,” *J. Nucl. Med. Technol.*, vol. 35, no. 4, pp. 213–225, Dec. 2007, doi: 10.2967/JNMT.106.037846.

[120] H. Alsleem and R. Davidson, “Quality parameters and assessment methods of digital radiography images,” *Radiographer*, vol. 59, no. 2, pp. 46–55, Jun. 2012, doi: 10.1002/J.2051-3909.2012.TB00174.X.

[121] M. B. Williams *et al.*, “Digital Radiography Image Quality: Image Acquisition,” *J. Am. Coll. Radiol.*,

vol. 4, no. 6, pp. 371–388, Jun. 2007, doi: 10.1016/J.JACR.2007.02.002.

[122] "[PDF] Performance of Digital Radiographic Detectors : Quantification and Assessment Methods 1 | Semantic Scholar." https://www.semanticscholar.org/paper/Performance-of-Digital-Radiographic-Detectors-%3A-and-Samei/9559675f1c909eb268edcdb3e8431846faab8932 (accessed Mar. 11, 2022).

[123] E. Samei, N. T. Ranger, J. T. Dobbins, and Y. Chen, "Intercomparison of methods for image quality characterization. I. Modulation transfer functiona)," *Med. Phys.*, vol. 33, no. 5, pp. 1454–1465, May 2006, doi: 10.1118/1.2188816.

[124] P. W. Nugent, J. A. Shaw, M. R. Kehoe, C. W. Smith, T. S. Moon, and R. C. Swanson, "Measuring the modulation transfer function of an imaging spectrometer with rooflines of opportunity," *https://doi-org.sid2nomade-1.grenet.fr/10.1117/1.3497051*, vol. 49, no. 10, p. 103201, Oct. 2010, doi: 10.1117/1.3497051.

[125] K. K. Ceelen *et al.*, "Compression-induced damage and internal tissue strains are related," *J. Biomech.*, vol. 41, no. 16, pp. 3399–3404, Dec. 2008, doi: 10.1016/J.JBIOMECH.2008.09.016.

[126] R. J. Talmadge, R. R. Roy, V. J. Caiozzo, and V. Reggie Edgerton, "Mechanical properties of rat soleus after long-term spinal cord transection," *J. Appl. Physiol.*, 2002, doi: 10.1152/japplphysiol.00053.2002.

[127] I. Hoogendoorn, J. Reenalda, B. F. J. M. Koopman, and J. S. Rietman, "The effect of pressure and shear on tissue viability of human skin in relation to the development of pressure ulcers: a systematic review," *J. Tissue Viability*, vol. 26, no. 3, pp. 157–171, Aug. 2017, doi: 10.1016/J.JTV.2017.04.003.

[128] A. Lustig, R. Margi, A. Orlov, D. Orlova, L. Azaria, and A. Gefen, "The mechanobiology theory of the development of medical device-related pressure ulcers revealed through a cell-scale computational modeling framework," *Biomech. Model. Mechanobiol.*, vol. 20, no. 3, pp. 851–860, Jun. 2021, doi: 10.1007/S10237-021-01432-W/FIGURES/5.

[129] M. Yavuz, A. Tajaddini, G. Botek, and B. L. Davis, "Temporal characteristics of plantar shear distribution: Relevance to diabetic patients," *J. Biomech.*, 2008, doi: 10.1016/j.jbiomech.2007.10.008.

[130] A. Gefen *et al.*, "A review of deep tissue injury development, detection, and prevention: Shear savvy," *Ostomy Wound Manag.*, 2013.

[131] A. Levy and A. Gefen, "Computer Modeling Studies to Assess Whether a Prophylactic Dressing Reduces the Risk for Deep Tissue Injury in the Heels of Supine Patients with Diabetes.," *Ostomy.*

Wound. Manage., vol. 62, no. 4, pp. 42–52, Apr. 2016, Accessed: Jul. 20, 2022. [Online]. Available: https://europepmc.org/article/med/27065218.

[132] C. W. J. Oomens, D. L. Bader, S. Loerakker, and F. Baaijens, "Pressure Induced Deep Tissue Injury Explained," *Ann. Biomed. Eng.*, vol. 43, no. 2, pp. 297–305, Feb. 2015, doi: 10.1007/S10439-014-1202-6/FIGURES/9.

[133] A. Erdemir, M. L. Viveiros, J. S. Ulbrecht, and P. R. Cavanagh, "An inverse finite-element model of heel-pad indentation," *J. Biomech.*, vol. 39, no. 7, pp. 1279–1286, Jan. 2006, doi: 10.1016/J.JBIOMECH.2005.03.007.

[134] R. Friedman, N. Shabshin, Y. Payan, and A. Gefen, "Heel ulcers: investigating injurious tissue load thresholds in humans, based on a patient-specific computational heel model," *Innov. Emerg. Technol. Wound Care*, pp. 123–139, Jan. 2020, doi: 10.1016/B978-0-12-815028-3.00007-9.

[135] W. G. H. van Zwam, M. C. van Turnhout, and C. W. J. Oomens, "Risk factors for developing heel ulcers for bedridden patients: A finite element study," *Clin. Biomech.*, vol. 78, p. 105094, Aug. 2020, doi: 10.1016/J.CLINBIOMECH.2020.105094.

[136] A. Trebbi *et al.*, "MR-based quantitative measurement of human soft tissue internal strains for pressure ulcer prevention," *Med. Eng. Phys.*, vol. 108, p. 103888, Oct. 2022, doi: 10.1016/J.MEDENGPHY.2022.103888.

[137] C. W. J. Oomens, O. F. J. T. Bressers, E. M. H. Bosboom, C. V. C. Bouten, and D. L. Bader, "Can Loaded Interface Characteristics Influence Strain Distributions in Muscle Adjacent to Bony Prominences?," *http://dx.doi.org.sid2nomade-1.grenet.fr/10.1080/10255840310001210 34*, vol. 6, no. 3, pp. 171–180, 2011, doi: 10.1080/10255840310001210 34.

[138] A. Isihara, N. Hashitsume, and M. Tatibana, "Statistical Theory of Rubber-Like Elasticity. IV. (Two-Dimensional Stretching)," *J. Chem. Phys.*, vol. 19, no. 12, p. 1508, Dec. 2004, doi: 10.1063/1.1748111.

[139] A. Ní Annaidh, K. Bruyère, M. Destrade, M. D. Gilchrist, and M. Otténio, "Characterization of the anisotropic mechanical properties of excised human skin," *J. Mech. Behav. Biomed. Mater.*, vol. 5, no. 1, pp. 139–148, Jan. 2012, doi: 10.1016/J.JMBBM.2011.08.016.

[140] L. L. Gras, D. Mitton, P. Viot, and S. Laporte, "Hyper-elastic properties of the human sternocleidomastoideus muscle in tension," *J. Mech. Behav. Biomed. Mater.*, vol. 15, pp. 131–140, Nov. 2012, doi: 10.1016/J.JMBBM.2012.06.013.

[141] R. Obuchowicz *et al.*, "Interfascicular matrix-mediated transverse deformation and sliding of discontinuous tendon subcomponents control the viscoelasticity and failure of tendons," *J. Mech.*

Behav. Biomed. Mater., vol. 97, pp. 238–246, Sep. 2019, doi: 10.1016/J.JMBBM.2019.05.027.

[142] K. M. Moerman, C. K. Simms, and T. Nagel, "Control of tension–compression asymmetry in Ogden hyperelasticity with application to soft tissue modelling," *J. Mech. Behav. Biomed. Mater.*, vol. 56, pp. 218–228, Mar. 2016, doi: 10.1016/J.JMBBM.2015.11.027.

[143] P. H. Mott, J. R. Dorgan, and C. M. Roland, "The bulk modulus and Poisson's ratio of 'incompressible' materials," *J. Sound Vib.*, vol. 312, no. 4–5, pp. 572–575, May 2008, doi: 10.1016/J.JSV.2008.01.026.

[144] M. Akrami, Z. Qian, Z. Zou, D. Howard, C. J. Nester, and L. Ren, "Subject-specific finite element modelling of the human foot complex during walking: sensitivity analysis of material properties, boundary and loading conditions," *Biomech. Model. Mechanobiol.*, 2018, doi: 10.1007/s10237-017-0978-3.

[145] R. Sopher, J. Nixon, E. McGinnis, and A. Gefen, "The influence of foot posture, support stiffness, heel pad loading and tissue mechanical properties on biomechanical factors associated with a risk of heel ulceration," *J. Mech. Behav. Biomed. Mater.*, vol. 4, no. 4, pp. 572–582, May 2011, doi: 10.1016/J.JMBBM.2011.01.004.

[146] L. Peko, M. Barakat-Johnson, and A. Gefen, "Protecting prone positioned patients from facial pressure ulcers using prophylactic dressings: A timely biomechanical analysis in the context of the COVID-19 pandemic," *Int. Wound J.*, vol. 17, no. 6, pp. 1595–1606, Dec. 2020, doi: 10.1111/IWJ.13435.